Doctoral Dissertation

博士論文

Gravitational waves induced by scalar perturbations in the early Universe

(初期宇宙におけるスカラー揺らぎを起源とする重力波生成)

A Dissertation Submitted for the Degree of Doctor of Philosophy

December 2019

令和 元年 12 月 博士(理学) 申請

Department of Physics, Graduate School of Science,

The University of Tokyo

東京大学大学院理学系研究科

物理学専攻

Keisuke Inomata

猪又 敬介

Abstract

We study the gravitational waves (GWs) induced by scalar perturbations in the early Universe. Scalar perturbations can induce not only fluctuations of cosmic microwave background (CMB) and the large scale structures (LSSs), but also GWs through their non-linear interactions. Observations of the induced GWs enable us to access small-scale ($k \gtrsim 1\,\mathrm{Mpc}^{-1}$) scalar perturbations, which are difficult to measure through CMB or LSS observations. For this reason, many authors have focused on the induced GWs recently.

In this thesis, we discuss the induced GWs in terms of the amplitude of the small-scale perturbations and the effects of an early matter-dominated (eMD) era on the induced GWs.

As for the amplitude of the small-scale perturbations, we derive existing and expected limits on the amplitude of the small-scale perturbations using induced GWs. To this end, we use accurate methods to calculate the induced GWs and carefully take into account the sensitivities of different experiments to the induced GWs and the profile of the power spectrum of the scalar perturbations.

As for the effects of an eMD era, we discuss how the existence of an eMD era, preceding the radiation dominated (RD) era, changes the spectrum of the induced GWs. We carefully take into account the evolution of the scalar perturbations before, during, and after the transition from an eMD era to the RD era. To make the discussion concrete, we consider two scenarios for the transition: the gradual transition and the sudden transition. In the gradual (sudden) transition scenario, the transition from an eMD era to the RD era occurs with the timescale comparable to (much shorter than) the Hubble timescale at that time. As a result, we find that the induced GWs are suppressed in the gradual transition scenario, or on the other hand are much enhanced in the sudden transition scenario. In particular, in the sudden transition scenario, the enhanced GWs could be detected by future observations and be used to determine the reheating temperature.

Contents

Chapter 1

Introduction

On February 11, 2016, the first direct detection of gravitational waves (GWs) from the merger of black holes was announced by the LIGO and Virgo Scientific Collaboration [1]. The existence of GWs was first predicted by Albert Einstein in 1916 [2] and indirectly proved by the observation of the binary pulsar system PSR B1913+16 in 1974 [3, 4]. The first direct detection is the dawn of a new era of astronomy and cosmology with GWs.

In this thesis, we discuss GWs in the aspect of the early Universe.

Historically, in 1950's and 60's, there were two remarkable models for the early Universe: the Big Bang cosmology [5] and the steady-state cosmology [6, 7]. The Big Bang cosmology claims that the Universe started from the high-temperature state, has been expanding since then, and has finally become a present low-temperature state. On the other hand, the steady-state cosmology claims that the Universe expands, but the energy density of the Universe remains constant with the assumption that the matter is continually created by some mechanism. In 1965, the detection of the cosmic microwave background (CMB) [8, 9] decided the winner, supporting the Big Bang cosmology. Since then, the Big Bang cosmology has been widely accepted by many researchers. In the Big Bang cosmology, the abundances of light elements, such as ^{4}He, ^{3}He, D, and ^{7}Li, are mainly determined a few minutes after the birth of the Universe, which is called the Big Bang Nucleosynthesis (BBN) [10–12]. The observations of the light elements in the Universe are almost consistent with the prediction of the BBN theory, which also supports the Big Bang cosmology (see Ref. [13] for a recent review of BBN).[1] In this sense, the Big Bang cosmology succeeds in explaining the early Universe from a few minutes after the birth of the Universe to the present.

However, the Big Bang cosmology has some problems, such as the horizon problem [14, 15] and the flatness problem [16]. The horizon problem is a difficulty in realizing the current homogeneous and isotropic Universe. In the Big Bang cosmology, the universe naturally becomes inhomogeneous and anisotropic at present because many parts of the universe cannot interact with each other before they enter the observable universe due to the causality. To realize the observed homogeneous and isotropic Universe, we need a fine-tuning, which is a problem. The flatness problem[2] is a difficulty in realizing the current flat Universe. If we do not assume fine-tuning, the Big Bang cosmology predicts that the contribution of the metric curvature to the evolution of the Universe is much larger

[1] There is a discrepancy between the theoretical prediction and observations in the abundance of ^{7}Li, which is called the lithium problem [13].

[2] This problem can be reinterpreted as the longevity problem of the Universe, which is a difficulty of letting the Universe live much longer than the Planck time.

than that of the matter components, such as radiation and non-relativistic matter, at present. However, the observation of the current Universe indicates that the contribution of the curvature is zero or very small [17]. The inflation theory elegantly solves the problems and therefore has been studied by many authors since it was invented in 1980 and 1981 [18–22]. In the inflation theory, the early Universe experiences the accelerating expansion before the Big Bang, which makes the Universe homogeneous, isotropic and flat. After the inflation era, the Universe is reheated and smoothly connected to that in the Big Bang cosmology.

The inflation theory automatically includes the mechanism for the production of the perturbations from the quantum fluctuations, which can be the origins of the CMB fluctuations and the large scale structures (LSSs), and the properties of the perturbations depend on the detail of the inflation models. In this sense, the perturbations have important information about the inflation theory. In particular, the scalar perturbations on the large scale ($k \lesssim 1\,\mathrm{Mpc}^{-1}$, k: wavenumber of the perturbations) have already been measured by the observations of the CMB and LSSs. To be concrete, we have already known the amplitude and tilt of the power spectrum of the scalar perturbations on the large scale as $\mathcal{P}_\zeta \simeq 2.1 \times 10^{-9}(k/0.05\,\mathrm{Mpc}^{-1})^{-0.04}$ [17], which means the energy density perturbation on the large scale is given as $\delta\rho/\rho \sim \mathcal{O}(10^{-5})$.

The connection between the early Universe and GWs has been studied by many authors. For example, the primordial GWs originating from the quantum fluctuations during the inflation era are closely related to the inflation energy scale [23], which are the targets of the CMB B-mode observation [24–26]. Furthermore, GWs can also be produced from the cosmological topological defects [27–29], the bubble collisions originating from the first-order phase transition [30–33], and the preheating [34–37]. In this thesis, we focus on another kind of GWs, which are induced by the scalar perturbations. The scalar perturbations can induce GWs through the non-linear interaction between the scalar perturbations and tensor perturbations [38–44]. Since we already know that there exist scalar perturbations in the Universe, the induced GWs necessarily exist. In some cases, the induced GWs are enhanced and could be a target of the current and future observations, such as pulsar timing array (PTA) experiments (EPTA [45], PPTA [46], NANOGrav [47], SKA [48, 49]), ground-based GW detectors (advanced LIGO (aLIGO) [50], Virgo [51], KAGRA [52], Einstein Telescope [48, 53, 54], Cosmic Explorer [55]), and space-based GW detectors (LISA [48, 53, 56], DECIGO [57, 58], BBO [58, 59]).

Throughout this thesis, we discuss the GWs induced by the scalar perturbations as a probe of the early Universe. In particular, we study the induced GWs from two points of view.

Investigation of the amplitude of small-scale perturbations

One viewpoint is the investigation of the amplitude of small-scale perturbations with the use of the induced GWs. Unlike the large-scale scalar perturbations, the small-scale perturbations ($k \gtrsim 1\mathrm{Mpc}^{-1}$) are difficult to investigate through the CMB or LSS observations. This is due to the diffusion (or Silk) damping [60, 61] for the CMB observations and the resolution limit of the Lyman-α forest for the LSS observations [62–64]. Therefore, the current constraints on the amplitude of the small-scale perturbations are much weaker than those on the large-scale ones.

The amplitudes of the scalar perturbations, including those on the small scales, are related to the details of the inflation models. Some inflation models predict the large amplitude of the small-scale perturbations [65–68], being consistent with the results on the large scale. If the small-scale perturbations have the large amplitude, they could produce

some unique compact objects, such as primordial black holes (PBHs) (see Ref. [69] for a recent review) and ultracompact minihalos (UCMHs) [70–73]. In particular, PBHs have recently been studied by a number of authors because PBHs are one of the good candidates for dark matter (DM) [74–76] and the black holes observed through the direct detection of GWs [77–79]. In these senses, the investigation of the amplitude of the small-scale perturbations is one of the hottest topics in modern cosmology.

The large-amplitude scalar perturbations on the small scales can also produce large-amplitude GWs through the interaction between them at the second-order level, which can be a target of the current and future GW projects. For this reason, the induced GWs have attracted a lot of attention recently, especially in the context of PBHs [80–102]. In this thesis, we discuss how much the current and future GW projects could measure or constrain the amplitude of the small-scale perturbations.

Effects of an early matter-dominated era on induced gravitational waves

The other viewpoint is the effects of an early matter-dominated era on the induced GWs. In some scenarios, there is a matter-dominated era preceding the radiation-dominated (RD) era, during which the BBN occurs. The matter-dominated era is often called an early matter-dominated (eMD) era. An eMD era might be realized by the coherent oscillation of an inflaton [103], which is a field causing inflation with its vacuum energy during the inflation era. An eMD era ends with the decay of the massive field to radiation, which is called the reheating, and the RD era begins. Therefore the investigation of an eMD era might reveal the properties of the inflaton. In addition, we also mention that PBHs could also be produced during an eMD era [104] and their properties are different from those of PBHs produced during the RD era [105, 106]. Since the existence of an eMD era has not been proved yet, it is meaningful to discuss how to extract information about an eMD era from observations.

Since the small-scale perturbations can enter the horizon during an eMD era and behave differently from those during the RD era, the induced GWs might be enhanced [81, 107, 108]. To probe the existence of an eMD era with the use of the induced GWs, we need to know the spectrum of the GWs induced by the scalar perturbations that have experienced an eMD era. In this thesis, we revisit the effects of an eMD era on the induced GWs taking into account how the scalar perturbations evolve before, during, and after the transition from an eMD era to the RD era. Then, we show the previous results are not correct and the spectrum of the induced GWs strongly depends on the timescale of the transition.

Organization of this thesis

This thesis is divided into two parts: review part (Part I) and part on our original works (Part II).

In Part I (Chaps. 2-4), we review the formulas used in Part II. We divide the review part into Chaps. 2-4 depending on the level of perturbations. In Chap. 2, we discuss the evolution of the Universe without considering the perturbations (zeroth order in perturbations). In Chap. 3, we review the cosmological perturbations at the linear level (first order in perturbations). In Chap. 4, we derive the basic formulas to calculate the GWs induced by the scalar perturbations through the second-order interaction between scalar and tensor perturbations (second order in perturbations). In Part I, we use the Mathematica package xPand [109] for some calculations.

In Part II (Chaps. 5 and 6), we show our original works, using the formulas derived in Part I. In Chap. 5, we reveal how much the future or current GW projects can investigate the amplitude of the small-scale perturbations through the observation of the induced GWs. In Chap. 6, we revisit the effects of an eMD era on the induced GWs. To be concrete, in Sec. 6.1, we discuss the effects in the case where the eMD era ends with the gradual reheating, whose timescale is comparable to the Hubble timescale at that time. In Sec. 6.2, contrary to Sec. 6.1, we discuss the induced GWs in the case of the sudden reheating, whose timescale is much shorter than the Hubble timescale at that time.

We devote Chap. 7 to the conclusions of this thesis.

Notations and Conventions

Before closing this chapter, we summarize the notations and conventions which are used in this thesis unless otherwise noted.

- When we use the Greek characters, such as μ, ν, ρ, and σ, for super/subscripts, they indicate the space-time coordinates. In other words, they run over the set $\{0, 1, 2, 3\}$.
- When we use the Latin characters, such as i, j, k, and l, for super/subscripts, they indicate the space coordinates. In other words, they run over the set $\{1, 2, 3\}$.
- We adopt the Einstein summation convention, such as $a^i b_i = a^1 b_1 + a^2 b_2 + a^3 b_3$.
- We adopt the relativistic units $\hbar = c = 1$, where $\hbar$ is the reduced Planck constant and c is the speed of light.
- We use the reduced Planck mass $M_{\rm Pl} = 1/\sqrt{8\pi G}$ instead of the gravitational constant.
- We take the signature $(-, +, +, +)$ for metric, which means the Minkowski metric is expressed as

$$\mathrm{d}s^2 = -\mathrm{d}t^2 + \mathrm{d}x^2 + \mathrm{d}y^2 + \mathrm{d}z^2. \tag{1.1}$$

- For the Fourier transform of $f(x)$ in d-dimension, we take the following normalizations:

$$f(x) = \int \frac{\mathrm{d}^d k}{(2\pi)^d} \tilde{f}(k) e^{ik\cdot x}, \tag{1.2}$$

$$\tilde{f}(k) = \int \mathrm{d}^d x f(x) e^{-ik\cdot x}. \tag{1.3}$$

Part I

Review Part

Chapter 2

Expanding Universe: zeroth order in perturbations

Modern cosmology is based on the Cosmological principle, which states that the spatial distribution of matter in the Universe is homogeneous and isotropic when the matter is averaged on the scale larger than the LSS, which leads to the Friedmann–Lemaître–Robertson–Walker (FLRW) metric. In addition, the flatness of the Universe is measured with the combination of the CMB and baryon acoustic oscillation (BAO) data as $\Omega_{\rm K} = 0.0007^{+0.0037}_{-0.0037}$ [17], where $\Omega_{\rm K}$ is the energy density parameter for the spatial curvature. In this chapter, we review the evolution of background quantities in the flat FLRW Universe.

2.1 Basic formulas

In this section, we summarize the basic formulas to describe the expansion of the Universe. We start from the flat FLRW metric, given as

$$\mathrm{d}s^2 = g_{\mu\nu}\mathrm{d}x^\mu \mathrm{d}x^\nu, \tag{2.1}$$

$$g_{\mu\nu} = \begin{cases} -a(\eta)^2 & (\mu=\nu=0) \\ a(\eta)^2 & (\mu=\nu=i) \\ 0 & (\text{otherwise}) \end{cases}, \tag{2.2}$$

where a is the scale factor, which depends on time, and $x^0 (= \eta)$ is the conformal time, defined as $\eta = \int \mathrm{d}t/a$.

The evolution of all quantities in the Universe should satisfy the Einstein equations, given as

$$G_{\mu\nu} + \Lambda g_{\mu\nu} = \frac{1}{M_{\rm Pl}^2} T_{\mu\nu}, \tag{2.3}$$

where Λ is the cosmological constant, $T_{\mu\nu}$ is the energy-momentum tensor, and $G_{\mu\nu}$ is the Einstein tensor, defined as $G_{\mu\nu} \equiv R_{\mu\nu} - \frac{1}{2} R g_{\mu\nu}$. The Ricci tensor and the Ricci scalar are defined as

$$R_{\mu\nu} \equiv \Gamma^\lambda{}_{\mu\nu,\lambda} - \Gamma^\lambda{}_{\mu\lambda,\nu} + \Gamma^\kappa{}_{\mu\nu}\Gamma^\lambda{}_{\kappa\lambda} - \Gamma^\kappa{}_{\mu\lambda}\Gamma^\lambda{}_{\nu\kappa}, \tag{2.4}$$

$$R \equiv g^{\mu\nu} R_{\mu\nu}, \tag{2.5}$$

where the subscript ",μ" means the derivative with respect to the spacetime and the Christoffel symbol is defines as

$$\Gamma^{\lambda}{}_{\mu\nu} \equiv \frac{1}{2} g^{\lambda\rho}(g_{\rho\mu,\nu} + g_{\rho\nu,\mu} - g_{\mu\nu,\rho}). \tag{2.6}$$

Note that the inverse metric $g^{\mu\nu}$ is defined with the relation $g^{\mu\nu}g_{\nu\rho} = \delta^{\mu}_{\rho}$, where δ^{μ}_{ν} is the unit tensor. Then, we can explicitly write $g^{\mu\nu}$ as

$$g^{\mu\nu} = \begin{cases} -\dfrac{1}{a(\eta)^2} & (\mu = \nu = 0), \\ \dfrac{1}{a(\eta)^2} & (\mu = \nu = i), \\ 0 & (\text{otherwise}). \end{cases} \tag{2.7}$$

Hereafter, the transformation between the superscript and subscript in the 4-dimensional spacetime is performed with $g^{\mu\nu}$ or $g_{\mu\nu}$ as $T^{\mu}{}_{\nu} \equiv g^{\mu\lambda}T_{\lambda\nu}$. In the flat FLRW metric, the Christoffel symbols are given as

$$\Gamma^{0}{}_{00} = \frac{a'}{a}, \quad \Gamma^{i}{}_{0j} = \frac{a'}{a}\delta^{i}{}_{j}, \quad \Gamma^{0}{}_{ij} = \frac{a'}{a}\delta_{ij}, \quad \Gamma^{i}{}_{00} = \Gamma^{0}{}_{0i} = \Gamma^{i}{}_{jk} = 0, \tag{2.8}$$

where the prime represents the derivative with respect to the conformal time. Then, the Ricci tensor and scalar can be expressed as

$$R_{00} = -3\frac{a''}{a} + 3\left(\frac{a'}{a}\right)^2, \tag{2.9}$$

$$R_{0i} = 0, \tag{2.10}$$

$$R_{ij} = \left(\frac{a''}{a} + \left(\frac{a'}{a}\right)^2\right)\delta_{ij}, \tag{2.11}$$

$$R = \frac{6}{a^2}\frac{a''}{a}. \tag{2.12}$$

On the other hand, since the matter can be approximated as a perfect fluid on large scales, we can express the energy-momentum tensor as

$$T_{\mu\nu} = (\rho + P)u_{\mu}u_{\nu} + Pg_{\mu\nu}, \tag{2.13}$$

where ρ and P are the energy density and the pressure of matter and u_{μ} is 4-velocity, which satisfies $u^{\mu}u_{\mu} = -1$. In the homogeneous universe, which we consider here, the 4-velocities are given as $u^{\mu} = \frac{1}{a}(1,0,0,0)$ and $u_{\mu} = -a(1,0,0,0)$ in the background level (zeroth order in perturbations).

From the $\{00\}$ and $\{ij\}$ components in Eq. (2.3), we obtain the following equations:

$$\left(\frac{a'}{a}\right)^2 = \frac{a^2\rho}{3M_{\rm Pl}^2} + \frac{\Lambda a^2}{3}, \tag{2.14}$$

$$\frac{a''}{a} = \frac{1}{2}\left(\frac{a'}{a}\right)^2 + \frac{\Lambda a^2}{2} - \frac{a^2 P}{2M_{\rm Pl}^2}. \tag{2.15}$$

These equations are often called the Friedman equations. From these equations, we can see that the contribution from the cosmological constant can be regarded as that from the

matter whose equation-of-state parameter is given as $w = P_\Lambda/\rho_\Lambda = -1$, where $\rho_\Lambda \equiv M_{\rm Pl}^2\Lambda$ and $P_\Lambda \equiv -M_{\rm Pl}^2\Lambda$. Substituting Eq. (2.14) into Eq. (2.15), we derive

$$\frac{a''}{a} = \frac{1}{6M_{\rm Pl}^2}(\rho + \rho_\Lambda - 3(P + P_\Lambda))a^2. \tag{2.16}$$

To get insights of the evolution of the Universe, we rewrite Eqs. (2.14) and (2.16) with the physical time t as

$$\left(\frac{\dot{a}}{a}\right)^2 = \frac{1}{3M_{\rm Pl}^2}(\rho + \rho_\Lambda), \tag{2.17}$$

$$\frac{\ddot{a}}{a} = -\frac{1}{6M_{\rm Pl}^2}(\rho + \rho_\Lambda + 3(P + P_\Lambda)), \tag{2.18}$$

where the dot represents the derivative with respect to the physical time. From these equations, we can see that the matter with $w < -1/3$ accelerates the expansion.

From the Bianchi identity, the covariant derivative of the energy-momentum tensor should be zero as

$$T^\mu{}_{\nu;\mu} = 0, \tag{2.19}$$

where the covariant derivative is defined as

$$T^\mu{}_{\nu;\mu} \equiv T^\mu{}_{\nu,\mu} + \Gamma^\mu{}_{\mu\lambda}T^\lambda{}_\nu - \Gamma^\lambda{}_{\nu\mu}T^\mu{}_\lambda. \tag{2.20}$$

Substituting Eqs. (2.8) and (2.13) into Eq. (2.19), we get the energy conservation law as

$$\rho' = -3\frac{a'}{a}(\rho + P). \tag{2.21}$$

Note that, we can also derive this equation from Eqs. (2.14) and (2.15) without using $T^\mu{}_{\nu;\mu} = 0$. To be concrete, substituting the derivative of Eq. (2.14) into (2.15), we can obtain Eq. (2.21). This means that there are only two independent equations in Eqs. (2.14), (2.15), and (2.21).

2.2 Evolution of the Universe

Here, we discuss the evolution of the Universe. As we will see in the following, the evolution of the Universe depends on the equation-of-state parameter ($w \equiv P/\rho$) of the dominant matter at that time.

First, we discuss the era during which the Universe is dominated by the matter with $w \neq -1$. We can derive the scale-factor dependence of the energy density through Eq. (2.21) as

$$\rho \propto a^{-3(1+w)}. \tag{2.22}$$

We can also derive the time dependence of the scale factor substituting this equation into Eq. (2.17) and solving the differential equation. As a result, we find

$$a \propto t^{\frac{2}{3(1+w)}} \propto \eta^{\frac{2}{1+3w}} \quad (\text{for } w \neq -1). \tag{2.23}$$

Here, we derive the expressions for realistic matters, such as radiation and non-relativistic matter. Since the equation-of-state parameter is given as $w = 1/3$ during a RD era or $w = 0$ during a (non-relativistic) matter-dominated (MD) era[1], we can derive the following expressions:

$$\rho \propto \begin{cases} a^{-4} & \text{(RD era)} \\ a^{-3} & \text{(MD era)} \end{cases}, \tag{2.24}$$

$$a \propto \begin{cases} t^{1/2} \propto \eta & \text{(RD era)} \\ t^{2/3} \propto \eta^2 & \text{(MD era)} \end{cases}. \tag{2.25}$$

For later convenience, we define the Hubble parameter and the conformal Hubble parameter as

$$H \equiv \frac{\dot{a}}{a} = \begin{cases} \dfrac{1}{2t} & \text{(RD era)} \\ \dfrac{2}{3t} & \text{(MD era)} \end{cases}, \tag{2.26}$$

$$\mathcal{H} \equiv \frac{a'}{a} = \begin{cases} \dfrac{1}{\eta} & \text{(RD era)} \\ \dfrac{2}{\eta} & \text{(MD era)} \end{cases}. \tag{2.27}$$

Next, we discuss the case of $w = -1$. This case corresponds to the era during which the Universe is dominated by the cosmological constant (ΛD era) or the vacuum energy of the inflaton (inflation era). Here, we consider the ΛD era. In this case, we can see from Eq. (2.21) that the dominant component of the energy density $\rho_\Lambda (= M_{\rm Pl}^2 \Lambda)$ is constant with time. Then, from Eq. (2.17), we get

$$a \propto \exp\left(\sqrt{\frac{\Lambda}{3}} t\right) \quad (\Lambda\text{D era}). \tag{2.28}$$

To characterize the amount of energy, we define the energy density parameters as

$$\Omega_{a,0} \equiv \frac{\rho_a}{\rho_{\rm tot,0}} = \frac{\rho_a}{3 M_{\rm Pl}^2 H_0^2}, \tag{2.29}$$

where $\rho_{\rm tot}$ means the total energy density, the subscript "a" indicates the each component, and the subscript "0" represents the present value. In particular, H_0 is the Hubble constant, defined as $H_0 \equiv \dot{a}/a|_{t=t_0}$ (t_0: the present time of the Universe). From the Planck CMB observation [17], the present values of cosmological parameters for matter and cosmological constant are measured as

$$\Omega_{\rm m,0} = 0.3153 \pm 0.0073, \tag{2.30}$$

$$\Omega_{\Lambda,0} = 0.6847 \pm 0.0073. \tag{2.31}$$

Although the energy density parameter of radiation is not explicitly shown in Ref. [17], we can derive the energy density parameter from the CMB temperature $T_{\rm CMB} = 2.7255\,{\rm K}$ [110].

[1] In the context of cosmology, the matter with $w = 0$ is often simply called "matter" in contrast to radiation. In this thesis, we follow this convention.

Here, we assume the neutrinos are massless for simplicity. Then, we derive the mean value of the parameter as

$$\Omega_{\mathrm{r},0}h^2 = 4.183 \times 10^{-5}, \tag{2.32}$$

where h is the dimensionless parameter, which is related to the Hubble constant as

$$H_0 = 100\,h\,\mathrm{km\,s^{-1}\,Mpc^{-1}}. \tag{2.33}$$

The Planck CMB observation determines the dimensionless parameter as [17][2]

$$h = 0.6736 \pm 0.0054. \tag{2.34}$$

From the present values of the energy density parameters (Eqs. (2.30), (2.31), and (2.32)) and the scale factor dependence of the energy density (Eq. (2.24)), we can predict the evolution of the Universe as follows. At first, the Universe is dominated by radiation. After a while, the Universe experiences the transition from the RD era to MD era at $z \sim 3400$ [17] (z: the redshift parameter) and then, the Universe gets dominated by the non-relativistic matter. Finally, the Universe is dominated by the cosmological constant. This picture of the Universe is consistent with the current observations, such as CMB/LSS observations and light element observations. Note that, however, we do not know much about how the Universe evolved before the BBN due to the lack of observational data. For example, there could exist an eMD era, which ends and is smoothly connected to the RD era before the BBN begins. We consider this case in Sec. 2.3.2.

2.3 Transition between RD era and MD era

In this section, we discuss the evolution of the quantities during the transition between a RD era and a MD era.

2.3.1 Transition from RD era to MD era

First, we consider the transition from the RD era to the MD era, which happened at $z \sim 3400$. We assume that there are only radiation and matter in the Universe and the other components are negligible, which is the case in the early Universe. Then, the total energy density can be written as

$$\rho = \rho_{\mathrm{m}} + \rho_{\mathrm{r}} = \frac{\rho_{\mathrm{eq}}}{2}\left(\left(\frac{a_{\mathrm{eq}}}{a}\right)^3 + \left(\frac{a_{\mathrm{eq}}}{a}\right)^4\right), \tag{2.35}$$

where the subscript "tot" is omitted and the subscript "eq" means the value at the equality time, when $\rho_{\mathrm{m}} = \rho_{\mathrm{r}}$ holds. From Eq. (2.16), we can derive

$$a'' = \frac{1}{12M_{\mathrm{Pl}}^2}\rho_{\mathrm{eq}}a_{\mathrm{eq}}^3. \tag{2.36}$$

[2]Note that there is a tension between the values of the Hubble parameter measured through the CMB observation and the local measurement of Cepheids and Type Ia supernovae. The most recent result for the local measurement is $h = 0.7403 \pm 0.0142$ [111]. This tension might come from the systematics in the CMB result considering the fact that the WMAP9 result shows $h = 0.700 \pm 0.022$ [112].

Solving this equation, we obtain

$$a(\eta) = \frac{1}{24M_{\rm Pl}^2}\rho_{\rm eq}a_{\rm eq}^3\eta^2 + C\eta, \tag{2.37}$$

where C is one of the integration constants and we kill the other integration constant imposing $a(\eta \to 0) = 0$. Here, we determine the value of C. When $a \ll a_{\rm eq}$, from Eqs. (2.35) and (2.37), we find

$$\rho \simeq \frac{\rho_{\rm eq}}{2}\left(\frac{a_{\rm eq}}{a}\right)^4, \tag{2.38}$$

$$a' \simeq C. \tag{2.39}$$

Substituting these equation into Eq. (2.14), we get

$$C = \left(\frac{1}{6M_{\rm Pl}^2}\rho_{\rm eq}a_{\rm eq}^4\right)^{1/2}. \tag{2.40}$$

Then, we can rewrite Eq. (2.37) as

$$a(\eta) = a_{\rm eq}\left(\left(\frac{\eta}{\eta_*}\right)^2 + 2\left(\frac{\eta}{\eta_*}\right)\right), \tag{2.41}$$

where η_* is defined as

$$\eta_* = \left(\frac{1}{24M_{\rm Pl}^2}\rho_{\rm eq}a_{\rm eq}^2\right)^{-1/2} = \frac{\eta_{\rm eq}}{\sqrt{2}-1}. \tag{2.42}$$

From the Planck result, the conformal equality time is measured as [17]

$$\eta_{\rm eq} = 113.14 \pm 0.91\,{\rm Mpc}, \tag{2.43}$$

where we have used the relation $k_{\rm eq} \equiv a_{\rm eq}H_{\rm eq} = (4-2\sqrt{2})/\eta_{\rm eq}$ [113].

2.3.2 Transition from MD era to RD era

Next, we consider the transition from a MD era to the RD era, which could happen in the early Universe. For example, a coherent oscillation of a purely massive scalar field could realize a MD era preceding the RD era and the decay of the scalar field leads to the transition from a MD era to the RD era [103]. Here, we consider the case where the matter decays to radiation with a decay rate of Γ, which can be applied to a coherently oscillating field [114].[3] In this case, the energy-momentum conservation can be expressed as [116, 117]

$$T^{\mu}_{{\rm m}\,\nu;\mu} = \Gamma\, T^{\mu}_{{\rm m}\,\nu}u_{{\rm m}\,\mu}, \tag{2.44}$$

$$T^{\mu}_{{\rm r}\,\nu;\mu} = -\Gamma\, T^{\mu}_{{\rm m}\,\nu}u_{{\rm m}\,\mu}, \tag{2.45}$$

[3] In most cases, the thermalization instantaneously occurs after/during the decay of the oscillating field in the early Universe [115]. Therefore, we assume the instantaneous thermalization throughout this thesis.

where the subscript "m" and "r" represent the matter and radiation components, respectively. Note that Γ is the decay rate of the matter per unit proper time of the matter and therefore the decay rate appears with $u_{\mathrm{m}\,\mu}$. The total energy-momentum tensor is given as $T^{\mu}_{\mathrm{tot}\,\nu} = T^{\mu}_{\mathrm{m}\,\nu} + T^{\mu}_{\mathrm{r}\,\nu}$ and the energy-momentum conservation law is satisfied for the total tensor as $T^{\mu}_{\mathrm{tot}\,\nu;\mu} = 0$. In the early Universe, the interaction between radiations are very strong and the radiation fluid can be regarded as the perfect fluid, as well as the matter fluid.[4] Substituting Eq. (2.13) into Eqs. (2.44) and (2.45), we derive the following equations:

$$\rho'_{\mathrm{m}} + 3\mathcal{H}\rho_{\mathrm{m}} = -a\Gamma\rho_{\mathrm{m}}, \tag{2.46}$$

$$\rho'_{\mathrm{r}} + 4\mathcal{H}\rho_{\mathrm{r}} = a\Gamma\rho_{\mathrm{m}}. \tag{2.47}$$

Note $T^{0}_{\mathrm{m}\,0} = -\rho_{\mathrm{m}}$ in our notation. Unfortunately, there are no analytical solutions for these equations and we need to perform a numerical calculation to solve them, as we do in Sec. 6.1.

For later convenience, we introduce the expression for the scale factor that experiences the sudden transition from a MD era to a RD era at η_{R}. In this case, the scale factor dependence of the energy density instantaneously changes from $\rho \propto a^{-3}$ to $\rho \propto a^{-4}$. Then, from Eq. (2.14), we obtain

$$\frac{a(\eta)}{a(\eta_{\mathrm{R}})} = \begin{cases} \left(\dfrac{\eta}{\eta_{\mathrm{R}}}\right)^2 & (\eta < \eta_{\mathrm{R}}) \\ 2\dfrac{\eta}{\eta_{\mathrm{R}}} - 1 & (\eta \geq \eta_{\mathrm{R}}) \end{cases}, \tag{2.48}$$

where we have imposed the scale factor and its derivative are continuous at η_{R} because the energy density does not change during the sudden transition. From this expression for the scale factor, we can express the conformal Hubble parameter as

$$\mathcal{H} = \begin{cases} \dfrac{2}{\eta} & (\eta < \eta_{\mathrm{R}}) \\ \dfrac{1}{\eta - \eta_{\mathrm{R}}/2} & (\eta \geq \eta_{\mathrm{R}}) \end{cases}. \tag{2.49}$$

[4]The temperature dependence of the diffusion length, coming from the anisotropic stress of radiation fluid, is calculated in Ref. [118]. In the reference, we can see that the diffusion length is much smaller than the horizon scale in the early Universe, which means that the anisotropic stress can be neglected at least in our analysis of the induced GWs.

Chapter 3

Cosmological Perturbations: first order in perturbations

In this chapter, we review the cosmological perturbations. Throughout this chapter, we focus on the scalar perturbations because the vector perturbation decays even on superhorizon scales [119] and the tensor perturbation can be expected to be smaller than the scalar perturbations from the constraints on the tensor-to-scalar ratio, $r < 0.065$ [17].[1] In this chapter, we take into account the perturbations up to first order. We discuss the second-order perturbations in the next chapter. Note that some parts of this chapter are based on the discussion in Ref. [119].

3.1 Basic quantities in perturbations

In this section, we summarize the basic quantities in perturbations.

The metric with the perturbations can be expressed as

$$\mathrm{d}s^2 = \left[\bar{g}_{\mu\nu} + \delta g_{\mu\nu}(x^\alpha)\right], \tag{3.1}$$

where $\bar{g}_{\mu\nu}$ is the background value, given as Eq. (2.2), and $|\delta g_{\mu\nu}| \ll |\bar{g}_{\mu\nu}|$ is satisfied except for the case of $\bar{g}_{\mu\nu} = 0$ such as $\bar{g}_{i0}, \bar{g}_{0i}$, and $\bar{g}_{ij}$ with $i \neq j$. The scalar metric perturbations can be expressed as

$$\delta g_{00} = -2a^2\Phi, \tag{3.2}$$
$$\delta g_{0i} = a^2 B_{,i}, \tag{3.3}$$
$$\delta g_{ij} = 2a^2(-\Psi\delta_{ij} + E_{,ij}), \tag{3.4}$$

where Φ, B, Ψ, and E are the scalar perturbations. We can explicitly write the metric with the perturbations as

$$\mathrm{d}s^2 = a(\eta)^2(-(1+2\Phi)\mathrm{d}\eta^2 + 2B_{,i}\mathrm{d}\eta\mathrm{d}x^i + ((1-2\Psi)\delta_{ij} + 2E_{,ij})\mathrm{d}x^i\mathrm{d}x^j). \tag{3.5}$$

[1] The blue-tilted primordial GWs can be realized in some models, such as kinetically-driven G-inflation [120, 121] and inflation with the nonminimal coupling to the Gauss-Bonnet term [122–125]. This means the tensor perturbation on the small scales could be larger than that on the large scales, constrained by the CMB B-mode observation. However, the study on the GWs induced by the blue-tilted primordial GWs is beyond the scope of this thesis and we do not consider this case.

Then, the perturbations of the Christoffel symbols can be written as

$$\delta\Gamma^0{}_{00} = \Phi', \tag{3.6}$$

$$\delta\Gamma^0{}_{0i} = \Phi_{,i} + \frac{a'}{a}B_{,i}, \tag{3.7}$$

$$\delta\Gamma^i{}_{00} = \frac{a'}{a}B_{,i} + B'_{,i} + \Phi_{,i}, \tag{3.8}$$

$$\delta\Gamma^0{}_{ij} = -2\frac{a'}{a}\Phi\delta^i{}_j - B_{,ij} - 2\frac{a'}{a}\Psi\delta_{ij} - \Psi'\delta_{ij} + 2\frac{a'}{a}E_{,ij} + E'_{,ij}, \tag{3.9}$$

$$\delta\Gamma^i{}_{0j} = -\Psi'\delta_{ij} + E'_{,ij}, \tag{3.10}$$

$$\delta\Gamma^i{}_{jk} = -\Psi_{,j}\delta_{ik} - \Psi_{,k}\delta_{ij} + \Psi_{,i}\delta_{jk} - \frac{a'}{a}B_{,i}\delta_{jk} + E_{,ijk}. \tag{3.11}$$

The perturbed Einstein tensor is given as

$$\delta G^0{}_0 = \frac{1}{a^2}\left[6\left(\frac{a'}{a}\right)^2\Phi + 6\frac{a'}{a}\Psi' + 2\frac{a'}{a}B^{,i}{}_{,i} - 2\Psi^{,i}{}_{,i} - 2\frac{a'}{a}E^{,i}{}_{,i}\right], \tag{3.12}$$

$$\delta G^0{}_i = \frac{1}{a^2}\left(-2\frac{a'}{a}\Phi_{,i} - 2\Psi'_{,i}\right), \tag{3.13}$$

$$\delta G^i{}_0 = \frac{1}{a^2}\left(4\left(\frac{a'}{a}\right)^2 B_{,i} - 2\frac{a''}{a}B_{,i} + 2\frac{a'}{a}\Phi_{,i} + 2\Psi'_{,i}\right), \tag{3.14}$$

$$\begin{aligned}\delta G^i{}_j = \frac{1}{a^2}\Bigg[&\left(2\frac{a'}{a}\Phi' + 4\frac{a''}{a}\Phi - 2\left(\frac{a'}{a}\right)^2\Phi + \Phi^{,i}{}_{,i} + 4\frac{a'}{a}\Psi' + 2\Psi''\right.\\ &\left. - \Psi^{,i}{}_{,i} + 2\frac{a'}{a}B^{,i}{}_{,i} + B^{,i}{}_{,i}{}' + 2\frac{a'}{a}E^{,i}{}_{,i}{}' - E^{,i}{}_{,i}{}''\right)\delta_{ij}\\ &+ \left(-\Phi + \Psi - 2\frac{a'}{a}B - B' + 2\frac{a'}{a}E' + E''\right)^{,i}{}_{,j}\Bigg].\end{aligned} \tag{3.15}$$

Note that the transformation between the superscript and subscript in the 3-dimensional space is performed by δ_{ij} because we consider the flat universe.

For the perturbations of the energy-momentum tensor, substituting $\rho = \bar{\rho} + \delta\rho$, $P = \bar{P} + \delta P$, $u^\mu = (1/a + \delta u^0, \delta u^i)$, and $u_\mu = (-a + \delta u_0, \delta u_i)$ into Eq. (2.13), we derive

$$\delta T^0{}_0 = -\delta\rho, \tag{3.16}$$

$$\delta T^0{}_i = \frac{1}{a}(\bar{\rho} + \bar{P})\delta u_{,i}, \tag{3.17}$$

$$\delta T^i{}_0 = \frac{1}{a}(\bar{\rho} + \bar{P})\left(aB_{,i} - \delta u_{,i}\right), \tag{3.18}$$

$$\delta T^i{}_j = -\delta P\delta^i{}_j, \tag{3.19}$$

where the overline indicates the background value and we have expressed the velocity perturbation δu_i with the scalar perturbation δu as $\delta u_i = \delta u_{,i}$ because we neglect the vector perturbation. Note that, from the normalization condition $g^{\mu\nu}u_\mu u_\nu = -1$, we can obtain

$$\delta u_0 = -a\Phi. \tag{3.20}$$

3.2 Gauge transformation

Here, we explain the gauge transformation of the perturbations.

When we transform the coordinates as

$$x^\mu \to \tilde{x}^\mu = x^\mu + \xi^\mu, \tag{3.21}$$

the spacetime metric in the coordinates $\tilde{x}^\mu$ is given as

$$\tilde{g}_{\mu\nu}(\tilde{x}^\alpha) = \frac{\partial x^\rho}{\partial \tilde{x}^\mu}\frac{\partial x^\sigma}{\partial \tilde{x}^\nu} g_{\rho\sigma}(x^\alpha) \simeq \bar{g}_{\mu\nu}(x^\alpha) + \delta g_{\mu\nu} - \bar{g}_{\mu\sigma}\xi^\sigma_{,\nu} - \bar{g}_{\rho\nu}\xi^\rho_{,\mu}, \tag{3.22}$$

where ξ^μ is the infinitesimal small function and the contributions from second-order perturbations are neglected. In other words, "$\simeq$" in this equation means that the equality holds in the first-order level. Hereafter in this section, we use "$=$" in the sense that the equality holds in the first-order level. Here, we divide $\tilde{g}_{\mu\nu}$ into the background and the perturbation as

$$\tilde{g}_{\mu\nu}(\tilde{x}^\alpha) = \bar{g}_{\mu\nu}(\tilde{x}^\alpha) + \delta\tilde{g}_{\mu\nu}. \tag{3.23}$$

Comparing Eqs. (3.22) with (3.23), we can see that the coordinate transformation given by Eq. (3.21) leads to the transformation of the metric perturbation as

$$\delta g_{\mu\nu} \to \delta\tilde{g}_{\mu\nu} = \delta g_{\mu\nu} - \bar{g}_{\mu\nu,\rho}\xi^\rho - \bar{g}_{\mu\rho}\xi^\rho_{,\nu} - \bar{g}_{\rho\nu}\xi^\rho_{,\mu}, \tag{3.24}$$

where we have used the relation given as

$$\bar{g}_{\mu\nu}(x^\alpha) = \bar{g}_{\mu\nu}(\tilde{x}^\alpha) - \bar{g}_{\mu\nu,\rho}\xi^\rho. \tag{3.25}$$

Similarly, the matter quantities, such as $\delta\rho$, δP, and δu, are transformed as

$$\delta\rho \to \delta\tilde{\rho} = \delta\rho - \bar{\rho}_{,\mu}\xi^\mu, \tag{3.26}$$

$$\delta P \to \delta\tilde{P} = \delta P - \bar{P}_{,\mu}\xi^\mu, \tag{3.27}$$

$$\delta u_\mu \to \delta\tilde{u}_\mu = \delta u_\mu - \bar{u}_{\mu,\nu}\xi^\nu - \bar{u}_\nu\xi^\nu_{,\mu}. \tag{3.28}$$

From Eqs. (3.24) and (3.26)-(3.28), we can see that if the coordinates are transformed, the perturbations are also transformed. This kind of transformation of the perturbations, originating from the coordinate transformation, is called the gauge transformation. The gauge transformation comes from the freedom on how to divide the quantities into backgrounds and perturbations.

Taking advantage of the gauge transformation, we can kill the redundant freedom of the perturbations, which makes the calculation simple. Here, we show the advantage concretely. From Eqs. (3.24) and (3.26)-(3.28), we can derive the gauge transformation law for the metric and matter perturbations as

$$\Phi \to \tilde{\Phi} = \Phi - \frac{1}{a}(a\xi^0)', \tag{3.29}$$

$$B \to \tilde{B} = B - \chi' + \xi^0, \tag{3.30}$$

$$\Psi \to \tilde{\Psi} = \Psi + \frac{a'}{a}\xi^0, \tag{3.31}$$

$$E \to \tilde{E} = E - \chi, \tag{3.32}$$

$$\delta\rho \to \delta\tilde{\rho} = \delta\rho - \bar{\rho}'\xi^0, \tag{3.33}$$

$$\delta P \to \delta\tilde{P} = \delta P - \bar{P}'\xi^0, \tag{3.34}$$

$$\delta u_0 \to \delta\tilde{u}_0 = \delta u_0 + (a\xi^0)', \tag{3.35}$$

$$\delta u \to \delta\tilde{u} = \delta u + a\xi^0, \tag{3.36}$$

where we express the components of the infinitesimal function as $\xi^\mu = (\xi^0, \delta^{ij}\chi_{,j})$. Taking appropriate ξ and χ, we can kill two degrees of freedom in the scalar perturbations. For example, the gauge satisfying $B = E = 0$ is called the conformal Newtonian gauge or longitudinal gauge, and that satisfying $\Phi = B = 0$ is called the synchronous gauge. In particular, Φ in the conformal Newtonian gauge is often called the gravitational potential.[2]

Combining the perturbations, we can make gauge-invariant quantity. For example, we can define the curvature perturbation in the conformal Newtonian gauge as

$$\zeta \equiv -\Psi + \frac{\delta\rho}{3(\bar{\rho} + \bar{P})}, \tag{3.38}$$

and this quantity is gauge invariant. This is often used to characterize the primordial perturbation because it is constant on superhorizon scales for the adiabatic perturbation. The gauge-invariant curvature perturbation can also be defined with δu as

$$\mathcal{R} \equiv -\Psi + H\delta u. \tag{3.39}$$

This becomes the same as ζ on superhorizon scales as we will see in the next section.

3.3 Evolution of perturbations in one fluid

In this section, we discuss the evolution of the perturbations in one fluid.

From the Einstein equation, the perturbations of the Einstein tensor and the energy-momentum tensor satisfy

$$\delta G^\mu{}_\nu = \frac{1}{M_{\rm Pl}^2}\delta T^\mu{}_\nu, \tag{3.40}$$

where we have neglected the cosmological constant because we focus on the early Universe throughout this thesis. Here, we write the concrete expressions of the perturbed Einstein equation. From the $\{00\}$ component, given by Eqs. (3.12) and (3.16), we can derive

$$\frac{1}{a^2}\left[6\left(\frac{a'}{a}\right)^2\Phi + 6\frac{a'}{a}\Psi' + 2\frac{a'}{a}B^{,i}{}_{,i} - 2\Psi^{,i}{}_{,i} - 2\frac{a'}{a}E^{,i}{}_{,i}\right] = -\frac{1}{M_{\rm Pl}^2}\delta\rho. \tag{3.41}$$

From the $\{0i\}$ component, given by Eqs. (3.13) and (3.17), we can derive

$$\frac{1}{a^2}\left(-2\frac{a'}{a}\Phi_{,i} - 2\Psi'_{,i}\right) = \frac{1}{aM_{\rm Pl}^2}(\bar{\rho} + \bar{P})\delta u_{,i}. \tag{3.42}$$

From the $\{i0\}$ component, given by Eqs. (3.14) and (3.18), we can derive

$$\frac{1}{a^2}\left(4\left(\frac{a'}{a}\right)^2 B_{,i} - 2\frac{a''}{a}B_{,i} + 2\frac{a'}{a}\Phi_{,i} + 2\Psi'_{,i}\right) = \frac{1}{aM_{\rm Pl}^2}(\bar{\rho} + \bar{P})\left(aB_{,i} - \delta u_{,i}\right). \tag{3.43}$$

[2]For example, we can write the Schwarzschild metric as

$$\mathrm{d}s^2 = -\left(1 - \frac{2GM}{r}\right)\mathrm{d}t^2 + \frac{\mathrm{d}r^2}{1 - 2GM/r} + r^2(\mathrm{d}\theta^2 + \sin^2\theta\mathrm{d}\varphi^2), \tag{3.37}$$

where G is the gravitational constant and M is the mass of the point mass located at $r = 0$. Comparing this metric with Eq. (3.5), we can see that Φ corresponds to the gravitational potential $-GM/r$.

From the $\{ij\}$ component, given by Eqs. (3.12) and (3.16), we can derive

$$\frac{1}{a^2}\left[\left(2\frac{a'}{a}\Phi' + 4\frac{a''}{a}\Phi - 2\left(\frac{a'}{a}\right)^2\Phi + \Phi^{,i}{}_{,i} + 4\frac{a'}{a}\Psi' + 2\Psi'' \right.\right.$$
$$\left. -\Psi^{,i}{}_{,i} + 2\frac{a'}{a}B^{,i}{}_{,i} + B^{,i}{}_{,i}{}' + 2\frac{a'}{a}E^{,i}{}_{,i}{}' - E^{,i}{}_{,i}{}''\right)\delta_{ij}$$
$$\left. + \left(-\Phi + \Psi - 2\frac{a'}{a}B - B' + 2\frac{a'}{a}E' + E''\right)^{,i}{}_{,j}\right] = -\frac{1}{M_{\rm Pl}^2}\delta P\delta_{ij}. \tag{3.44}$$

In the rest of this section, to understand evolution of the perturbations concretely, we take the conformal Newtonian gauge. In the conformal Newtonian gauge, Eqs. (3.41), (3.42), and (3.44) can be expressed as

$$\Delta\Psi - 3(\Psi' + \mathcal{H}\Phi) = \frac{a^2}{2M_{\rm Pl}^2}\delta\rho, \tag{3.45}$$
$$(\Psi' + \mathcal{H}\Phi)_{,i} = -\frac{a}{2M_{\rm Pl}^2}(\bar{\rho} + \bar{P})\delta u_{,i}, \tag{3.46}$$
$$\left[\Phi'' + (2\Psi + \Phi)' + (2\mathcal{H}' + \mathcal{H}^2)\Phi + \frac{1}{2}\Delta(\Phi - \Psi)\right]\delta_{ij} - \frac{1}{2}(\Phi - \Psi)_{,ij} = \frac{a^2}{2M_{\rm Pl}^2}\delta P, \tag{3.47}$$

where Δ indicates the Laplacian as $\Delta A = A^{,i}{}_{,i}$. From Eq. (3.47), we can derive

$$(\Phi - \Psi)_{,ij} = 0$$
$$\Rightarrow \quad \Phi = \Psi. \tag{3.48}$$

Then, we can rewrite Eqs. (3.41), (3.43), and (3.44) as

$$\Delta\Phi - 3\mathcal{H}(\Phi' + \mathcal{H}\Phi) = \frac{a^2}{2M_{\rm Pl}^2}\delta\rho, \tag{3.49}$$
$$(a\Phi)'_{,i} = -\frac{a^2}{2M_{\rm Pl}^2}(\bar{\rho} + \bar{P})\delta u_{,i}, \tag{3.50}$$
$$\Phi'' + 3\mathcal{H}\Phi' + (2\mathcal{H}' + \mathcal{H}^2)\Phi = \frac{a^2}{2M_{\rm Pl}^2}\delta P. \tag{3.51}$$

Substituting Eq. (3.50) into Eq. (3.49), we can relate $\delta\rho$ to δu as

$$\delta\rho - \frac{2M_{\rm Pl}^2}{a^2}\Delta\Phi = \frac{3}{a}\mathcal{H}(\bar{\rho} + \bar{P})\delta u. \tag{3.52}$$

Using this relation, we can derive the relation between the two curvature perturbations defined in Eqs. (3.38) and (3.39) as

$$\zeta = \mathcal{R} + \frac{2M_{\rm Pl}^2\Delta\Phi}{3a^2(\bar{\rho} + \bar{P})}. \tag{3.53}$$

From this equation, we can see that $\zeta \simeq \mathcal{R}$ is satisfied on superhorizon scales. Since we consider one fluid, the pressure perturbations can be expressed with energy density perturbations as

$$\delta P = c_s^2\delta\rho, \tag{3.54}$$

where c_s is the sound speed. Substituting this equation into Eq. (3.51) and using Eq. (3.49), we can derive

$$\Phi'' + 3(1+c_s^2)\mathcal{H}\Phi' - c_s^2\Delta\Phi + (2\mathcal{H}' + (1+3c_s^2)\mathcal{H}^2)\Phi = 0. \tag{3.55}$$

In the following, we discuss the evolution of the perturbations specifying the era of the Universe.

3.3.1 Matter-dominated era: $c_s^2 = 0$

Here, we consider the perturbations during a MD era, which corresponds to the case of $c_s^2 = 0$. In this case, Eq. (3.55) becomes

$$\Phi'' + \frac{6}{\eta}\Phi' = 0, \tag{3.56}$$

where we have used the relation $\mathcal{H} = 2/\eta$ given in Eq. (2.27). Solving this equation, we obtain

$$\Phi = C_1(\boldsymbol{x}) + \frac{C_2(\boldsymbol{x})}{\eta^5}, \tag{3.57}$$

where C_1 and C_2 only depend on the space coordinates. From this equation, we can see that if the decaying mode ($\propto 1/\eta^5$) is neglected, Φ is always constant during a MD era whether on superhorizon scales or on subhorizon scales. Substituting this solution of Φ into Eq. (3.49), we get the solution for the energy density perturbation as

$$\frac{\delta\rho}{\bar{\rho}} = \frac{1}{6}\left[(\Delta C_1\eta^2 - 12C_1) + (\Delta C_2\eta^2 + 18C_2)\frac{1}{\eta^5}\right]. \tag{3.58}$$

In the Fourier space, this equation becomes

$$\frac{\delta\rho_{\boldsymbol{k}}}{\bar{\rho}} = \frac{1}{6}\left[(-C_{1\boldsymbol{k}}(k\eta)^2 - 12C_{1\boldsymbol{k}}) + (-C_{2\boldsymbol{k}}(k\eta)^2 + 18C_{2\boldsymbol{k}})\frac{1}{\eta^5}\right], \tag{3.59}$$

where the subscript "$\boldsymbol{k}$" indicates the Fourier modes of perturbations.

On superhorizon scales ($k\eta \ll 1$), the perturbation is approximated as

$$\frac{\delta\rho_{\boldsymbol{k}}}{\bar{\rho}} \simeq -2C_{1\boldsymbol{k}} \quad (k\eta \ll 1), \tag{3.60}$$

where we have neglected the decaying mode. From this equation, we can see that the energy density perturbation is constant on superhorizon scales. On the other hand, the perturbation on subhorizon scales ($k\eta \gg 1$) is approximated as

$$\frac{\delta\rho_{\boldsymbol{k}}}{\bar{\rho}} \simeq -\frac{1}{6}C_{1\boldsymbol{k}}(k\eta)^2 \propto a \quad (k\eta \gg 1), \tag{3.61}$$

where we have neglected the decaying mode again. This equation means that the energy density perturbation grows proportionally to the scale factor on subhorizon scales during a MD era.

For later convenience, we mention the velocity potential δu on superhorizon scales. From Eq. (3.50), we can derive the expression of δu which is valid only on superhorizon scales as

$$\frac{\delta u_{\boldsymbol{k}}}{a} \simeq -\frac{\eta}{3}\Phi_{\boldsymbol{k}} \quad (k\eta \ll 1). \tag{3.62}$$

This condition is used as the initial condition when we calculate the perturbations numerically in Sec. 6.1.

3.3.2 Radiation-dominated era: $c_s^2 = 1/3$

Here, we discuss the case of $c_s^2 = 1/3$, which corresponds to a RD era. In this case, we can express Eq. (3.55) in the Fourier space as

$$\Phi_{\boldsymbol{k}}'' + \frac{4}{\eta}\Phi_{\boldsymbol{k}}' + \frac{k^2}{3}\Phi_{\boldsymbol{k}} = 0. \tag{3.63}$$

Note that $\mathcal{H} = 1/\eta$ during a RD era. Solving this equation, we finally obtain

$$\Phi_{\boldsymbol{k}} = \frac{3\sqrt{3}}{x}\left[C_{1\boldsymbol{k}} j_1(x/\sqrt{3}) + C_{2\boldsymbol{k}} y_1(x/\sqrt{3})\right], \tag{3.64}$$

where $x \equiv k\eta$ and j_1 and y_1 are the second spherical Bessel functions, defined as

$$j_1(x) = \frac{\sin x - x\cos x}{x^2}, \tag{3.65}$$

$$y_1(x) = -\frac{\cos x + x \sin x}{x^2}. \tag{3.66}$$

Substituting the expression of Φ into Eq. (3.49), we derive

$$\begin{aligned}\frac{\delta\rho_{\boldsymbol{k}}}{\bar{\rho}} =& \frac{6C_{1\boldsymbol{k}}}{x^3}\left[x(x^2-6)\cos(x/\sqrt{3}) - 2\sqrt{3}(x^2-3)\sin(x/\sqrt{3})\right] \\ &+ \frac{6C_{2\boldsymbol{k}}}{x^3}\left[x(x^2-6)\sin(x/\sqrt{3}) + 2\sqrt{3}(x^2-3)\cos(x/\sqrt{3})\right].\end{aligned} \tag{3.67}$$

Since $j_1(x \to 0) = x/3$ and $y_1(x \to 0) = -\infty$, we discard the C_2 term in Eq. (3.67) in the rest of this section on the basis of the initial conditions. Then, the gravitational potential on superhorizon scales can be expressed as

$$\Phi_{\boldsymbol{k}} \simeq C_{1\boldsymbol{k}} \quad (k\eta \ll 1). \tag{3.68}$$

On subhorizon scales, the gravitational potential is expressed as

$$\Phi_{\boldsymbol{k}} \simeq -\frac{9C_{1\boldsymbol{k}}}{x^2}\cos(x/\sqrt{3}) \quad (k\eta \gg 1). \tag{3.69}$$

From this equation, we can see that the gravitational potential oscillates and decays proportionally to $1/x^2$ on subhorizon scales during a RD era, unlike the gravitational potential during a MD era, discussed in the previous subsection.

From Eq. (3.67), we can express the energy density perturbations on superhorizon scales as

$$\frac{\delta\rho_{\boldsymbol{k}}}{\bar{\rho}} \simeq -2C_{1\boldsymbol{k}} \quad (k\eta \ll 1). \tag{3.70}$$

On subhorizon scales, the energy density is given as

$$\frac{\delta\rho_{\boldsymbol{k}}}{\bar{\rho}} \simeq 6C_{1\boldsymbol{k}}\cos(x/\sqrt{3}) \quad (k\eta \gg 1). \tag{3.71}$$

From this equation, we can see that the energy density perturbation does not grow on subhorizon scales during a RD era, unlike the perturbation during a MD era. This is because of the radiation pressure.

From Eq. (3.50), we can derive the expression for the velocity perturbation on superhorizon scales as

$$\frac{\delta u_{\boldsymbol{k}}}{a} \simeq -\frac{\eta}{2}\Phi_{\boldsymbol{k}} \quad (k\eta \ll 1). \tag{3.72}$$

This relation shows the initial condition of the velocity perturbation during a RD era.

3.3.3 Conservation of curvature perturbations

In this subsection, we show that the curvature perturbations are conserved on superhorizon scales in the case of one fluid. Here, to give a general discussion, we do not assume that the sound speed is constant. When the Universe experiences the transition between the eras, the sound speed depends on the time.

First, we define the quantity v as

$$v \equiv \exp\left(\frac{3}{2}\int(1+c_s^2)\mathcal{H}\mathrm{d}\eta\right)\Phi \tag{3.73}$$

$$= \exp\left(-\frac{1}{2}\int\left(1+\frac{\bar{P}'}{\bar{\rho}'}\right)\frac{\bar{\rho}'}{(\bar{\rho}+\bar{P})}\mathrm{d}\eta\right)\Phi = \frac{\Phi}{(\bar{\rho}+\bar{P})^{1/2}}, \tag{3.74}$$

where we have used the relation $c_s^2(=\delta P/\delta\rho) = \bar{P}'/\bar{\rho}'$, valid only on superhorizon scales, and $\mathcal{H} = -\rho'/(3(\bar{\rho}+\bar{P}))$ (see Eq. (2.21)). Substituting $\Phi = (\bar{\rho}+\bar{P})^{1/2}v$ into Eq. (3.55), we obtain

$$\begin{aligned}&(\bar{\rho}+\bar{P})^{1/2}v'' - (\bar{\rho}+\bar{P})^{1/2}c_s^2\Delta v \\ &- (\bar{\rho}+\bar{P})^{1/2}\left[\frac{1}{M_{\rm Pl}^2}a^2(\bar{\rho}+\bar{P}) + \mathcal{H}\frac{(\bar{\rho}+\bar{P})'}{(\bar{\rho}+\bar{P})} + \frac{3}{4}\frac{((\bar{\rho}+\bar{P})')^2}{(\bar{\rho}+\bar{P})^2} - \frac{1}{2}\frac{(\bar{\rho}+\bar{P})''}{(\bar{\rho}+\bar{P})}\right]v = 0.\end{aligned} \tag{3.75}$$

Finally, we can rewrite Eq. (3.55) as

$$v'' - c_s^2\Delta v - \frac{\theta''}{\theta}v = 0, \tag{3.76}$$

where θ is defined as

$$\theta \equiv \frac{1}{a}\left(1+\frac{\bar{P}}{\bar{\rho}}\right)^{-1/2} = \frac{1}{a}\left[\frac{2}{3}\left(1-\frac{\mathcal{H}'}{\mathcal{H}^2}\right)\right]^{-1/2}. \tag{3.77}$$

In the Fourier space, Eq. (3.76) becomes

$$v_{\boldsymbol{k}}'' + c_s^2k^2v_{\boldsymbol{k}} - \frac{\theta''}{\theta}v_{\boldsymbol{k}} = 0. \tag{3.78}$$

Since the goal of this subsection is to show the conservation of the curvature perturbations on superhorizon scales, we focus on the case of $c_sk\eta \ll 1$. Then, Eq. (3.78) can be approximated as

$$v_{\boldsymbol{k}}'' - \frac{\theta''}{\theta}v_{\boldsymbol{k}} \simeq 0 \quad (c_sk\eta \ll 1). \tag{3.79}$$

The curvature perturbation $\mathcal{R}$, defined in Eq. (3.39) can be expressed with v and θ as

$$\mathcal{R}_{\boldsymbol{k}} = -\frac{2\sqrt{3}M_{\rm Pl}}{3}\theta^2\left(\frac{v_{\boldsymbol{k}}}{\theta}\right)', \tag{3.80}$$

where we have used the relation $\Phi = \Psi$. The derivative of $\theta^2(v_{\boldsymbol{k}}/\theta)'$ satisfies

$$\left[\theta^2\left(\frac{v_{\boldsymbol{k}}}{\theta}\right)'\right]' = \theta\left(v_{\boldsymbol{k}}'' - \frac{\theta''}{\theta}v_{\boldsymbol{k}}\right) \simeq 0. \tag{3.81}$$

Then, we can see that the curvature perturbations become constant on superhorizon scales ($\mathcal{R}'_{\boldsymbol{k}} = 0$ ($k\eta \ll 1$)).

Finally, we mention the relation between the curvature perturbations and Φ. Using Eq. (3.50), we can also express the curvature perturbation without δu as

$$\mathcal{R}_{\boldsymbol{k}} = -\frac{2}{3}\frac{\mathcal{H}^{-1}\Phi'_{\boldsymbol{k}} + \Phi_{\boldsymbol{k}}}{1+w} - \Phi_{\boldsymbol{k}}. \tag{3.82}$$

Since $\Phi'_{\boldsymbol{k}} = 0$ on superhorizon scales, we can express the following relation

$$\mathcal{R}_{\boldsymbol{k}} \simeq \zeta_{\boldsymbol{k}} \simeq -\frac{5+3w}{3(1+w)}\Phi_{\boldsymbol{k}} = \begin{cases} -\frac{5}{3}\Phi_{\boldsymbol{k}} & \text{(MD era)} \\ -\frac{3}{2}\Phi_{\boldsymbol{k}} & \text{(RD era)} \end{cases}, \tag{3.83}$$

where this relation is valid only on superhorizon scales. From this relation, we can see that Φ is suppressed by the factor 9/10 during the transition from the RD era to the MD era.

3.4 Equations for perturbations experiencing the transition from a MD era to a RD era

In this section, we derive the equations for the perturbations that experiences the transition from a MD era to a RD era, which will be used in Chap. 6. Here, we consider the case where non-relativistic matter decays to radiation, as we mentioned in Sec. 2.3.2. In this case, as we have seen in Sec. 2.3.2, the energy-momentum conservation can be expressed as [116, 117][3][4]

$$T^{\mu}_{\mathrm{m}\,\nu;\mu} = \Gamma\, T^{\mu}_{\mathrm{m}\,\nu} u_{\mathrm{m}\,\mu}, \tag{2.44}$$

$$T^{\mu}_{\mathrm{r}\,\nu;\mu} = -\Gamma\, T^{\mu}_{\mathrm{m}\,\nu} u_{\mathrm{m}\,\mu}. \tag{2.45}$$

[3] Since there is only the (non-relativistic) matter fluid well before the decay of the non-relativistic matter, the perturbation can be regarded as an adiabatic perturbation on superhorizon scales. Therefore, the curvature perturbations on superhorizon scales are conserved even during the transition. However, on subhorizon scales, the perturbations of matter and radiation behave differently (or the entropy perturbation appears) and therefore the evolution cannot be described with the one-fluid formulation, given in the previous section.

[4] One might wonder if collision terms between the massive particle and radiation could appear in the right-hand side of Eqs. (2.44) and (2.45). Here, assuming that the massive particle decays through the Yukawa interaction, we naively discuss the condition that we can neglect the collision terms. In this case, the order of the decay rate is given as $\Gamma \sim y^2 m$ (y: Yukawa coupling constant, m: mass of the massive particle decaying to radiation). Then, the number density of the massive particle can be approximated around the transition as $n_{\mathrm{m}} \sim 3M_{\mathrm{Pl}}^2\Gamma^2/m \sim y^4 M_{\mathrm{Pl}}^2 m$, where note that the transition occurs around $\Gamma \sim H$. Since the order of the cross section between the massive particle and radiation is given as $\sigma \sim y^4/m^2$ (or could be smaller for high-momentum radiation ($p \gg m$)) [126], the mean scattering time between the massive particle and radiation can be estimated as $t_{\mathrm{sc}} = (n_{\mathrm{m}}\sigma)^{-1} \sim (y^8 M_{\mathrm{Pl}}^2/m)^{-1}$. Comparing the mean scattering time with the Hubble timescale at that time ($H^{-1} \sim \Gamma^{-1}$), we can find that if $y^6 M_{\mathrm{Pl}}^2/m^2 \ll 1$ holds, the mean scattering time becomes larger than the Hubble timescale and the collision terms can be negligible. Note that the long-lasting eMD era, which we focus on in Chap. 6, leads to a small coupling constant. From this result, we can naively expect that if the massive particle decays through the Planck-suppressed operator, the collision terms can be neglected. Hereafter, we assume that the interaction between the massive particle and radiation is weak enough that we can neglect the collision terms.

The goal of this section is to derive the formulas for the perturbations from these equations. The perturbations of the covariant derivative of the energy-momentum tensor can be written as

$$\delta(T^{\mu}_{\ \nu;\mu}) = \delta T^{\mu}_{\ \nu,\mu} + \bar{\Gamma}^{\mu}_{\ \mu\lambda}\delta T^{\lambda}_{\ \nu} - \bar{\Gamma}^{\lambda}_{\ \mu\nu}\delta T^{\mu}_{\ \lambda} + \delta\Gamma^{\mu}_{\ \mu\lambda}\bar{T}^{\lambda}_{\ \nu} - \delta\Gamma^{\lambda}_{\ \mu\nu}\bar{T}^{\mu}_{\ \lambda}. \tag{3.84}$$

Substituting Eqs. (3.6)-(3.11) and (3.16)-(3.19) into this expression, we get

$$\begin{aligned}\delta(T^{\mu}_{\ 0;\mu}) =&\delta T^{0}_{\ i,0} + \delta T^{i}_{\ 0,i} + 3\frac{a'}{a}\delta T^{0}_{\ 0} - \frac{a'}{a}\delta T^{i}_{\ i} - \delta\Gamma^{i}_{\ i0}\bar{P} - \delta\Gamma^{i}_{\ i0}\bar{\rho}\\ =&-\delta\rho' + \frac{1}{a}(\bar{\rho}+\bar{P})(a\Delta B - \Delta\delta u) - 3\frac{a'}{a}\delta\rho - 3\frac{a'}{a}\delta P - (-3\Psi' + \Delta E')(\bar{\rho}+\bar{P}),\end{aligned} \tag{3.85}$$

$$\begin{aligned}\delta(T^{\mu}_{\ i;\mu}) =&\delta T^{0}_{\ i,0} + \delta T^{j}_{\ i,j} + 3\frac{a'}{a}\delta T^{0}_{\ i} - \frac{a'}{a}\delta T^{i}_{\ 0} + \delta\Gamma^{0}_{\ 0i}\bar{P} + \delta\Gamma^{0}_{\ 0i}\bar{\rho}\\ =&\frac{1}{a}((\bar{\rho}+\bar{P})\delta u_{,i})' + \delta P_{,i} + \frac{4a'}{a^2}(\bar{\rho}+\bar{P})\delta u_{,i} + (\bar{\rho}+\bar{P})\Phi_{,i}.\end{aligned} \tag{3.86}$$

For later convenience, we write down the expressions for $(\delta(T^{\mu}_{i;\mu}))^{,i}$ as

$$(\delta(T^{\mu}_{\ i;\mu}))^{,i} = \frac{1}{a}((\bar{\rho}+\bar{P})\Delta\delta u)' + \Delta\delta P + \frac{4a'}{a^2}(\bar{\rho}+\bar{P})\Delta\delta u + (\bar{\rho}+\bar{P})\Delta\Phi. \tag{3.87}$$

The perturbation of the right-hand side in Eqs. (2.44) and (2.45) can be written as

$$\delta(\Gamma\, T^{\mu}_{\mathrm{m}\,0}u_{\mathrm{m}\,\mu}) = a\delta\Gamma\rho_{\mathrm{m}} + a\Gamma\delta\rho_{\mathrm{m}} + a\Gamma\rho_{\mathrm{m}}\Phi, \tag{3.88}$$

$$\delta(\Gamma\, T^{\mu}_{\mathrm{m}\,i}u_{\mathrm{m}\,\mu}) = -\Gamma\bar{\rho}_{\mathrm{m}}\delta u_{\mathrm{m},i}, \tag{3.89}$$

$$(\delta(\Gamma\, T^{\mu}_{\mathrm{m}\,i}u_{\mathrm{m}\,\mu}))^{,i} = -\Gamma\bar{\rho}_{\mathrm{m}}\Delta\delta u_{\mathrm{m}}, \tag{3.90}$$

where we have used the relation $\delta u_0 = -a\Phi$, given in Eq. (3.20). Note that we take into account the perturbation of the decay rate because the decay rate can depend on a scalar field and be perturbed by the perturbations of the scalar field in some models, such as the models given in Appendix A.

3.4.1 Equations for matter perturbations

In this subsection, we focus on the equations for matter perturbations ($\bar{P}_{\mathrm{m}} = \delta P_{\mathrm{m}} = 0$).

From Eqs. (3.85) and (3.88), we can derive the equations for the energy density perturbation as

$$-\delta\rho'_{\mathrm{m}} + \frac{1}{a}\bar{\rho}_{\mathrm{m}}(a\Delta B - \Delta\delta u_{\mathrm{m}}) - 3\frac{a'}{a}\delta\rho_{\mathrm{m}} - (-3\Psi' + \Delta E')\bar{\rho}_{\mathrm{m}} = a\delta\Gamma\rho_{\mathrm{m}} + a\Gamma\delta\rho_{\mathrm{m}} + a\Gamma\rho_{\mathrm{m}}\Phi. \tag{3.91}$$

Dividing both sides by ρ_{m}, we obtain

$$\delta'_{\mathrm{m}} - (\Delta B - \theta_{\mathrm{m}}) + (-3\Psi' + \Delta E') = -a\delta\Gamma - a\Gamma\Phi, \tag{3.92}$$

where we have defined $\delta \equiv \delta\rho/\rho$ and $\theta \equiv T^{0}_{\ i}{}^{,i}/(\rho + P) = \frac{1}{a}\Delta u$ for later convenience. From Eqs. (3.87) and (3.90), we can derive the equations for the velocity divergence as

$$(\bar{\rho}_{\mathrm{m}}\theta_{\mathrm{m}})' + \frac{4a'}{a}\bar{\rho}_{\mathrm{m}}\theta_{\mathrm{m}} + \bar{\rho}_{\mathrm{m}}\Delta\Phi = -a\Gamma\bar{\rho}_{\mathrm{m}}\theta_{\mathrm{m}}. \tag{3.93}$$

Dividing both sides by $\bar{\rho}_{\rm m}$, we obtain

$$\theta'_{\rm m} + \frac{a'}{a}\theta_{\rm m} + \Delta\Phi = 0. \tag{3.94}$$

Eqs. (3.92) and (3.94) are consistent with the equations given in Ref. [127].

3.4.2 Equations for radiation perturbations

Here, we derive the equations for the radiation perturbations ($\bar{P}_{\rm r} = \bar{\rho}_{\rm r}/3$, $\delta P_{\rm r} = \delta\rho_{\rm r}/3$).

From Eqs. (3.85) and (3.88), we obtain

$$-\delta\rho'_{\rm r} + \frac{4}{3a}\bar{\rho}_{\rm r}(a\Delta B - \Delta\delta u_{\rm r}) - 4\frac{a'}{a}\delta\rho_{\rm r} - \frac{4}{3}(-3\Psi' + \Delta E')\bar{\rho}_{\rm r} = -(a\delta\Gamma\rho_{\rm m} + a\Gamma\delta\rho_{\rm m} + a\Gamma\rho_{\rm m}\Phi). \tag{3.95}$$

Dividing both sides by $\bar{\rho}_{\rm r}$, we obtain

$$\delta'_{\rm r} + \frac{4}{3}(\Delta B - \theta_{\rm r}) - \frac{4}{3}(-3\Psi' + \Delta E') = a\frac{\rho_{\rm m}}{\rho_{\rm r}}\Gamma\left(\frac{\delta\Gamma}{\Gamma} + \delta_{\rm m} - \delta_{\rm r} + \Phi\right). \tag{3.96}$$

From Eqs. (3.87) and (3.90), we can derive the equations for the velocity divergence as

$$\left(\frac{4}{3}\rho_{\rm r}\theta_{\rm r}\right)' + \frac{1}{3}\Delta\delta\rho_{\rm r} + \frac{4}{3}\frac{4a'}{a}\bar{\rho}_{\rm r}\theta_{\rm r} + \frac{4}{3}\rho_{\rm r}\Delta\Phi = a\Gamma\bar{\rho}_{\rm m}\theta_{\rm m}. \tag{3.97}$$

Dividing both sides by $\frac{4}{3}\bar{\rho}_{\rm r}$, we obtain

$$\theta'_{\rm r} + \frac{1}{4}\Delta\delta_{\rm r} + \Delta\Phi = a\Gamma\frac{3\bar{\rho}_{\rm m}}{4\bar{\rho}_{\rm r}}\left(\theta_{\rm m} - \frac{4}{3}\theta_{\rm r}\right). \tag{3.98}$$

Eqs. (3.96) and (3.98) are consistent with the equations given in Ref. [127].

We will show the numerical solutions of Eqs. (3.92), (3.94), (3.96), and (3.98) in Fig. 6.2.

Chapter 4

Induced Gravitational Waves: second order in perturbations

In this chapter, we review the formulas for the GWs induced by scalar perturbations. Although scalar perturbations are independent of tensor perturbations at the linear order, scalar perturbations can be sources of tensor perturbations at the second order. Therefore, we focus on the second-order interaction between scalar and tensor perturbations in this chapter. Note that some parts of this chapter are based on the discussion in Ref. [81].

4.1 Equation of motion for the induced GWs

Similarly to Chaps. 2 and 3, we start from the Einstein equation and derive the equations describing the induced GWs.

Up to second order, metric perturbations in the conformal Newtonian gauge can be expressed as

$$\begin{aligned} \mathrm{d}s^2 = a^2(\eta) \Big[&-(1+2\Phi^{(1)}+2\Phi^{(2)})\mathrm{d}\eta^2 + 2V_i^{(2)}\mathrm{d}\eta\mathrm{d}x^i \\ &+ \left\{ (1-2\Psi^{(1)}-2\Psi^{(2)})\delta_{ij} + \frac{1}{2}h_{ij}^{(2)} \right\} \mathrm{d}x^i\mathrm{d}x^j \Big], \end{aligned} \tag{4.1}$$

where the superscript "(1)" and "(2)" represent the 1st-order and 2nd-order perturbations and we neglect $h_{ij}^{(1)}$ and $V_i^{(1)}$ to spotlight the GWs induced by scalar perturbations.

For later convenience, we mention the Fourier transformation of the tensor perturbations here. The tensor perturbations can be expressed with the polarization tensors and the Fourier modes as

$$h_{ij}(\boldsymbol{x}) = \sum_{\lambda=+,\times} \int \frac{\mathrm{d}^3k}{(2\pi)^3} \mathrm{e}_{ij}^{\lambda}(\hat{k}) h_{\boldsymbol{k}}^{\lambda} e^{i\boldsymbol{k}\boldsymbol{x}}, \tag{4.2}$$

where $\hat{k} \equiv \boldsymbol{k}/|\boldsymbol{k}|$. The polarization tensors are defined as

$$\mathrm{e}_{ij}^{+}(\hat{k}) \equiv \frac{1}{\sqrt{2}} \left[\mathrm{e}_i(\hat{k})\mathrm{e}_j(\hat{k}) - \bar{\mathrm{e}}_i(\hat{k})\bar{\mathrm{e}}_j(\hat{k}) \right], \tag{4.3}$$

$$\mathrm{e}_{ij}^{\times}(\hat{k}) \equiv \frac{1}{\sqrt{2}} \left[\mathrm{e}_i(\hat{k})\bar{\mathrm{e}}_j(\hat{k}) + \bar{\mathrm{e}}_i(\hat{k})\mathrm{e}_j(\hat{k}) \right], \tag{4.4}$$

where e_i and $\bar{\mathrm{e}}_i$ are the unit vectors perpendicular to $\hat{k}$. By definition, the polarization tensors satisfy the following equations:

$$k^i \mathrm{e}^{\lambda}_{ij} = 0,\ \mathrm{e}^{\lambda\, i}_{\ \ i} = 0,\ \mathrm{e}^{\lambda\, ij}\mathrm{e}^{\lambda'}_{ij} = \delta^{\lambda\lambda'}. \tag{4.5}$$

Note again the transformation between the superscript and the subscript is done by δ_{ij}. When we take $\hat{k}$ as z-axis and e_i and $\bar{\mathrm{e}}_i$ as the unit vectors along x-axis and y-axis respectively, the polarization tensors are explicitly given as

$$\mathrm{e}^{+}_{ij} = \frac{1}{\sqrt{2}}\begin{pmatrix} 1 & 0 & 0 \\ 0 & -1 & 0 \\ 0 & 0 & 0 \end{pmatrix}, \quad \mathrm{e}^{\times}_{ij} = \frac{1}{\sqrt{2}}\begin{pmatrix} 0 & 1 & 0 \\ 1 & 0 & 0 \\ 0 & 0 & 0 \end{pmatrix}. \tag{4.6}$$

In the second-order level, the Einstein tensor can be written as

$$\begin{aligned}\delta G^{(2)}_{ij} =& \frac{1}{4}\left(h^{(2)\prime\prime}_{ij} + 2\mathcal{H}h^{(2)\prime}_{ij} - 2\mathcal{H}^2 h^{(2)}_{ij} - 4\mathcal{H}'h^{(2)}_{ij} - \Delta h^{(2)}_{ij}\right) + 2\Phi^{(1)}_{,i}\Phi^{(1)}_{,j} + 4\Phi^{(1)}\Phi^{(1)}_{,ij} \\ &+ (\Phi^{(2)}, \Psi^{(2)}, V^{(2)}_i \text{ terms}) + (\text{ diagonal part})\,\delta^i_j. \end{aligned} \tag{4.7}$$

The energy-momentum tensor in the second order is given by

$$\delta T^{(2)}{}_{ij} = (\bar{\rho} + \bar{P})\delta u^{(1)}_{,i}\delta u^{(1)}_{,j} + \delta P^{(2)}\bar{g}_{ij} + \delta P^{(1)}\delta g^{(1)}_{ij} + \bar{P}\delta g^{(2)}_{ij}. \tag{4.8}$$

From the background equations given by Eq. (2.15), the background pressure can be written as

$$\bar{P} = -\frac{2M_{\rm Pl}^2}{a^2}\left(\mathcal{H}' + \frac{1}{2}\mathcal{H}^2\right), \tag{4.9}$$

where we have used the relation $\mathcal{H}' = a''/a - \mathcal{H}^2$ and neglected the cosmological constant. From Eq. (3.42), we can express the velocity perturbation as

$$\delta u^{(1)}_{,i} = -\frac{2M_{\rm Pl}^2}{a(\bar{\rho} + \bar{P})}\left(\mathcal{H}\Phi^{(1)} + \Psi^{(1)\prime}\right)_{,i}. \tag{4.10}$$

To focus on the induced GWs, we apply the projection operator to both sides of the Einstein equation as

$$\hat{\mathcal{T}}^{\lambda}{}_{ij}{}^{lm}\delta G^{(2)}_{lm} = \frac{1}{M_{\rm Pl}^2}\hat{\mathcal{T}}^{\lambda}{}_{ij}{}^{lm}\delta T^{(2)}_{lm}, \tag{4.11}$$

where $\hat{\mathcal{T}}^{\lambda}{}_{ij}{}^{lm}$ is the projection operator onto the traceless-transverse space. The projection operator can be expressed explicitly as

$$\hat{\mathcal{T}}^{\lambda}{}_{ij}{}^{lm}A_{lm}(\boldsymbol{x}) = \int \frac{\mathrm{d}^3k}{(2\pi)^3}e^{i\boldsymbol{k}\cdot\boldsymbol{x}}\mathrm{e}^{\lambda}_{ij}(\hat{k})\mathrm{e}^{\lambda\, lm}(\hat{k})A_{lm}(\boldsymbol{k}), \tag{4.12}$$

where $A_{lm}(\boldsymbol{k}) = \int d^3x' A_{lm}(\boldsymbol{x}')e^{-i\boldsymbol{k}\cdot\boldsymbol{x}}$.

From Eqs. (4.7) - (4.11), we obtain the formulas for the tensor perturbations induced by scalar perturbations as

$$h^{\lambda\,(2)\prime\prime}_{ij} + 2\mathcal{H}h^{\lambda\,(2)\prime}_{ij} - \Delta h^{\lambda\,(2)}_{ij} = -4\hat{\mathcal{T}}^{\lambda}{}_{ij}{}^{lm}\mathcal{S}_{lm}. \tag{4.13}$$

The source term $\mathcal{S}_{ij}$ comes from the second-order scalar perturbations and can be expressed as

$$\mathcal{S}_{ij} \equiv 2\Phi^{(1)}_{,i}\Phi^{(1)}_{,j} + 4\Phi^{(1)}\Phi^{(1)}_{,ij} - \frac{4}{3(1+\omega)\mathcal{H}^2}(\mathcal{H}\Phi^{(1)} + \Psi^{(1)\,\prime})_{,i}(\mathcal{H}\Phi^{(1)} + \Psi^{(1)\,\prime})_{,j}. \tag{4.14}$$

In the Fourier space, Eq. (4.13) can be written as

$$h^{\lambda\prime\prime}_{\boldsymbol{k}} + 2\mathcal{H}h^{\lambda\prime}_{\boldsymbol{k}} + k^2 h^{\lambda}_{\boldsymbol{k}} = 4\mathcal{S}^{\lambda}(\boldsymbol{k},\eta). \tag{4.15}$$

The source function $\mathcal{S}^{\lambda}(\boldsymbol{k},\eta)$ is defined as

$$\begin{aligned}\mathcal{S}^{\lambda}(\boldsymbol{k},\eta) &\equiv -\mathrm{e}^{\lambda\, lm}(\hat{k})\mathcal{S}_{lm}(\boldsymbol{k}) \\ &= \int \frac{\mathrm{d}^3k'}{(2\pi)^3}\mathrm{e}^{\lambda\, lm}(\hat{k})k'_l k'_m \Bigg[2\Phi_{\boldsymbol{k}'}(\eta)\Phi_{\boldsymbol{k}-\boldsymbol{k}'}(\eta) \\ &\qquad + \frac{4}{3(1+\omega)}\left(\Phi_{\boldsymbol{k}'}(\eta) + \frac{\Psi'_{\boldsymbol{k}'}(\eta)}{\mathcal{H}}\right)\left(\Phi_{\boldsymbol{k}-\boldsymbol{k}'}(\eta) + \frac{\Psi'_{\boldsymbol{k}-\boldsymbol{k}'}(\eta)}{\mathcal{H}}\right)\Bigg],\end{aligned} \tag{4.16}$$

where we have used the relation $\mathrm{e}^{\lambda\, ij}(\hat{k})k_j = 0$ and omitted the superscripts indicating the order of perturbations for simplicity.

4.2 Solution for tensor perturbations

Here, we solve Eq. (4.15) using the Green functions. We can rewrite Eq. (4.15) as

$$(ah^{\lambda}_{\boldsymbol{k}})'' + \left(k^2 - \frac{a''}{a}\right)(ah^{\lambda}_{\boldsymbol{k}}) = 4a\mathcal{S}^{\lambda}(\boldsymbol{k},\eta). \tag{4.17}$$

Then, we obtain the solution as

$$h^{\lambda}_{\boldsymbol{k}}(\eta) = \frac{4}{a}\int^{\eta} \mathrm{d}\bar{\eta} G_k(\eta;\bar{\eta})a(\bar{\eta})\mathcal{S}^{\lambda}(\boldsymbol{k},\bar{\eta}), \tag{4.18}$$

where G_k is the causal Green function being the solution of following equation:

$$G''_k + \left(k^2 - \frac{a''}{a}\right)G_k = \delta(\eta - \bar{\eta}). \tag{4.19}$$

Note that the prime means the derivative with respect to η, not $\bar{\eta}$. The explicit expression for the Green function depends on the era. During a RD era, the scale factor is written as $a \propto \eta$ and therefore the causal Green function is given as

$$kG^{\mathrm{RD}}_k(\eta;\bar{\eta}) = \Theta(\eta - \bar{\eta})\sin(x - \bar{x}), \tag{4.20}$$

where $x = k\eta$ and $\bar{x} = k\bar{\eta}$ and $\Theta(\eta)$ is the step function defined as

$$\Theta(x) = \begin{cases} 1 & (\eta \geq 0) \\ 0 & (\eta < 0) \end{cases}. \tag{4.21}$$

During a MD era, the Green function is given by

$$kG_k^{\rm MD}(\eta;\bar{\eta}) = -\Theta(\eta-\bar{\eta})x\bar{x}\left(j_1(x)y_1(\bar{x}) - j_1(\bar{x})y_1(x)\right), \tag{4.22}$$

where we have used the relation $a \propto \eta^2$, which is valid during a MD era.

For later convenience, we introduce the Green function for the tensor perturbations that are induced during a MD era and experience the transition to a RD era. Here, we assume that the scale factor changes as

$$\frac{a(\eta)}{a(\eta_{\rm R})} = \begin{cases} \left(\dfrac{\eta}{\eta_{\rm R}}\right)^2 & (\eta < \eta_{\rm R}) \\ 2\dfrac{\eta}{\eta_{\rm R}} - 1 & (\eta \geq \eta_{\rm R}) \end{cases}, \tag{2.48}$$

where we have derived this expression in Chap. 2 and $\eta_{\rm R}$ is the conformal time at the transition. Since the Green function should be expressed with $\sin x$ and $\cos x$ during a RD era, we need two conditions to match the Green function during a MD era, given in Eq. (4.22), to the Green function during the RD era. One condition is the continuity of the Green function at the transition. We need one more condition to determine the coefficients. In the following, we show the derivative of G should also be continuous at the transition. The source-free equation of motion for the Green function can be written as

$$\left(a^2\left(\frac{G_k}{a}\right)'\right)' = -a^2k^2\left(\frac{G_k}{a}\right). \tag{4.23}$$

If we integrate both sides between $\eta_{\rm R}-\epsilon$ and $\eta_{\rm R}+\epsilon$ and take $\epsilon \to 0$, the right-hand side becomes zero because G_k and a are continuous at $\eta_{\rm R}$. Then, we can see that $a^2(G_k/a)' = aG_k' - a'G_k$ should be continuous. Since $\mathcal{H}$ (and therefore a') are continuous, G_k' should also be continuous. Imposing that G_k and G_k' are continuous at $\eta_{\rm R}$, we finally derive the Green function that experiences the transition from a MD era to a RD era as

$$\begin{aligned} kG_k^{\rm MD\to RD}(\eta;\bar{\eta}) &= kG_k^{\rm MD}(\eta_{\rm R};\bar{\eta})\cos(x-x_{\rm R}) + kG_k^{\rm MD\prime}(\eta_{\rm R};\bar{\eta})\sin(x-x_{\rm R}) \\ &= C(x,x_{\rm R})\bar{x}j_1(\bar{x}) + D(x,x_{\rm R})\bar{x}y_1(\bar{x}), \end{aligned} \tag{4.24}$$

where $\bar{\eta} < \eta_{\rm R}$ and $C(x,x_{\rm R})$ and $D(x,x_{\rm R})$ are defined as

$$C(x,x_{\rm R}) = \frac{\sin x - 2x_{\rm R}(\cos x + x_{\rm R}\sin x) + \sin(x-2x_{\rm R})}{2x_{\rm R}^2}, \tag{4.25}$$

$$D(x,x_{\rm R}) = \frac{(2x_{\rm R}^2-1)\cos x - 2x_{\rm R}\sin x + \cos(x-2x_{\rm R})}{2x_{\rm R}^2}. \tag{4.26}$$

Note that the Green function $G_k^{\rm MD\to RD}$ is defined only in $\eta > \eta_{\rm R}$.

4.3 Energy density of induced GWs

In this section, we derive the energy density of the induced GWs because it is often used to parametrize the amplitude of the induced GWs. Here, we assume that the frequencies of the GWs are much larger than the Hubble parameter (and therefore $k \gg \mathcal{H}$). Since

GWs oscillate on subhorizon scales, the leading contribution to the energy density comes from the second-order tensor perturbations (linear × linear). The leading contribution to the Einstein tensor is given as

$$\delta G^0{}_0|_{\text{2nd-order tensor}} = \frac{1}{16a^2}\left(\frac{1}{2}h'_{ij}h^{ij\prime} + 4\mathcal{H}h_{ij}h^{ij\prime} - 2h_{ij}\Delta h^{ij} + h_{ij,k}h^{ik,j} - \frac{3}{2}h_{ij,k}h^{ij,k}\right). \tag{4.27}$$

Then, the energy density of GWs is given as [128]

$$\rho_{\rm GW} = M_{\rm Pl}^2 \left\langle \overline{\delta G^0{}_0}|_{\text{2nd-order tensor}} \right\rangle, \tag{4.28}$$

where the bracket means the expectation value and the overline indicates the time average over the oscillation period ($\simeq 1/k$). The power spectrum of the tensor perturbations are defined as

$$\langle h^\lambda_{\boldsymbol{k}} h^{\lambda'}_{\boldsymbol{k}'} \rangle = (2\pi)^3 \delta(\boldsymbol{k}+\boldsymbol{k}')\delta^{\lambda\lambda'}\frac{2\pi^2}{k^3}\mathcal{P}_h(k,\eta). \tag{4.29}$$

Substituting Eq. (4.2) into Eq. (4.28), we obtain

$$\rho_{\rm GW}(\eta) \simeq \int \frac{{\rm d}k}{k}\left(\frac{M_{\rm Pl}^2}{8}\left(\frac{k}{a}\right)^2 \overline{\mathcal{P}_h(k,\eta)}\right), \tag{4.30}$$

where we have neglected the second term in Eq. (4.27) because we focus on the GWs whose frequencies are much larger than the Hubble parameter. For later convenience, we define the energy density of GWs per logarithmic interval of k as

$$\rho_{\rm GW}(\eta,k) \equiv \frac{M_{\rm Pl}^2}{8}\left(\frac{k}{a}\right)^2 \overline{\mathcal{P}_h(k,\eta)}. \tag{4.31}$$

Using this parameter, we also define the energy density parameter of GWs as

$$\Omega_{\rm GW}(\eta,k) \equiv \frac{\rho_{\rm GW}(\eta,k)}{\rho_{\rm tot}} = \frac{1}{24}\left(\frac{k}{\mathcal{H}}\right)^2 \overline{\mathcal{P}_h(k,\eta)}. \tag{4.32}$$

4.4 Formulas for GW spectrum

In this section, we derive the formulas for $\mathcal{P}_h$ and $\Omega_{\rm GW}$, defined in Eqs. (4.29) and (4.32). In the following, we neglect the anisotropic stress and take $\Psi = \Phi$.

4.4.1 General expression

In this subsection, we derive the general expressions for the induced GWs. Note that we do not assume any specific era in this subsection.

First, we define the transfer function of the gravitational potential as

$$\Phi_{\boldsymbol{k}}(\eta) = \phi_{\boldsymbol{k}}\Phi(k\eta), \tag{4.33}$$

where we normalize the transfer function as $\Phi(x\to 0)\to 1$ and then $\phi_{\boldsymbol{k}}$ corresponds to the amplitude of the gravitational potential on superhorizon scales, e.g. $\phi_{\boldsymbol{k}} \sim \mathcal{O}(10^{-5})$

for $\mathcal{P}_\zeta = 2.1 \times 10^{-9}$. Substituting Eq. (4.15) into the left-hand side of Eq. (4.29), we can rewrite the expectation value of the Fourier modes as

$$\langle h^\lambda_{\boldsymbol{k}} h^{\lambda'}_{\boldsymbol{k}'} \rangle = \frac{16}{a^2} \int^\eta \mathrm{d}\eta_1 \int^\eta \mathrm{d}\eta_2 \, a(\eta_1) a(\eta_2) G_k(\eta;\eta_1) G_k(\eta;\eta_2) \left\langle \mathcal{S}^\lambda(\boldsymbol{k},\eta_1) \mathcal{S}^{\lambda'}(\boldsymbol{k}',\eta_2) \right\rangle . \tag{4.34}$$

The expectation value of the source terms can be written as

$$\begin{aligned} \langle \mathcal{S}^\lambda_{\boldsymbol{k}}(\eta_1) \mathcal{S}^{\lambda'}_{\boldsymbol{k}'}(\eta_2) \rangle = \int \frac{\mathrm{d}^3\tilde{k} \mathrm{d}^3\tilde{k}'}{(2\pi)^6} \mathrm{e}^{\lambda\, ij}(\hat{k}) \tilde{k}_i \tilde{k}_j \mathrm{e}^{\lambda'\, lm}(\hat{k}') \tilde{k}'_l \tilde{k}'_m \\ \times f(\tilde{k}, |\boldsymbol{k} - \tilde{\boldsymbol{k}}|, \eta_1) f(\tilde{k}', |\boldsymbol{k}' - \tilde{\boldsymbol{k}}'|, \eta_2) \left\langle \phi_{\tilde{\boldsymbol{k}}} \phi_{\boldsymbol{k} - \tilde{\boldsymbol{k}}} \phi_{\tilde{\boldsymbol{k}}'} \phi_{\boldsymbol{k}' - \tilde{\boldsymbol{k}}'} \right\rangle , \end{aligned} \tag{4.35}$$

where $f(k_1, k_2, \eta)$ is the source function, including the transfer functions as

$$f(k_1, k_2, \eta) \equiv 2\Phi(k_1\eta)\Phi(k_2\eta) + \frac{4}{3(1+\omega)} \left(\Phi(k_1\eta) + \frac{\Phi'(k_1\eta)}{\mathcal{H}} \right) \left(\Phi(k_2\eta) + \frac{\Phi'(k_2\eta)}{\mathcal{H}} \right) . \tag{4.36}$$

Throughout this thesis, we assume that $\phi_{\boldsymbol{k}}$ follows the Gaussian distribution for simplicity.[1] The power spectrum of the gravitational potential is given as

$$\langle \phi_{\boldsymbol{k}} \phi'_{\boldsymbol{k}} \rangle = (2\pi)^3 \delta(\boldsymbol{k} + \boldsymbol{k}') \frac{2\pi^2}{k^3} \mathcal{P}_\Phi(k). \tag{4.37}$$

Then, we can express the expectation value of the scalar perturbations with their power spectra as

$$\begin{aligned} \left\langle \phi_{\tilde{\boldsymbol{k}}} \phi_{\boldsymbol{k} - \tilde{\boldsymbol{k}}} \phi_{\tilde{\boldsymbol{k}}'} \phi_{\boldsymbol{k}' - \tilde{\boldsymbol{k}}'} \right\rangle &= \left\langle \phi_{\tilde{\boldsymbol{k}}} \phi_{\tilde{\boldsymbol{k}}'} \right\rangle \left\langle \phi_{\boldsymbol{k} - \tilde{\boldsymbol{k}}} \phi_{\boldsymbol{k}' - \tilde{\boldsymbol{k}}'} \right\rangle + \left\langle \phi_{\tilde{\boldsymbol{k}}} \phi_{\boldsymbol{k}' - \tilde{\boldsymbol{k}}'} \right\rangle \left\langle \phi_{\boldsymbol{k} - \tilde{\boldsymbol{k}}} \phi_{\tilde{\boldsymbol{k}}'} \right\rangle \\ &= (2\pi)^3 \delta(\tilde{\boldsymbol{k}} + \tilde{\boldsymbol{k}}') (2\pi)^3 \delta(\boldsymbol{k} - \tilde{\boldsymbol{k}} + \boldsymbol{k}' - \tilde{\boldsymbol{k}}') \frac{2\pi^2}{\tilde{k}^3} \mathcal{P}_\Phi(\tilde{k}) \frac{2\pi^2}{|\boldsymbol{k}' - \tilde{\boldsymbol{k}}'|^3} \mathcal{P}_\Phi(|\boldsymbol{k}' - \tilde{\boldsymbol{k}}'|) \\ &\quad + (2\pi)^3 \delta(\tilde{\boldsymbol{k}} + \boldsymbol{k}' - \tilde{\boldsymbol{k}}') (2\pi)^3 \delta(\boldsymbol{k} - \tilde{\boldsymbol{k}} + \tilde{\boldsymbol{k}}') \frac{2\pi^2}{\tilde{k}^3} \mathcal{P}_\Phi(\tilde{k}) \frac{2\pi^2}{\tilde{k}'^3} \mathcal{P}_\Phi(\tilde{k}'). \end{aligned} \tag{4.38}$$

Here, we express the wave vector with the spherical coordinates as

$$\tilde{\boldsymbol{k}} = (\tilde{k} \sin\theta \cos\varphi, \tilde{k} \sin\theta \sin\varphi, \tilde{k} \cos\theta), \tag{4.39}$$

where $\boldsymbol{k}$ is along z-axis. Then, we get the following expressions:

$$\mathrm{e}^{+\, ij}(\hat{k}) \tilde{k}_i \tilde{k}_j = \frac{\tilde{k}^2}{\sqrt{2}} \sin^2\theta \cos 2\varphi, \quad \mathrm{e}^{\times\, ij}(\hat{k}) \tilde{k}_i \tilde{k}_j = \frac{\tilde{k}^2}{\sqrt{2}} \sin^2\theta \sin 2\varphi. \tag{4.40}$$

Integrating with respect to the azimuthal angle φ, we obtain

$$\begin{aligned} \langle \mathcal{S}^\lambda_{\boldsymbol{k}}(\eta_1) \mathcal{S}^{\lambda'}_{\boldsymbol{k}'}(\eta_2) \rangle &= (2\pi)^3 \delta(\boldsymbol{k} + \boldsymbol{k}') \delta^{\lambda\lambda'} \frac{2\pi^2}{k^3} \frac{1}{4} \int_0^\infty \mathrm{d}\tilde{k} \int_{-1}^1 \mathrm{d}\mu \frac{k^3 \tilde{k}^3}{|\boldsymbol{k} - \tilde{\boldsymbol{k}}|^3} (1-\mu^2)^2 \\ &\quad \times f(|\boldsymbol{k} - \tilde{\boldsymbol{k}}|, \tilde{k}, \eta_1) f(|\boldsymbol{k} - \tilde{\boldsymbol{k}}|, \tilde{k}, \eta_2) \mathcal{P}_\Phi(\tilde{k}) \mathcal{P}_\Phi(|\boldsymbol{k} - \tilde{\boldsymbol{k}}|) \\ &= (2\pi)^3 \delta(\boldsymbol{k} + \boldsymbol{k}') \frac{2\pi^2}{k^3} \left(\frac{3(1+w_\mathrm{h})}{5+3w_\mathrm{h}} \right)^4 \frac{1}{4} \int_0^\infty \mathrm{d}\tilde{k} \int_{-1}^1 \mathrm{d}\mu \frac{k^3 \tilde{k}^3}{|\boldsymbol{k} - \tilde{\boldsymbol{k}}|^3} (1-\mu^2)^2 \\ &\quad \times f(|\boldsymbol{k} - \tilde{\boldsymbol{k}}|, \tilde{k}, \eta_1) f(|\boldsymbol{k} - \tilde{\boldsymbol{k}}|, \tilde{k}, \eta_2) \mathcal{P}_\zeta(\tilde{k}) \mathcal{P}_\zeta(|\boldsymbol{k} - \tilde{\boldsymbol{k}}|), \end{aligned} \tag{4.41}$$

[1] The effects of the non-Gaussianity on the induced GWs are discussed in Refs. [82, 85, 129, 130].

where the relation between ζ and Φ on superhorizon scales, given in Eq. (3.83), has been used and μ is the cosine function with the angle between $\boldsymbol{k}$ and $\tilde{\boldsymbol{k}}$, defined as $\mu \equiv \boldsymbol{k}\cdot\tilde{\boldsymbol{k}}/(k\tilde{k})$. We also used the relation $f(k_1,k_2,\eta) = f(k_2,k_1,\eta)$.[2] Note that $w_{\rm h}$ in Eq. (4.41) represents the equation-of-state parameter when the scalar perturbations enter the horizon. We can rewrite Eq. (4.41) with $u \equiv |\boldsymbol{k}-\tilde{\boldsymbol{k}}|/k$ and $v \equiv \tilde{k}/k$ instead of $\tilde{k}$ and μ as

$$\langle \mathcal{S}^{\lambda}_{\boldsymbol{k}}(\eta_1)\mathcal{S}^{\lambda'}_{\boldsymbol{k}'}(\eta_2)\rangle = (2\pi)^3\delta(\boldsymbol{k}+\boldsymbol{k}')\delta^{\lambda\lambda'}\frac{2\pi^2}{k^3}\left(\frac{3(1+w_{\rm h})}{5+3w_{\rm h}}\right)^4 \times \frac{k^4}{4}\int_0^\infty {\rm d}v\int_{|1-v|}^{|1+v|}{\rm d}u\left[\frac{4v^2-(1+v^2-u^2)^2}{4uv}\right]^2 \times f(uk,vk,\eta_1)f(uk,vk,\eta_2)\mathcal{P}_\zeta(uk)\mathcal{P}_\zeta(vk), \tag{4.42}$$

where we have used the relation $\mu = (1+v^2-u^2)/2v$. Comparing this equation with Eq. (4.34), we obtain the expressions for the power spectrum of the induced GWs as

$$\mathcal{P}_h(\eta,k) = 4\left(\frac{3(1+w_{\rm h})}{5+3w_{\rm h}}\right)^4\int_0^\infty {\rm d}v\int_{|1-v|}^{|1+v|}{\rm d}u\left[\frac{4v^2-(1+v^2-u^2)^2}{4uv}\right]^2 \times I^2(u,v,x)\mathcal{P}_\zeta(uk)\mathcal{P}_\zeta(vk), \tag{4.43}$$

where $I(u,v,x)$ is defined as

$$I(u,v,x) \equiv \int^x {\rm d}\bar{x}\frac{a(\bar{\eta})}{a(\eta)}kG_k(\eta;\bar{\eta})f(u,v,\bar{x}). \tag{4.44}$$

Note that we have rewritten the arguments of f as $f(u,v,\bar{x}) \equiv f(uk,vk,\bar{\eta})$, which can be expressed as

$$f(u,v,\bar{x}) = \frac{1}{3(1+w)}\left(2(5+3w)\Phi(u\bar{x})\Phi(v\bar{x}) + 4\mathcal{H}^{-1}(\Phi'(u\bar{x})\Phi(v\bar{x})+\Phi(u\bar{x})\Phi'(v\bar{x})) + 4\mathcal{H}^{-2}\Phi'(u\bar{x})\Phi'(v\bar{x})\right), \tag{4.45}$$

where $\mathcal{H}$ means $\mathcal{H}(\bar{\eta})$ and the prime means the derivative with respect to $\bar{\eta}$ (not $\bar{x}$).

Here, we mention another choice of the variables. If we use the variables $t \equiv u+v-1$ and $s \equiv u-v$ instead u and v, we can rewrite Eq. (4.43) as

$$\mathcal{P}_h(\eta,k) = 2\left(\frac{3(1+w_{\rm h})}{5+3w_{\rm h}}\right)^4\int_0^\infty {\rm d}t\int_{-1}^1 {\rm d}s\left[\frac{t(2+t)(s^2-1)}{(1-s+t)(1+s+t)}\right]^2 \times I^2(u,v,x)\mathcal{P}_\zeta(uk)\mathcal{P}_\zeta(vk), \tag{4.46}$$

where u and v are given with s and t as $u = (t+s+1)/2$ and $v = (t-s+1)/2$.

[2] Although the function $f(k_1,k_2,\eta)$ defined in Eq. (4.36) is symmetric under the exchange of k_1 and k_2, we can make $f(k_1,k_2,\eta)$ asymmetric under the exchange if we perform the Fourier transform of Eq. (4.14) to make the integrand in Eq. (4.16) asymmetric with respect to $\boldsymbol{k}$ and $\boldsymbol{k}-\boldsymbol{k}'$. However, in that case, the integrand in Eq. (4.41) includes $f(\tilde{k},|\boldsymbol{k}-\tilde{\boldsymbol{k}}|,\eta_1)\frac{1}{2}(f(\tilde{k},|\boldsymbol{k}-\tilde{\boldsymbol{k}}|,\eta_2)+f(|\boldsymbol{k}-\tilde{\boldsymbol{k}}|,\tilde{k},\eta_2))$ instead of $f(\tilde{k},|\boldsymbol{k}-\tilde{\boldsymbol{k}}|,\eta_1)f(\tilde{k},|\boldsymbol{k}-\tilde{\boldsymbol{k}}|,\eta_2)$, which means that the asymmetric part does not contribute to the induced GWs.

Finally, we can rewrite the energy density of the induced GWs (Eq. (4.32)) as

$$\Omega_{\rm GW}(\eta,k) = \frac{1}{6}\left(\frac{3(1+w_{\rm h})}{5+3w_{\rm h}}\right)^4\left(\frac{k}{\mathcal{H}}\right)^2 \times\int_0^\infty {\rm d}v\int_{|1-v|}^{|1+v|}{\rm d}u\left[\frac{4v^2-(1+v^2-u^2)^2}{4uv}\right]^2\overline{I^2(u,v,x)}\mathcal{P}_\zeta(uk)\mathcal{P}_\zeta(vk). \tag{4.47}$$

4.4.2 GWs induced by scalar perturbations entering horizon during RD era

In this subsection, we focus on the GWs induced by the scalar perturbations entering the horizon during a RD era. Note that we do not take into account the effects of the late MD era in this subsection, which will be discussed in Sec. 4.5.

The transfer function of the gravitational potential during a RD era is given by (see Eq. (3.64))

$$\Phi(x) = \frac{9}{x^2}\left(\frac{\sin(x/\sqrt{3})}{x/\sqrt{3}} - \cos(x/\sqrt{3})\right). \tag{4.48}$$

Substituting this equation and $w = 1/3$ into Eq. (4.45), we obtain

$$\begin{aligned} f_{\rm RD}(u,v,x) = \frac{27}{u^3v^3x^6}\Bigg(&18uvx^2\cos\frac{ux}{\sqrt{3}}\cos\frac{vx}{\sqrt{3}} \\ &+(54-6(u^2+v^2)x^2+u^2v^2x^4)\sin\frac{ux}{\sqrt{3}}\sin\frac{vx}{\sqrt{3}} \\ &+2\sqrt{3}ux(v^2x^2-9)\cos\frac{ux}{\sqrt{3}}\sin\frac{vx}{\sqrt{3}} \\ &+2\sqrt{3}vx(u^2x^2-9)\sin\frac{ux}{\sqrt{3}}\cos\frac{vx}{\sqrt{3}}\Bigg), \end{aligned} \tag{4.49}$$

where we have used the relation $\mathcal{H}^{-1} = \eta$, given in Eq. (2.27).

Then, we perform the integral in Eq. (4.44) from 0 to x and finally obtain[3]

$$\begin{aligned} I_{\rm RD}(u,v,x) =& \frac{27}{16u^3v^3x}\Bigg(-\frac{4}{x^3}\Bigg(uv(u^2+v^2-3)x^3\sin x - 6uvx^2\cos\frac{ux}{\sqrt{3}}\cos\frac{vx}{\sqrt{3}} \\ &+6\sqrt{3}ux\cos\frac{ux}{\sqrt{3}}\sin\frac{vx}{\sqrt{3}}+6\sqrt{3}vx\sin\frac{ux}{\sqrt{3}}\cos\frac{vx}{\sqrt{3}} \\ &-3(6+(u^2+v^2-3)x^2)\sin\frac{ux}{\sqrt{3}}\sin\frac{vx}{\sqrt{3}}\Bigg) \\ &+(u^2+v^2-3)^2\Bigg(\sin x\left(\mathrm{Ci}\left[\left(1-\frac{v-u}{\sqrt{3}}\right)x\right]+\mathrm{Ci}\left[\left(1+\frac{v-u}{\sqrt{3}}\right)x\right]\right. \\ &\left.-\mathrm{Ci}\left[\left|1-\frac{v+u}{\sqrt{3}}\right|x\right]-\mathrm{Ci}\left[\left(1+\frac{v+u}{\sqrt{3}}\right)x\right]+\log\left|\frac{3-(u+v)^2}{3-(u-v)^2}\right|\right) \\ &+\cos x\left(-\mathrm{Si}\left[\left(1-\frac{v-u}{\sqrt{3}}\right)x\right]-\mathrm{Si}\left[\left(1+\frac{v-u}{\sqrt{3}}\right)x\right]\right. \end{aligned}$$

[3]To perform the integral, we need to use the trigonometric addition theorem and perform the integration by parts (see Appendix B.1).

$$+\mathrm{Si}\left[\left(1-\frac{v+u}{\sqrt{3}}\right)x\right]+\mathrm{Si}\left[\left(1+\frac{v+u}{\sqrt{3}}\right)x\right]\Bigg)\Bigg), \tag{4.50}$$

where Si and Ci are the sine integral and cosine integral, defined as

$$\mathrm{Si}(x)=\int_0^x\frac{\sin t}{t}\mathrm{d}t,\quad \mathrm{Ci}(x)=-\int_x^\infty\frac{\cos t}{t}\mathrm{d}t. \tag{4.51}$$

In the late-time limit ($x\gg 1$), we get

$$I_{\mathrm{RD}}(u,v,x\to\infty)=\frac{27(u^2+v^2-3)}{16u^3v^3x}\left(\sin x\left(-4uv+(u^2+v^2-3)\log\left|\frac{3-(u+v)^2}{3-(u-v)^2}\right|\right)\right.$$
$$\left.-\pi(u^2+v^2-3)\Theta(v+u-\sqrt{3})\cos x\right). \tag{4.52}$$

The late time behavior of $I(\propto a^{-1})$ represents the redshift of the induced GWs ($h_{ij}\propto a^{-1}$). Using this equation, we can write the oscillation average of I^2 as

$$\overline{I^2_{\mathrm{RD}}(u,v,x\to\infty)}=\frac{1}{2}\left(\frac{27(u^2+v^2-3)}{16u^3v^3x}\right)^2\left(\left(-4uv+(u^2+v^2-3)\log\left|\frac{3-(u+v)^2}{3-(u-v)^2}\right|\right)^2\right.$$
$$\left.+\pi^2(u^2+v^2-3)^2\Theta(v+u-\sqrt{3})\right). \tag{4.53}$$

If we use the variables $t(=u+v-1)$ and $s(=u-v)$ instead of u and v, we get

$$\begin{aligned}\overline{I^2_{\mathrm{RD}}(u,v,x\to\infty)}=&\frac{1458(-5+s^2+t(2+t))^2}{x^2(1-s+t)^6(1+s+t)^6}\\&\times\left(\frac{\pi^2}{4}(-5+s^2+t(2+t))^2\Theta(t-(\sqrt{3}-1))\right.\\&+\left(-(t-s+1)(t+s+1)\right.\\&\left.\left.+\frac{1}{2}(-5+s^2+t(2+t))\log\left|\frac{-2+t(2+t)}{3-s^2}\right|\right)^2\right).\end{aligned} \tag{4.54}$$

The energy density parameter of the GWs induced during a RD era can be expressed as

$$\Omega_{\mathrm{GW}}(\eta,k)=\frac{8}{243}\left(\frac{k}{\mathcal{H}}\right)^2\int_0^\infty\mathrm{d}v\int_{|1-v|}^{|1+v|}\mathrm{d}u\left[\frac{4v^2-(1+v^2-u^2)^2}{4uv}\right]^2$$
$$\times\overline{I^2_{\mathrm{RD}}(u,v,x)}\mathcal{P}_\zeta(uk)\mathcal{P}_\zeta(vk). \tag{4.55}$$

Note that the x dependence of I^2_{RD} at late time ($I^2_{\mathrm{RD}}\propto x^{-2}$) is canceled by the factor $(k/\mathcal{H})^2$ and Ω_{GW} finally becomes constant during a RD era.

Here, to understand the scale dependence of the induced GWs, we assume the delta-function peak of the power spectrum as an example, which is defined as

$$\mathcal{P}_\zeta=A_s\delta(\log k-\log k_*), \tag{4.56}$$

where A_s is the amplitude and the k_* is the peak scale. Substituting this power spectrum into Eq. (4.55), we derive the energy density parameter in the late-time limit ($\eta \gg 1/k$) as

$$\begin{aligned}\Omega_{\rm GW}(\eta,k)|_{\eta\gg 1/k} \simeq & \frac{3A_s^2}{64}\left(\frac{4-\bar{k}^2}{4}\right)^2 \bar{k}^2(3\bar{k}^2-2)^2 \\ & \times\left(\pi - 2(3\bar{k}^2-2)^2\Theta(2-\sqrt{3}\bar{k})\right. \\ & \left.+\left(4+(3\bar{k}^2-2)\log\left|1-\frac{4}{3\bar{k}^2}\right|\right)^2\right)\Theta(2-\bar{k}),\end{aligned} \tag{4.57}$$

where $\bar{k} \equiv k/k_*$. Figure 4.1 shows the wavenumber dependence of the energy density parameter. The peak is located at $k = \frac{2}{\sqrt{3}}k_*$ and the factor $1/\sqrt{3}$ comes from the sound speed of the radiation fluid. The cutoff of $\Omega_{\rm GW}$ is given as $k = 2k_*$, which comes from the wavenumber conservation.

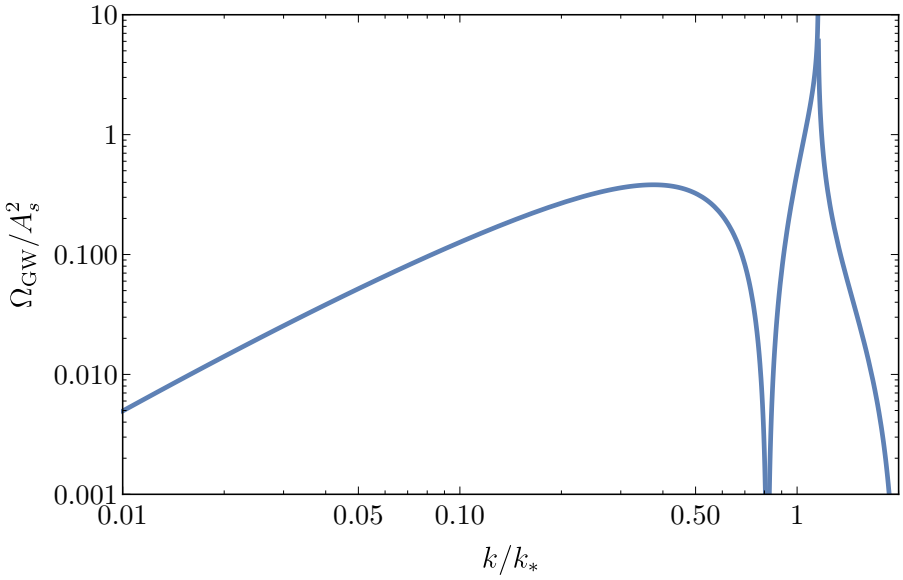

Figure 4.1: The energy density parameter for the GWs induced by the delta-function power spectrum, defined as Eq. (4.56). The parameter is normalized by A_s^2 and the analytical expression is given in Eq. (4.57). Note that this result is first shown in Ref. [43].

If we consider the scale-invariant spectrum as another example, the energy density parameter in the late-time limit is given as

$$\Omega_{\rm GW}(\eta,k)|_{\eta\gg 1/k} \simeq 0.8222 A_s^2, \tag{4.58}$$

where the power spectrum of curvature perturbations is assumed as $\mathcal{P}_\zeta = A_s$.

4.5 Late time evolution

During a RD era, the gravitational potential decays as $\Phi \propto a^{-2}$ on subhorizon scales (see Eq. (3.64)) and the production of GWs stops while after the perturbations enter the

horizon. Once GWs are produced and decouple from the source, the energy density of the induced GWs behave like that of radiation and therefore $\Omega_{\rm GW}$ finally becomes constant during the RD era, as we have seen in Sec. 4.4.2. Here, we define $\eta_{\rm c}$ as the conformal time when the energy density parameter becomes constant, which is the same order of magnitude as the conformal time at the horizon entry of the scalar perturbations.

Since the energy density of the induced GWs is proportional to a^{-4}, we can express the current energy density as

$$\rho_{\rm GW}(\eta_0, k) = \left(\frac{a_{\rm c}}{a_0}\right)^4 \rho(\eta_{\rm c}, k). \tag{4.59}$$

Note that the subscripts "c" and "0" mean the values at η_c and η_0 (the present time), respectively. Then, we can express the current value of the energy density parameter as

$$\Omega_{\rm GW}(\eta_0, k)h^2 = \left(\frac{a_{\rm c}}{a_0}\right)^4 \left(\frac{H_{\rm c}}{H_0}\right)^2 \Omega_{\rm GW}(\eta_{\rm c})h^2. \tag{4.60}$$

Here, let us mention the relation between a, H, and $\Omega_{\rm r,0}$. The ratio between $\rho_{\rm r,0}$ and $\rho_{\rm r,c}$ can be written as

$$\begin{aligned} &\frac{\rho_{\rm r,0}}{\rho_{\rm r,c}} = \frac{g_{*,0}T_0^4}{g_{*,{\rm c}}T_{\rm c}^4} \\ \Rightarrow \quad &\frac{\Omega_{\rm r,0}}{\Omega_{\rm r,c}} = \frac{H_{\rm c}^2 g_{*,0}T_0^4}{H_0^2 g_{*,{\rm c}}T_{\rm c}^4}, \end{aligned} \tag{4.61}$$

where g_* is the effective degrees of freedom for the radiation energy density and T represents the temperature of the photon. From the entropy conservation, we can relate the temperature to the scale factor as

$$g_{s*,0}a_0^3T_0^3 = g_{s*,{\rm c}}a_{\rm c}^3T_{\rm c}^3, \tag{4.62}$$

where g_{s*} is the effective degrees of freedom of the entropy density. From this equation and Eq. (4.61), we derive

$$\begin{aligned} \left(\frac{a_{\rm c}}{a_0}\right)^4 \left(\frac{H_{\rm c}}{H_0}\right)^2 &= \frac{\Omega_{\rm r,0}\, a_{\rm c}^4 T_{\rm c}^4\, g_{*,{\rm c}}}{\Omega_{\rm r,c}\, a_0^4 T_0^4\, g_{*,0}} \\ &= \Omega_{\rm r,0} \left(\frac{g_{s*,0}}{g_{s*,{\rm c}}}\right)^{4/3} \frac{g_{*,{\rm c}}}{g_{*,0}}, \end{aligned} \tag{4.63}$$

where $\Omega_{\rm r,c} = 1$ because we assume that the GW production stops during a RD era here. Since we focus on the GWs induced in the early Universe throughout this thesis, we take $g_{s*,{\rm c}} = g_{*,{\rm c}}$. Finally, we obtain

$$\Omega_{\rm GW}(\eta_0, k)h^2 = 0.39 \left(\frac{g_{*,{\rm c}}}{106.75}\right)^{-1/3} \Omega_{\rm r,0}h^2\Omega_{\rm GW}(\eta_{\rm c}, k), \tag{4.64}$$

where we have substituted $g_{*,0} = 3.36$ and $g_{s*,0} = 3.91$ [131] assuming three massless neutrino species.

Since the degrees of freedom are often given as the function of the photon temperature, it is useful to derive the relation between the conformal time and the temperature. From the Friedman equation, we obtain

$$\frac{aH}{a_{\rm eq}H_{\rm eq}} = \frac{a}{a_{\rm eq}}\sqrt{\frac{\rho}{2\rho_{\rm r,eq}}}. \tag{4.65}$$

Then, we can get the following equation:

$$\frac{1}{k_{\rm eq}\eta} = \frac{1}{\sqrt{2}} \left(\frac{g_{s*,{\rm eq}}}{g_{s*}} \right)^{1/3} \left(\frac{g_*}{g_{\rm eq}} \right)^{1/2} \frac{T}{T_{\rm eq}}, \tag{4.66}$$

where note that the subscript "eq" represents the value at the late-time equality time ($z \sim 3400$) and $k_{\rm eq} \equiv a_{\rm eq} H_{\rm eq}$ [113]. From the Planck result, $k_{\rm eq}$ is given as $k_{\rm eq} = 0.0103\,{\rm Mpc}^{-1}$ [17]. In addition, we take $g_{*,{\rm eq}} = 3.36 (= g_{*,0})$, $g_{s*,{\rm eq}} = 3.91 (= g_{s*,0})$, and $T_{\rm eq} = 8.0 \times 10^{-7}\,{\rm MeV}$ throughout this thesis [17, 131, 132].

Part II

Original Works

Chapter 5

Investigation of the amplitude of small-scale perturbations

Now, we are in a position to discuss the early Universe in terms of the GWs induced by the scalar perturbations. In this chapter, we discuss the possibility that the amplitudes of scalar perturbations on the small scales could be measured or constrained by the observation of the induced GWs.

Although it is difficult to investigate the amplitude of the small-scale perturbations, as we mentioned in Chap. 1, some constraints have been put on the small-scale perturbations so far. For example, the power spectrum of the small-scale perturbations has been constrained from non-detection of the CMB spectral distortion ($\mathcal{P}_\zeta \lesssim 10^{-4}$ on $k \lesssim 10^4 \mathrm{Mpc}^{-1}$ [72, 133, 134]), the consistency between the theoretical prediction of the BBN and the observational results of the light element abundances ($\mathcal{P}_\zeta \lesssim 10^{-2}$ on $10^4 \mathrm{Mpc}^{-1} \lesssim k \lesssim 10^5 \mathrm{Mpc}^{-1}$ [118, 135, 136]), non-detection of the gamma rays emitted from the annihilation of DM particles in the UCMH ($\mathcal{P}_\zeta \lesssim 10^{-6}$ on $k \lesssim 10^7 \mathrm{Mpc}^{-1}$ [137]), and non-detection of PBHs[1] ($\mathcal{P}_\zeta \lesssim 10^{-2}$ over a wide range of scales [139–141]). However, some of them have large uncertainties in their results. For example, the constraints from UCMHs strongly depend on the properties of DM [73, 137] and if the DM is axion, we cannot obtain the constraints from UCMHs. The constraints from PBHs also have uncertainties coming from the ambiguities in the relation between the PBH abundance and the amplitude of the curvature perturbations [142–145]. Therefore, it is meaningful to discuss the small-scale perturbations in terms of the induced GWs.

The study on the amplitude of the small-scale perturbations from the viewpoint of the induced GWs was first done by Assadullahi & Wands in Ref. [146]. However, since then, the formulas for the induced GWs have been corrected. The energy density parameter of the induced GWs calculated with the formulas that the authors used is different from that calculated with the latest formulas by an order of magnitude even if the same power spectrum of the curvature perturbations are assumed, as we will mention in Sec. 5.2. Since many future GW projects are expected to observe GWs in the near future, it is worth revisiting the possibility of the measurement of the induced GWs and deriving the amplitude and scale of the small-scale perturbations which can be accessed by the future GW observations more precisely.

Note that this chapter is mainly based on our previous work [87].

[1] The possibility that the OGLE project might detect PBHs with $M_{\mathrm{PBH}} \sim 10^{-5} M_\odot$ is discussed in Ref. [138].

5.1 Constraints on induced GWs

In this section, we briefly summarize the formulas and the sensitivity curves to discuss the measurement of the induced GWs. Since the induced GWs are stochastic, we follow the analysis in Ref. [147], which discusses the sensitivity curves for the stochastic GW backgrounds. Throughout this section, we use the frequencies of GWs instead of their wavenumbers for convenience, which are related to each other as $f = 1.546 \times 10^{-15} (k/1\mathrm{Mpc}^{-1})\,\mathrm{Hz}$.

If the noises of the multiple detectors or pulsars are uncorrelated, we can take advantage of the cross-correlation technique to look for the induced GWs. In this case, the signal-to-noise ratio of the GW observation with a collection of detectors or pulsars labeled by I and J is given as [148]

$$SNR = \sqrt{2T_{\rm obs}} \left[\int_{f_{\rm min}}^{f_{\rm max}} \mathrm{d}f \sum_{I=1}^{M} \sum_{J>I}^{M} \frac{\Gamma_{IJ}^2(f) S_h^2(f)}{P_{nI}(f) P_{nJ}(f)} \right]^{1/2}, \tag{5.1}$$

where M is the number of detectors or pulsars, $T_{\rm obs}$ is the observation time, P_n is the noise power spectrum, Γ_{IJ} is the overlap reduction function between I-th and J-th detectors or pulsars, $f_{\rm max}$ and $f_{\rm min}$ are the maximum and minimum observation frequencies respectively, and S_h is the power spectral density of the induced GWs, which are related to the energy density parameter as $\Omega_{\rm GW}(\eta_0, f) H_0^2 = 2\pi^2 f^3 S_h(f)/3$. Note that the signal defined in Eq. (5.1) assumes the weak-signal limit [149], which may not be applied to PTA experiments, depending on projects. We will mention the refined signal-to-noise ratio for the PTA experiments later in this section. The effective sensitivity curve for the energy density parameter is defined as

$$\Omega_{\rm GW,eff}(f) H_0^2 = \frac{2\pi^2}{3} f^3 \left[\sum_{I=1}^{M} \sum_{J>I}^{M} \frac{\Gamma_{IJ}^2(f)}{P_{nI}(f) P_{nJ}(f)} \right]^{-1/2}. \tag{5.2}$$

Then, we can rewrite Eq. (5.1) with this effective sensitivity curve as

$$SNR = \sqrt{2T_{\rm obs}} \left[\int_{f_{\rm min}}^{f_{\rm max}} \mathrm{d}f \left(\frac{\Omega_{\rm GW}(f)}{\Omega_{\rm GW,eff}(f)} \right)^2 \right]^{1/2}. \tag{5.3}$$

In Fig. 5.1, we plot $\Omega_{\rm GW,eff} h^2 / \sqrt{T_{\rm obs} f / 10}$ as the benchmark of the effective sensitivity curves for PTA experiments and projects with interferometers. In the figure, we take $T_{\rm obs} = 18$ years for EPTA [45], $T_{\rm obs} = 20$ years for SKA, $T_{\rm obs} = 4$ months for aLIGO(O2) [50], and $T_{\rm obs} = 1$ year for the others as fiducial values. We ignore the notches of the sensitivity curves, which come from the spikes of the overlap function for simplicity. Since we are interested in the signal-to-noise ratio, defined with the integral over $[f_{\rm min}, f_{\rm max}]$, the notches are not expected to affect our results. In addition, we show the constraints on $\Omega_{\rm GW} h^2$ from CMB, LSS, and BBN in Fig. 5.1, which do not use detectors of GWs or pulsars and therefore are different from $\Omega_{\rm GW,eff} h^2$, as we will explain later. We also plot the foreground that comes from extragalactic binary white dwarfs and main sequence stars.

In the following, we explain in detail the sensitivity curve or the constraint for each observation and foreground, plotted in Fig. 5.1.

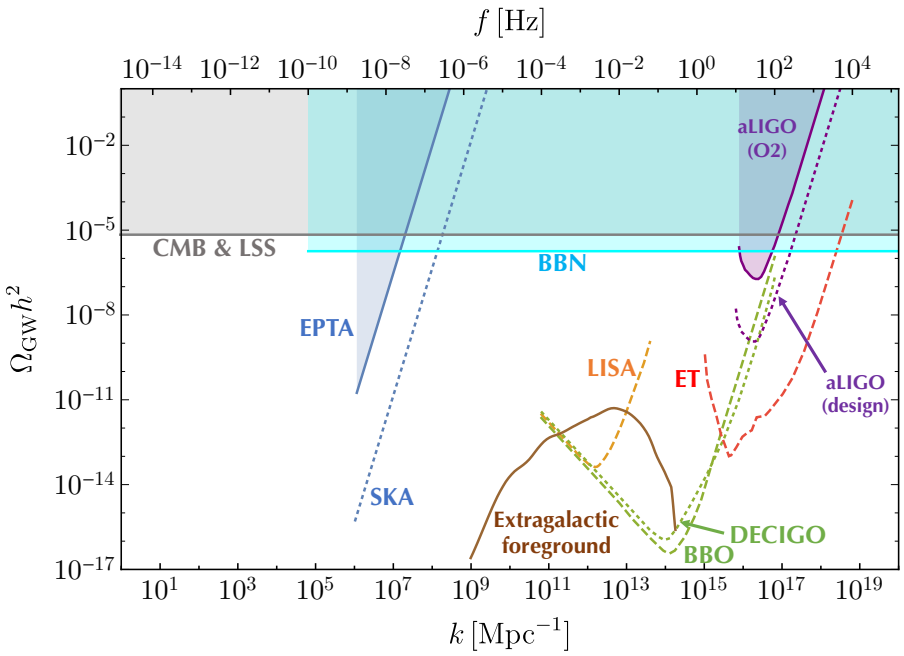

Figure 5.1: The effective sensitivities for the stochastic GWs of the future GW detectors and the current constraints on the GWs. Note that, except for the plots labeled as CMB & LSS and BBN, we plot $\Omega_{\rm GW,eff}h^2/\sqrt{T_{\rm obs}f/10}$ as benchmarks of the effective sensitivities, where $\Omega_{\rm GW,eff}$ is defined as Eq. (5.2) in the weak-signal limit. Hence, these curves should be distinguished from the power-law integrated curves derived in Ref. [147]. We include a current PTA observation by EPTA [45], a future PTA observation by SKA [48, 49], a second-generation ground-based GW interferometer (aLIGO, for which both the limits from the O2 run and design sensitivity are shown [50, 147, 150]), space-based GW interferometers (LISA [48, 56, 147], BBO [58, 59, 147], DECIGO [151]), and finally third-generation ground-based GW interferometers (Einstein Telescope (ET) [48,53,54]). We also plot other constraints coming from the observations of CMB and LSS [152], as well as BBN [81], which should be noted to be current limits on stochastic GWs. We take the observation time $T_{\rm obs}$ as 18 years for EPTA [45], 20 years for SKA, 4 months for aLIGO(O2) [50], and 1 year for the others. The shaded regions are already excluded by the current observational data. We also show the foreground from extragalactic binary white dwarfs and main sequence stars (Extragalactic foreground) [153]. See text for more details about each project and foreground.

Advanced LIGO. The effective sensitivity curve for the design sensitivity of aLIGO is derived in Ref. [147]. They consider the cross-correlation between the detectors in Hanford and Livingston. For the latest results of the O2 run, we obtain an approximation of $\Omega_{\rm GW,eff}$ by renormalizing the amplitude of and rescaling the frequency dependence of $\Omega_{\rm GW,eff}$ for the design sensitivity so that the minimum of the power-law integrated curve [147] calculated from the approximation reproduces the minimum of the power-law integrated curve for the O2 run presented in Ref. [50]. If the sensitivities of Virgo and KAGRA reach the same level as that of aLIGO in the near future, we could add the Virgo and KAGRA detectors to the cross-correlation analysis, which is expected to improve the sensitivity.

Space-based interferometers. The effective sensitivity curve for DECIGO is derived in Refs. [151,154], which is calculated with the cross-correlation between the Michelson interferometers located at opposite positions of the hexagonal form. The sensitivity curve for BBO is also derived in Ref. [147]. Since the sensitivity of BBO is expected to be similar to that of DECIGO [58], we extrapolate the sensitivity curve of BBO given in Ref. [147] to cover the same frequency range as that of DECIGO shown in Ref. [151].

Unlike LIGO, BBO, and DECIGO, we cannot apply the cross-correlation technique to LISA due to its triangle configuration [147,155]. However, some other techniques have been invented to discriminate the stochastic GW signals from the instrumental noise using its configuration [156–159]. To estimate the benchmark of LISA, we assume instrumental noise is removed perfectly, as the authors of Ref. [147] did. Then, we can redefine the effective sensitivity curve for LISA as [147]

$$\Omega_{\rm GW,eff}(f)H_0^2 = \sqrt{2}\,\frac{2\pi^2}{3} f^3 \frac{P_n(f)}{\Gamma(f)}, \tag{5.4}$$

where $\Gamma(f)$ is the transfer function of the detector and $P_n(f)$ is the noise power spectrum. The factor $\sqrt{2}$ in this equation comes from the fact that LISA corresponds to a single GW detector.

Third-generation ground-based interferometers. The configuration of Einstein Telescope (ET) is proposed to be the triangle shape, similar to that of LISA. Therefore, we expect that the technique of the noise subtraction, invented for LISA, can also be applied to ET. Then, we assume the perfect removal of the instrumental noise, as we did for LISA, and use Eq. (5.4) to obtain $\Omega_{\rm GW,eff}$, with the sensitivity curve given in Refs. [48, 53, 54]. On the other hand, the configuration of Cosmic Explorer (CE) is proposed to be the L-shaped geometry and we cannot use the technique for noise removal. For this reason, we do not plot $\Omega_{\rm GW,eff}$ for CE in Fig. 5.1. However, note that we could take advantage of the data of CE for cross-correlation analysis with other detectors, such as aLIGO and ET. In this sense, CE would improve the sensitivity curves on the induced GWs.

PTA. We can investigate the induced GWs by measuring residuals in arrival times of pulsar signals for a long time ($\mathcal{O}(10)$ years). In this case, each pulsar corresponds to each detector for GWs and therefore we can take cross-correlation between the pulsars. Unlike the observations using the interferometers, the inverse of the observation time of the PTA experiments is the same order of magnitude as the target frequencies. This means that the frequency integral in Eq. (5.1) does not increase the signal-to-noise ratio much. Therefore, the weak-signal limit might not be valid in the PTA experiments.[2]

[2]In Fig. 5.1, just for comparison, we plot $\Omega_{\rm eff}h^2$ for EPTA and PTA, defined as Eq. (5.2) in the weak-signal limit.

Here, we assume that all pulsars have the same noise characteristics for simplicity. Then, we redefine the signal-to-noise ratio for the PTA experiments as [149, 160, 161]

$$SNR = \sqrt{2T_{\rm obs}} \left(\sum_{I=1}^{M} \sum_{J>I}^{M} \chi_{IJ}^2 \right)^{1/2} \left[\int_{f_{\rm min}}^{f_{\rm max}} {\rm d}f \left(\frac{\Omega_{\rm GW}(f)}{\Omega_n(f) + \Omega_{\rm GW}(f)} \right)^2 \right]^{1/2}, \tag{5.5}$$

where χ_{IJ} is the Hellings and Downs coefficient for pulsars I and J [162] (see e.g. Eq. (13) in Ref. [161] for the concrete expression). When we discuss the signal-to-noise ratio for the PTA experiments, we assume the homogeneous distribution of pulsars and take the average over the angle between the pulsars.[3] The variable Ω_n is the energy density parameter for noise of each pulsar, given by

$$\Omega_n(f) H_0^2 = \frac{2\pi^2}{3} f^3 S_n(f), \tag{5.6}$$

where $S_n(f)$ is the power spectral density for noise and can be expressed with the noise power spectrum, $P_n(f)$, as $S_n(f) = 12\pi^2 f^2 P_n(f)$. Here, we assume the noise power spectrum is mainly determined by the white timing noise as $P_n(f) \simeq 2\Delta t \sigma^2$ [147], where $1/\Delta t$ is the cadence of the measurements and σ is the timing precision. Recent PTA experiments have been performed by the following projects: EPTA [45], PPTA [46], and NANOGrav [47]. Since their constraints on the GWs are almost the same, we take the EPTA results as a fiducial example for current constraints from PTA. Following the observational result of EPTA in Ref. [45], we take the parameters, $M = 6$, $T_{\rm obs} = 18$ years, $\Delta t = 14$ days, and $\sigma = 1\mu$s for EPTA.[4] For a future PTA project, we consider SKA as a concrete example. We take the parameters, $M = 100$, $T_{\rm obs} = 20$ years, $\Delta t = 14$ days, and $\sigma = 30\,$ns for SKA [48].

CMB, LSS, and BBN. We also mention the other constraints, which are related to CMB, LSS, and BBN. The induced GWs behave as an additional component of the radiation and could change the prediction of CMB, LSS, and BBN. Imposing the consistency between the prediction and the observation, we can put constraints on the GWs. The constraint from CMB and LSS is $\Omega_{\rm GW} h^2 < 6.9 \times 10^{-6}$ [152] and from BBN is $\Omega_{\rm GW} h^2 < 1.8 \times 10^{-6}$ [81]. Since they are constraints on the total GW energy density, not the GW energy density per logarithmic interval $\Omega_{\rm GW}(f)$, we must compare the constraints with the induced GWs integrated over frequency, $\int_{f_{\rm cut}} {\rm d}\ln f\, \Omega_{\rm GW}(f)$. The variable $f_{\rm cut}$ is the lower cutoff of the constraint, which corresponds to 10^{-15} Hz for the constraint from CMB and LSS, and 10^{-10} Hz for that from BBN.

Extragalactic foreground. Finally, we explain foreground coming from extragalactic binary white dwarfs and main sequence stars. Since it is difficult to identify the extragalactic binaries and subtract the extragalactic foreground, the foreground could

[3] After taking the average over the angle, we obtain

$$\frac{1}{4\pi} \int {\rm d}\phi \sin\theta {\rm d}\theta \sum_{I=1}^{M} \sum_{J>I}^{M} \chi_{IJ}^2(\theta) = \frac{1}{48} \frac{M(M-1)}{2}.$$

[4] Strictly speaking, since our analysis is based on the assumption of the homogeneous distribution of pulsars and the same noise characteristics for all pulsars, the current constraints from EPTA in Figs. 5.3 and 5.4 are rough estimates. However, we have checked that the constraints are almost the same as those that we derive imposing that $\Omega_{\rm GW}$ for the induced GWs should not touch the constraint curve given by the black dashed line in Fig.1 in Ref. [45].

affect the sensitivities of LISA, DECIGO, and BBO [153, 163, 164]. The foreground is dominated by stochastic GWs from the binary main sequence stars in $f < 10^{-4}$ Hz and dominated by those from the binary white dwarfs in $10^{-4}\text{Hz} < f < 10^{-1}\text{Hz}$ [153]. Although the foreground might be removed with the use of its spectral shape [159], we plot the extragalactic foreground in Fig. 5.1 for comparison [153]. The region below the brown line in the figure could be contaminated by the extragalactic foreground.

5.2 Constraints on curvature perturbations

In this section, we derive the amplitude of the small-scale perturbations that can be measured by the current and future observations. Throughout this chapter, we assume that GWs are induced by the scalar perturbations entering the horizon during the RD era.[5] We discuss the effects of an eMD era on the induced GWs in the next chapter. Then, we use the following formulas for the energy density parameter of the induced GWs:

$$\Omega_{\rm GW}(\eta,k) = \frac{8}{243}\left(\frac{k}{\mathcal{H}}\right)^2 \int_0^\infty {\rm d}v \int_{|1-v|}^{|1+v|} {\rm d}u \left[\frac{4v^2-(1+v^2-u^2)^2}{4uv}\right]^2 \times \overline{I^2_{\rm RD}(u,v,x)}\mathcal{P}_\zeta(uk)\mathcal{P}_\zeta(vk), \tag{4.55}$$

where $\overline{I^2_{\rm RD}(u,v,x)}$ in the late-time limit can be expressed as Eq. (4.53). Note that we have explained how to obtain this equation in Chap. 4.

The induced GWs depend on the scale-dependence of the power spectrum of the curvature perturbations. Since the induced GWs have attracted a lot of attention in the context of PBHs, which are often related to the peak-like profile of the power spectrum [75, 165, 166], we parametrize the profile of the power spectrum as

$$\mathcal{P}_\zeta(k) = A_s \exp\left(-\frac{(\log k - \log k_{\rm p})^2}{2\sigma^2}\right), \tag{5.7}$$

where A_s represents the amplitude of the curvature perturbations, $k_{\rm p}$ is the peak wavenumber, and σ corresponds to the width of the peak. Using Eq. (4.55), we calculate $\Omega_{\rm GW}(\eta,k)$ with this spectrum. In Fig. 5.2, we plot the squared power spectrum of curvature perturbations, $\mathcal{P}_\zeta^2$, and the quantity $\Omega_{\rm GW}(k,\eta_c)$, both of which are normalized by A_s^2. In the figure, we take $\sigma = 0.5$, $\sigma = 1$, and $\sigma = 2$ as examples. We can see that the peak height of the induced GWs, $\Omega_{\rm GW}(k_{\rm p},\eta_c)$, is the same order of magnitude as A_s^2. This relation ($\Omega_{\rm GW}(k_{\rm p},\eta_c) \sim A_s^2$) is different from the previous relation used in the pioneering work ($\Omega_{\rm GW}(k_{\rm p},\eta_c) \sim 30A_s^2$) [146] by an order of magnitude.[6] We can see that the scale dependence of $\Omega_{\rm GW}(k,\eta_c)$ is very similar to that of $\mathcal{P}_\zeta^2$ on the scales smaller than the peak scale ($k_{\rm p}^{-1}$). Meanwhile, on larger scales, the GWs decay as $\Omega_{\rm GW}h^2 \propto k^3$ even though the power spectrum of curvature perturbations decays more rapidly.[7]

[5] The scales potentially affected by an eMD era, preceding the RD era, could overlap the scales we consider in this chapter ($\mathcal{O}(10)\text{Mpc}^{-1} < k < \mathcal{O}(10^{20})\text{Mpc}^{-1}$), if the reheating temperature is less than roughly 10^{13}GeV.

[6] The work of Ref. [146] is based on the numerical result for a scale-invariant power spectrum ($\mathcal{P}_\zeta(k) = A_s$) in Ref. [41], which indicates $\Omega_{\rm GW}(k,\eta_c) \simeq 33.3A_s^2$. However, the latest result, which our analysis is based on, gives $\Omega_{\rm GW}(k,\eta_c) \simeq 0.8222A_s^2$ for the scale-invariant power spectrum [81].

[7] The wavenumber dependence of $\Omega_{\rm GW}h^2 \propto k^3$ on the large scale can be interpreted as the result

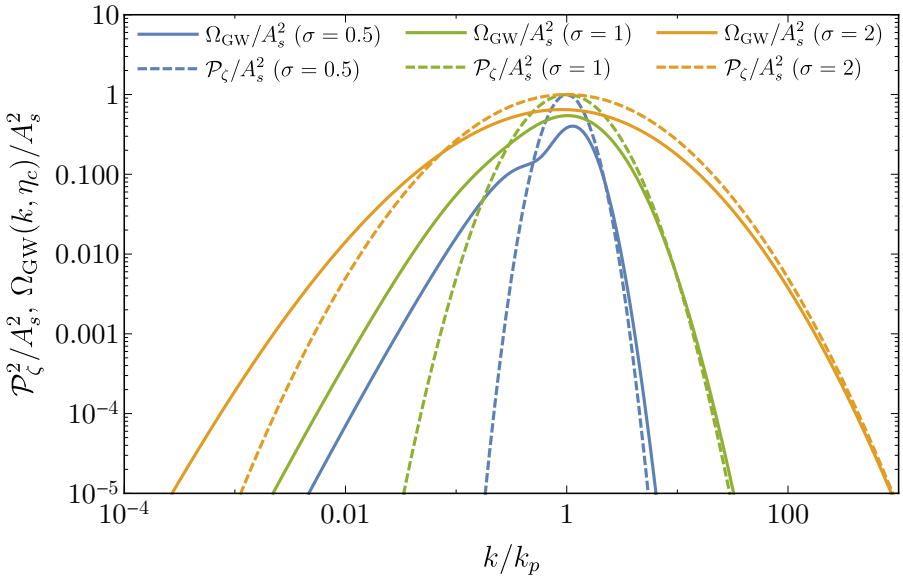

Figure 5.2: Normalized, squared power spectra of curvature perturbations ($\mathcal{P}_\zeta^2(k)/A_s^2$, dashed) and induced GWs ($\Omega_{\rm GW}(k,\eta_c)/A_s^2$, solid). The power spectrum of the curvature perturbation is given by Eq. (5.7) and $\sigma = 0.5$ (blue), $\sigma = 1$ (green), and $\sigma = 2$ (orange) are assumed. Note that the quantity $\Omega_{\rm GW}(k,\eta_c)$ here does not reflect the late-time evolution of induced GWs (see Sec. 4.5).

We derive (expected) limits on A_s for each σ and $k_{\rm p}$ by finding the value of A_s which yields the signal-to-noise ratio, given by Eq. (5.3) for interferometer experiments or Eq. (5.5) for PTA observations, unity, taking into account $\Omega_{\rm GW,eff}$ for each observation discussed above, except for the CMB and BBN constraints. As we do in Fig. 5.1, we take $T_{\rm obs} = 18$ years for EPTA, $T_{\rm obs} = 20$ years for SKA, $T_{\rm obs} = 4$ months for aLIGO (O2) [50], and $T_{\rm obs} = 1$ year for the others as fiducial values. For CMB and BBN constraints, we derive the limits by finding the value of A_s which makes the integral $\int {\rm d}\ln f\, \Omega_{\rm GW}(f)$ equal to the $\Omega_{\rm GW}$ constraints, plotted in Fig. 5.1.

Figure 5.3 shows the limits on A_s for $\sigma = 0.5, 1$ and 2.[8] We also show the parameter region that could be contaminated by the extragalactic foreground, which is derived simply imposing that the foreground at $k_{\rm p}$ should hold

$$\Omega_{\rm GW,\ foreground}h^2 < 0.39(g_{*,c}/106.75)^{-1/3}\Omega_{{\rm r},0}h^2\, 0.8222A_s^2, \tag{5.8}$$

where $\Omega_{\rm GW,\ foreground}h^2$ is plotted with a brown solid line in Fig. 5.1 and the right-hand side comes from Eqs. (4.58) and (4.64)[9]. The parameter space of the primordial spectrum that can be constrained by GW experiments is wider when σ is larger, due to the spread of the GW spectrum as shown in Fig. 5.2. The shaded regions show the constraints from the existing data of current observations. In particular, the current PTA observations

of the Poisson fluctuations of tensor perturbations on superhorizon scale at the GW production [167]. The similar wavenumber dependence is also explained with the correlation function in Ref. [168] (see Eqs. (26) and (27) in the reference).

[8] When we obtain the plots in Fig. 5.3, we find that, for SKA curves, both results based on Eqs. (5.3) and (5.5) are almost the same, which means the weak-signal limit is a good approximation. This is mainly because a large number of pulsars increases the signal-to-noise ratio sufficiently so that $SNR = 1$ is reached in the weak-signal regime.

[9] Note that, since the value of $0.39(g_{*,c}/1056.75)^{-1/3}\Omega_{{\rm r},0}h^2\, 0.8222A_s^2$ is based on the result of the scale invariant spectrum, the foreground in Fig. 5.3 is a rough estimate.

constrain the perturbations as $A_s \lesssim \mathcal{O}(10^{-2})$ on $k \sim \mathcal{O}(10^6)\mathrm{Mpc}^{-1}$. The noticeable scale dependence of constraints from CMB and BBN is due to the change in the relativistic degrees of freedom and the frequency cutoff of the constraints. As to future prospects, the amplitude of the curvature perturbations could be investigated over a wide range of scales. In particular, the curvature perturbations with $\mathcal{P}_\zeta = \mathcal{O}(10^{-4})-\mathcal{O}(10^{-6})$ could be observed or constrained by SKA, LISA, BBO, or ET. Note that, although we assume the concrete values of observation times and signal-to-noise ratio to derive Fig. 5.3, the parameter dependence of the constraints in the weak-signal limit is given by $A_s \propto (SNR)^{1/2} T_{\mathrm{obs}}^{-1/4}$, which we can easily see from Eq. (5.3).

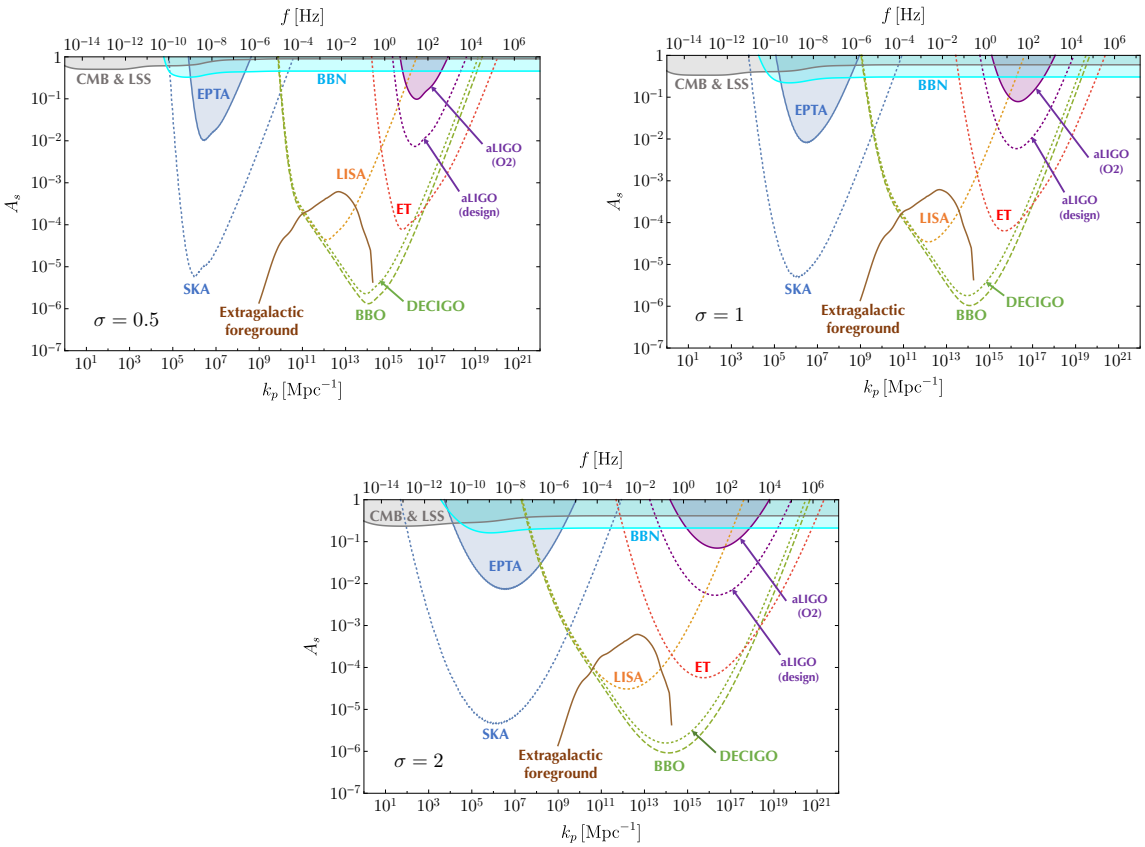

Figure 5.3: Limits on curvature perturbations with $\sigma = 0.5$ (upper left figure), $\sigma = 1$ (upper right figure) and $\sigma = 2$ (lower figure). The vertical axis is A_s and the lower horizontal axis is k_{p}, which are defined in Eq. (5.7). The upper horizontal axis shows the frequency corresponding to k_{p}. The colors and styles of the curves here correspond to those in Fig. 5.1 (e.g. the blue solid lines show the constraints from the current PTA observation, EPTA). The shaded regions are excluded by the current observations, as in Fig. 5.1.

5.3 Discussion

In this section, we discuss our results in this chapter.

As we mention at the beginning of this chapter, the constraints on the curvature perturbations from the induced GWs were also discussed in Ref. [146].[10] Here, let us

[10] A related paper [86] appeared when we were finalizing our paper [87], which this chapter is mainly

stress the updates that we have performed. Our updates are roughly divided into two parts. First, we have used updated equations for the induced GWs. The induced GWs predicted by these updated equations differ from those predicted by the equation used in the previous study by an order of magnitude. Second, we have performed a more precise analysis when we derive the constraints on the power spectrum of curvature perturbations from the sensitivity curves of the GW experiments. To take into account the frequency dependence of the induced GWs and sensitivity curves correctly, we have calculated the signal-to-noise ratio, defined in Eq. (5.3) or Eq. (5.5). We have also discussed the dependence of the limits on the profile of the power spectrum.

Next, let us discuss the foreground. The future observations might detect the stochastic GWs of astrophysical origins, or stochastic GWs of cosmological origins that are different from the induced GWs we have considered, such as those from quantum vacuum fluctuations during inflation, first-order phase transitions, or cosmic strings (see e.g. Ref. [169] for review). In such a case, the limits on the curvature perturbation would be affected, and a discussion about this issue depends on the experiment. For instance, at relatively low frequencies, relevant to SKA, stochastic GWs from mergers of supermassive black holes would be important. Although an estimation of such GWs inevitably involves uncertainties stemming from complex astrophysical processes, the amplitude of $\Omega_{\rm GW}h^2 \sim 10^{-11}(f/10^{-8}{\rm Hz})^{2/3}$ was noted to be a conservative lower limit [169], based on Refs. [170, 171]. If stochastic GWs from supermassive-black-hole mergers are indeed detected, stochastic GWs of cosmological origins, including induced GWs, would be buried, and this implies less information obtained about the early Universe. For instance, the limits on the curvature perturbation based on induced GWs would be weaker than those obtained from the null detection of stochastic GWs. Naively, in this case, one may constrain the curvature perturbation by requiring induced GWs to be less than the detected GW background from supermassive-black-hole-binary mergers. We may do a bit better than that by making use of the anisotropy of stochastic GWs from supermassive black holes, which is at the level of $\sim 20\%$ of the isotropic component [172–175]. In the case of BBO or DECIGO, there are foregrounds coming from binary neutron stars and black holes besides that from extragalactic binary white dwarfs and main sequence stars. Unlike the case of the extragalactic foreground from white dwarfs and main sequence stars, it may be possible to identify and subtract out $\sim 3 \times 10^5$ merging binaries composed of neutron stars and/or black holes, out to $z \sim 5$ [176]. If cosmological and stochastic GWs are indeed detected as a result of the successful subtraction of astrophysical foregrounds, differentiating between different kinds of cosmological GWs with the use of their properties such as the spectrum and chirality [169] would be crucial. In this case, if we fail to identify the source of the detected cosmological GW background, one would obtain the limit on the curvature perturbation by simply requiring induced GWs to be less than the detected GWs. Instead, if we can reliably exclude the possibility that the detected GWs are induced GWs, one may obtain limits tighter than that, possibly making use of the spectrum of the GWs. If we can conclude that the detected GWs are induced GWs, we would be able to determine the power spectrum of curvature perturbation. See also Ref. [177] for the subtraction of astrophysical foregrounds to detect cosmological GWs by ground-based detectors.

In Fig. 5.4, we summarize the current and future expected limits on the small-scale

based on. Although the authors focus on PBHs, the limits on the power spectrum from the induced GWs are also shown. However, they included only current and future PTA and LISA and also did not perform the analysis that we have done with the calculation of the signal-to-noise ratio in this chapter.

curvature perturbations. In this figure, for the constraints from the induced GWs, the vertical and the horizontal axis should be understood as A_s and $k_{\rm p}$, which corresponds to the amplitude and the wavenumber of a peak of the power spectrum we have used in this chapter. This makes a simple comparison of different limits possible, which would be instructive. We take $\sigma = 0.5$ to show conservative constraints. In addition to the constraints from the induced GWs, we also plot the conventional constraints from CMB and LSS observations, CMB distortions, and acoustic reheating. We derive the constraints from CMB distortions performing the integration of Eq. (10) in Ref. [134] with the profile of the power spectrum given in Eq. (5.7) in this chapter, using the limits on the μ and y parameters obtained by COBE/FIRAS, which are $\mu \lesssim 9 \times 10^{-5}$ and $y \lesssim 1.5 \times 10^{-5}$ [178]. We do not show constraints from UCMHs and PBHs because the constraints from such objects have some uncertainties, as we mentioned at the beginning of this chapter. Note again that, throughout this chapter, we assume that the induced GWs are induced by the scalar perturbations entering the horizon during the RD era. If there is an eMD era in the early Universe, the constraints could be changed. In the next chapter, we focus on the effects of an eMD era on the induced GWs, though we leave the analysis for the constraints on the curvature perturbations with an eMD era for future work. Note also that we have implicitly assumed the standard thermal history (no entropy production after reheating) in this chapter. If entropy production occurs after GWs are induced by the scalar perturbations, the constraints would be weaker.

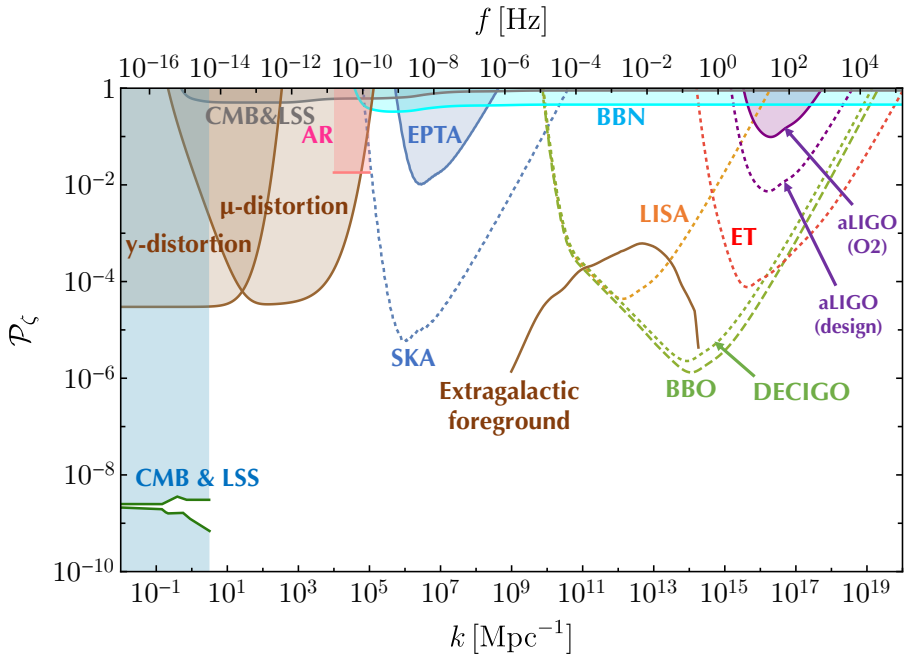

Figure 5.4: Existing and expected limits on the small-scale power spectrum of the curvature perturbation. The constraints from the induced GWs are the same as those shown in Fig. 5.3 ($\sigma = 0.5$). In addition to the constraints derived in this chapter, the constraints from acoustic reheating (AR) [136] (pink, see also [118] and [135]), CMB spectral distortions [72,134] (brown), and CMB/LSS observations on large scales [179] (dark green) are also plotted. The shaded regions are excluded by the current observations, whereas expected limits from future experiments are shown by the dashed and dotted lines.

Before closing this chapter, let us comment on the gauge dependence of the tensor perturbations induced by the scalar perturbations, following the discussion in Ref. [180].

At the second order, tensor perturbations depend on the gauge, though we take the Newtonian gauge throughout this thesis. The gauge dependence of the second-order tensor perturbation has been discussed in Refs. [181–184]. However, if we consider the GW induced by the small-scale perturbations, the gauge dependence is not a problem. In the Newtonian gauge ($B = E = 0$), the synchronous gauge ($\Phi = B = 0$), and the uniform curvature gauge ($E = \Psi = 0$), the tensor perturbation finally becomes the freely-propagating tensor perturbation, whose time dependence is expressed with $\sin(k\eta)/a$ or $\cos(k\eta)/a$, in the subhorizon limit during the RD era. It is already shown that the amount of the induced GWs calculated in the gauges coincides with each other [180, 184–186]. On the other hand, the tensor perturbation calculated in the comoving gauge ($E = \delta u = 0$) is different from those calculated in the other gauges even in the subhorizon limit [184]. However, this does not necessarily mean that the induced GWs are gauge dependent. According to Eq. (65) in Ref. [184], the time dependence of the difference between the comoving gauge and the other gauges is described with $\cos\left((u \pm v)k\eta/\sqrt{3}\right)$ or $\sin\left((u \pm v)k\eta/\sqrt{3}\right)$, not $\sin(k\eta)$ or $\cos(k\eta)$. This means that the difference is in the part of tensor perturbations coupling with the scalar perturbations, not in the freely-propagating tensor perturbations. In addition, the small-scale scalar perturbations finally disappear due to the diffusion damping (see e.g. Ref. [118] for the time dependence of the damping scale). Since the difference between the tensor perturbations in different gauges should be written with the square of scalar perturbations, the gauge dependence should disappear after the diffusion damping of the small-scale perturbations. Therefore, the tensor perturbations should finally become unique (the same as the ones in the Newtonian gauge). On the other hand, the gauge dependence of the tensor perturbations induced by large-scale scalar perturbations does not disappear because the large-scale perturbations remain until now. The observation for this kind of tensor perturbation might require the discussion about which gauge is correct for each observation [180]. Note again that we consider the GWs induced by the small-scale perturbations throughout this thesis and therefore we do not need to worry about the gauge dependence of the induced GWs.

Chapter 6

Effects of an early matter-dominated era on induced gravitational waves

In this chapter, we discuss the effects of an early matter-dominated (eMD) era on the induced GWs.

There could exist an eMD era, preceding the RD era, in the early Universe, as we have mentioned in Chap. 1. An eMD era ends with the decay of the dominant massive particles to radiation, which is called "reheating". Since an eMD era could be related to the coherent oscillation of inflaton, the study of an eMD era is important to understand the early Universe. As we have seen in Chap. 3, unlike during a RD era, the gravitational potential, the source of the induced GWs, does not decay even on subhorizon scales during a MD era. Therefore, we expect that the existence of an eMD era affects the spectrum of the induced GWs, which could shed light on the properties of the eMD era.

The effects of an eMD era on induced GWs were discussed in Refs. [81,107,108]. In the previous works, they assume that the gravitational potential is constant on subhorizon scales during an eMD era up to the moment of reheating. In addition, they implicitly assume that an eMD era ends suddenly and the amplitude of tensor perturbations does not change at the transition from an eMD era to the RD era. However, in realistic situations, the reheating occurs gradually and the tensor perturbations could change during the gradual reheating. Even if the reheating occurs suddenly, we need to care about the GWs induced after the sudden reheating.

In this chapter, we revisit the effects of an eMD era on the induced GWs. Since the effects depend on the detail of the transition, we consider them assuming two scenarios. In Sec. 6.1, we discuss the effects of the eMD era in the case of the gradual transition, whose timescale is comparable to the Hubble timescale at that time. To be concrete, we assume that the reheating is caused by the perturbative decay of the massive particles. This section is mainly based on our previous work [94]. In Sec. 6.2, we discuss the effects in the case of the sudden transition, whose timescale is much shorter than the Hubble timescale at that time. We carefully take into account the GWs induced after the sudden transition. This section is mainly based on our previous work [95]. Note that, throughout this chapter, we basically focus on the GWs induced by the scalar perturbations entering the horizon during an eMD era because the effects of an eMD era on induced GWs are mainly due to the behaviors of the perturbations on subhorizon scales during an eMD era, which are different from those during the RD era.

6.1 Gradual transition

In this section, we consider the gradual transition. Throughout this section, we assume the massive particles, dominant during an eMD era, decay to radiation with a constant decay rate Γ. This situation corresponds to the standard perturbative decay of massive particles. In this case, a large difference from the previous works [81, 107, 108] comes from the evolution of gravitational potential during the gradual transition, which was not taken into account in the previous works.[1]

6.1.1 Evolution of gravitational potential

In this subsection, we discuss the evolution of the gravitational potential around the gradual transition, which has large impacts on the resultant GWs. Since we assume a constant decay rate Γ in this section, we can use the formulas derived in Secs. 2.3.2 and 3.4 with $\delta\Gamma = 0$.[2] Then, the evolution of the energy densities is described by

$$\rho_{\rm m}' = -(3\mathcal{H} + a\Gamma)\rho_{\rm m}, \tag{2.46}$$
$$\rho_{\rm r}' = -4\mathcal{H}\rho_{\rm r} + a\Gamma\rho_{\rm m}, \tag{2.47}$$

where note again the subscripts "m" and "r" represent the matter and radiation, respectively. From Eqs. (3.92), (3.94), (3.96), and (3.98), we can write down the equations for perturbations in the Fourier space as

$$\delta_{\rm m}' = -\theta_{\rm m} + 3\Phi' - a\Gamma\Phi, \tag{6.1}$$
$$\theta_{\rm m}' = -\mathcal{H}\theta_{\rm m} + k^2\Phi, \tag{6.2}$$
$$\delta_{\rm r}' = -\frac{4}{3}(\theta_{\rm r} - 3\Phi') + a\Gamma\frac{\rho_{\rm m}}{\rho_{\rm r}}(\delta_{\rm m} - \delta_{\rm r} + \Phi), \tag{6.3}$$
$$\theta_{\rm r}' = \frac{k^2}{4}\delta_{\rm r} + k^2\Phi - a\Gamma\frac{3\rho_{\rm m}}{4\rho_{\rm r}}\left(\frac{4}{3}\theta_{\rm r} - \theta_{\rm m}\right), \tag{6.4}$$

where we have taken the Newtonian gauge and omitted the bar indicating the background quantity for simplicity. From Eq. (3.49), we can express the derivative of Φ as

$$\Phi' = -\frac{k^2\Phi + 3\mathcal{H}^2\Phi + \frac{3}{2}\mathcal{H}^2\left(\frac{\rho_{\rm m}}{\rho_{\rm tot}}\delta_{\rm m} + \frac{\rho_{\rm r}}{\rho_{\rm tot}}\delta_{\rm r}\right)}{3\mathcal{H}}, \tag{6.5}$$

[1] The effects of the decrease in the gravitational potential during a gradual transition and the resultant incomplete enhancement of induced GWs were also discussed in a talk by S. Kuroyanagi [187], though they neglected the difference between the evolution of the perturbations of matter and radiation. Some qualitative features of our results including the shape of the spectrum $\Omega_{\rm GW}$ are somewhat different from theirs.

[2] Strictly speaking, the perturbations of the coherently oscillating scalar field behave differently from the dust-like fluid for $k \gtrsim \sqrt{am\mathcal{H}}$ (m: mass of the oscillating field) [188,189] (see also Refs. [116,117,190]). However, for the perturbations that enter the horizon during an eMD era, which we focus on in this chapter, we can regard the fluid of the oscillating field as the dust-like fluid (even for the perturbations of the oscillating field). The reason is as follows. The comoving horizon scale at the beginning of the eMD era is given as $\sim (am)^{-1}$ at that time because the inflaton starts to oscillate and the eMD era begins when $\mathcal{H} \sim am$. Then, the wavenumber of the perturbation entering the horizon during the eMD era satisfies $k < ma|_{t=t_{\rm eMD,start}} < \sqrt{am\mathcal{H}}$ ($t_{\rm eMD,start}$: the start time of the eMD era), considering the fact that $\sqrt{am\mathcal{H}}$ is proportional to $a^{1/4}$ during the eMD era. Therefore, we can regard the fluid dominant during an eMD era as the dust-like fluid, whether or not the fluid is realized by the coherently-oscillating field.

where $\rho_{\rm tot} = \rho_{\rm m} + \rho_{\rm r}$.

Figure 6.1 shows the numerical results for the evolution of the background quantities, such as a, $\rho_{\rm m}$, $\rho_{\rm r}$, and $w(\equiv P/\rho)$. We define $\eta_{\rm eq}$ as the conformal time when $\rho_{\rm m} = \rho_{\rm r}$ in this section. Note that there is one-to-one correspondence between Γ and $\eta_{\rm eq}$ and hence this and the subsequent figures do not depend on the specific choice of Γ. As an approximation formula for the scale factor, we also plot

$$\frac{a_{\rm app}(\eta)}{a(\eta_{\rm R})} = \begin{cases} \left(\frac{\eta}{\eta_{\rm R}}\right)^2 & (\eta < \eta_{\rm R}), \\ 2\frac{\eta}{\eta_{\rm R}} - 1 & (\eta \geq \eta_{\rm R}), \end{cases} \tag{6.6}$$

where we take $\eta_{\rm R} = 0.83\eta_{\rm eq}$ in Fig. 6.1. This formula is derived in Eq. (2.48) with the assumption of the sudden transition from a MD era to a RD era. For a fitting formula for the equation-of-state parameter, we also plot

$$w_{\rm fit} = \frac{1}{3}\left(1 - \exp\left(-0.7\left(\frac{\eta}{\eta_{\rm eq}}\right)^3\right)\right). \tag{6.7}$$

We can see that both the formulas (Eqs. (6.6) and (6.7)) fit the numerical results very well. We have checked the errors are less than 10%. The fact that the approximation formula for the scale factor fits the numerical result well may indicate that using the exact solutions for the Green functions experiencing the sudden transition from a MD era to a RD era, given in Eq. (4.24), is a good approximation. This is because the Green functions are determined by the time dependence of the scale factor (see Eq. (4.19)).

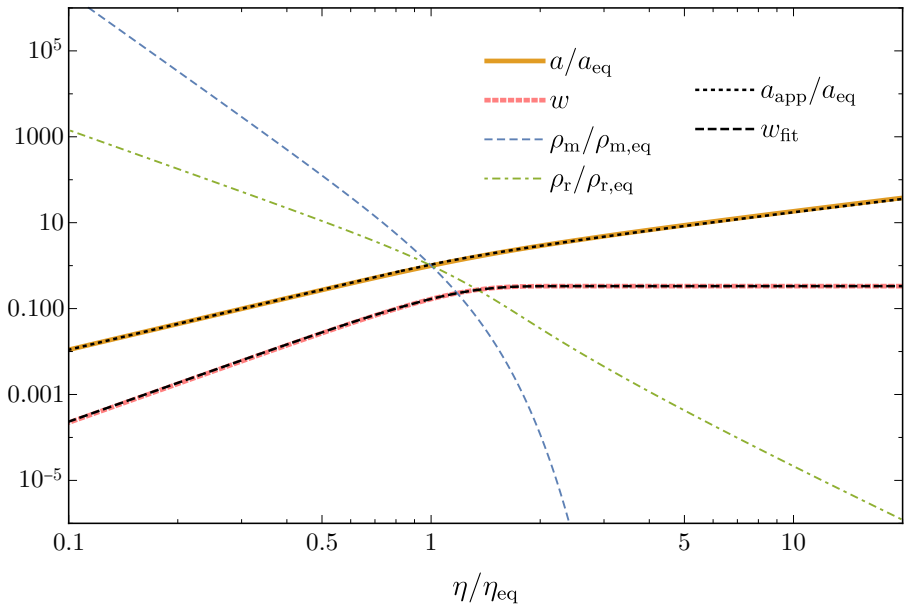

Figure 6.1: Time dependences of the scale factor, the energy densities, normalized by their values at $\eta = \eta_{\rm eq}$, and the equation-of-state parameter. $a_{\rm app}$ is given by Eq. (6.6) with $\eta_{\rm R} = 0.83\eta_{\rm eq}$ and $w_{\rm fit}$ is given by Eq. (6.7). Note that $\rho_{\rm m,eq} = \rho_{\rm r,eq}$ by definition.

Figure 6.2 shows the numerical results of the evolution of the perturbations. Following Sec. 3.3.1, we have assumed the following adiabatic initial conditions:

$$\delta_{\rm m,ini} = -2\Phi_{\rm ini},\ \ \delta_{\rm r,ini} = \frac{4}{3}\delta_{\rm m,ini},\ \ \theta_{\rm m,ini} = \theta_{\rm r,ini} = \frac{k^2\eta}{3}\Phi_{\rm ini}. \tag{6.8}$$

Note that we study the linear regime, and thus the overall normalization of perturbations does not matter in the figures, hence we take $\Phi_{\rm ini} = 1$, or equivalently we plot the transfer function. In Fig. 6.2, we can see that for perturbation modes that entered the horizon well before the transition ($k \gg 1/\eta_{\rm eq}$), the gravitational potential Φ exponentially decays soon after the equality time, and after a while, Φ starts to oscillate due to radiation pressure, with the amplitude decaying less rapidly ($\propto \eta^{-2}$).

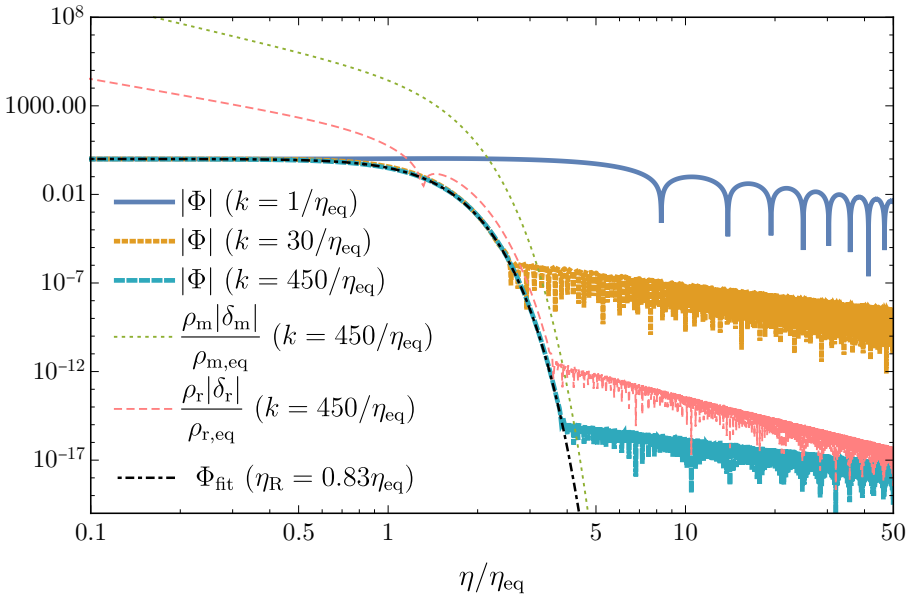

Figure 6.2: Evolution of transfer functions for the gravitational potential and the energy density perturbations. The approximate formula $\Phi_{\rm fit}$, given by Eq. (6.9), is also plotted.

Here, we explain how to derive an approximation formula of Φ which describes its exponential decay. The formula will be used to calculate the induced GWs. First, from Eq. (6.5), Φ can be approximated to be $k^2\Phi \simeq -\frac{3}{2}\mathcal{H}^2\left(\frac{\rho_{\rm m}}{\rho_{\rm tot}}\delta_{\rm m} + \frac{\rho_{\rm r}}{\rho_{\rm tot}}\delta_{\rm r}\right)$ in the subhorizon limit. For modes with $k \gg 1/\eta_{\rm eq}$, during $1/k \ll \eta \ll \eta_{\rm eq}$, $\delta_{\rm m}$ grows but $\delta_{\rm r}$ does not. Therefore, even after $\eta_{\rm eq}$, the evolution of Φ is dominated by $\rho_{\rm m}\delta_{\rm m}$ for a while. During this phase, $\rho_{\rm m}$ decays exponentially and then we can expect Φ is proportional to $\rho_{\rm m}$. Radiation density perturbations $\rho_{\rm r}\delta_{\rm r}$ also decay following the decay of Φ around this phase. After a while, the evolution of Φ is dominated by $\rho_{\rm r}\delta_{\rm r}$ and then Φ starts to oscillate. Neglecting this radiation term and the expansion of the Universe during the transition for simplicity, we can approximate Φ as

$$\begin{aligned}\Phi &\sim \exp\left(-\int^{\eta} {\rm d}\bar{\eta} a(\bar{\eta})\Gamma\right) \\ &= \begin{cases} \exp\left(-\frac{2}{3}\left(\frac{\eta}{\eta_{\rm R}}\right)^3\right) & (\eta < \eta_{\rm R}) \\ \exp\left(-2\left(\left(\frac{\eta}{\eta_{\rm R}}\right)^2 - \frac{\eta}{\eta_{\rm R}} + \frac{1}{3}\right)\right) & (\eta \geq \eta_{\rm R}) \end{cases} \\ &\equiv \Phi_{\rm fit},\end{aligned} \tag{6.9}$$

where we have used Eq. (6.6) and assumed $a(\eta_{\rm R})\Gamma = \mathcal{H}(\eta_{\rm R})(= 2/\eta_{\rm R})$.

Figure 6.3 is an enlarged view of the evolution of Φ for several modes around the transition. From this figure, we can see that, for $k \gtrsim 30/\eta_{\rm eq}$, the exponential decay of

Φ can be fitted by Eq. (6.9). We have checked that the error of the fitting formulas for $k = 30/\eta_{\rm eq}$ is less than 15% in $\eta < 2\eta_{\rm eq}$ and, for smaller scales, the error becomes smaller.

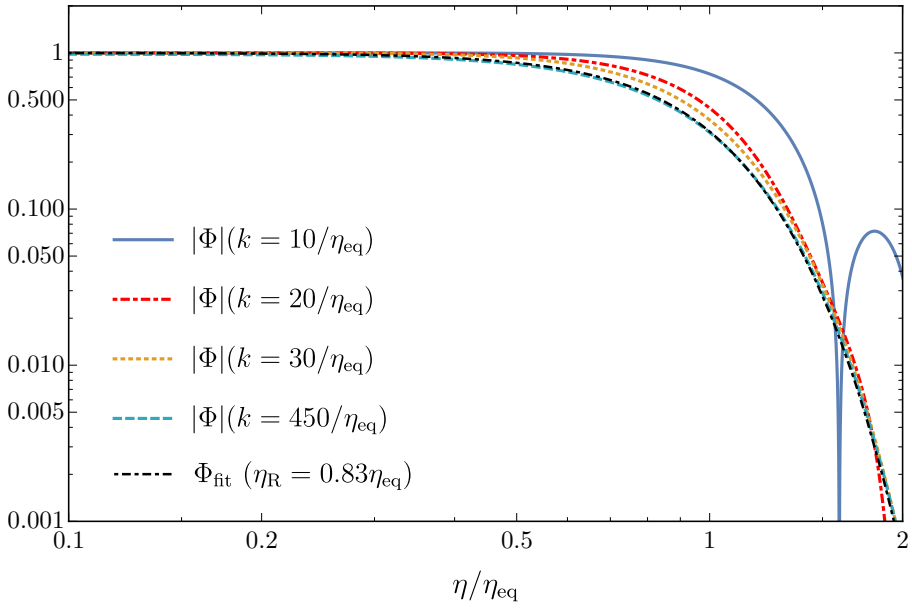

Figure 6.3: Evolution of Φ with different wave numbers ($10/\eta_{\rm eq} \leq k \leq 450/\eta_{\rm eq}$) and the fitting formula given in Eq. (6.9).

6.1.2 Suppression of induced GWs

Ultimately, to calculate the induced GWs precisely, we need to know the exact evolution for all quantities such as a, G_k, and Φ. Unfortunately, however, we have not been able to find exact analytic solutions of these quantities. In addition, obtaining numerical solutions and plugging them into the formula for the induced GWs to do the relevant integrations require high computational costs. Hence, in this section, we try to calculate the induced GWs approximately as the first step toward a more rigorous analysis.

First, we briefly summarize the formulas for the induced GWs, which we use throughout this section. From Eq. (4.47), the energy density parameter is given as

$$\Omega_{\rm GW}(\eta, k) = \frac{27}{1250}\left(\frac{k}{\mathcal{H}}\right)^2 \int_0^\infty {\rm d}v \int_{|1-v|}^{|1+v|} {\rm d}u \left[\frac{4v^2 - (1+v^2-u^2)^2}{4uv}\right]^2 \times \overline{I^2(u, v, x, x_{\rm R})}\mathcal{P}_\zeta(uk)\mathcal{P}_\zeta(vk), \tag{6.10}$$

where we have substituted $w_{\rm h} = 0$ into Eq. (4.47) because we consider the GWs induced by the scalar perturbation entering the horizon during an eMD era. From Eq. (4.44), $I(u, v, x, x_{\rm R})$ is defined as

$$I(u, v, x, x_{\rm R}) \equiv \int^x {\rm d}\bar{x} \frac{a(\bar{\eta})}{a(\eta)} k G_k(\eta; \bar{\eta}) f(u, v, \bar{x}, x_{\rm R}), \tag{6.11}$$

where $f(u, v, x, x_{\rm R})$ is given as (see Eq. (4.45))

$$f(u, v, \bar{x}, x_{\rm R}) = \frac{1}{3(1+w)}\left(2(5+3w)\Phi(u\bar{x})\Phi(v\bar{x}) + 4\mathcal{H}^{-1}(\Phi'(u\bar{x})\Phi(v\bar{x}) + \Phi(u\bar{x})\Phi'(v\bar{x})) + 4\mathcal{H}^{-2}\Phi'(u\bar{x})\Phi'(v\bar{x})\right). \tag{6.12}$$

The second argument of Φ is abbreviated in Eq. (6.12) for compact notation, that is, $\Phi(u\bar{x})$ actually means $\Phi(u\bar{x}, ux_{\rm R})$ and $\Phi(v\bar{x})$ should be understood similarly. $\Phi(\bar{x}, x_{\rm R})$ is the transfer function of the gravitational potential, which satisfies $\Phi(\bar{x} \to 0, x_{\rm R}) = 1$. The prime here denotes a differentiation with respect to $\bar{\eta}$. Here, we assume that the scale factor is given by Eq. (6.6) because the approximation formula fits the numerical result well. Then, in $\eta < \eta_{\rm R}$, $I(u, v, x, x_{\rm R})$ is expressed as

$$I(u, v, x, x_{\rm R}) = \int_0^x {\rm d}\bar{x} \left(\frac{\bar{x}}{x}\right)^2 kG_k^{\rm eMD}(\eta; \bar{\eta}) f(u, v, \bar{x}, x_{\rm R}). \qquad (\text{for } \eta < \eta_{\rm R}) \tag{6.13}$$

The Green function is given as (see Eq. (4.22))

$$kG_k^{\rm eMD}(\eta; \bar{\eta}) = -x\bar{x} \left(j_1(x) y_1(\bar{x}) - j_1(\bar{x}) y_1(x)\right), \tag{6.14}$$

where we have omitted the step function because $\bar{\eta} < \eta$. On the other hand, in $\eta > \eta_{\rm R}$, we obtain[3]

$$\begin{aligned} I(u, v, x, x_{\rm R}) = &\int_0^{x_{\rm R}} {\rm d}\bar{x} \left(\frac{1}{2(x/x_{\rm R}) - 1}\right) \left(\frac{\bar{x}}{x_{\rm R}}\right)^2 kG_k^{\rm eMD\to RD}(\eta; \bar{\eta}) f(u, v, \bar{x}, x_{\rm R}) \\ &+ \int_{x_{\rm R}}^x {\rm d}\bar{x} \left(\frac{2(\bar{x}/x_{\rm R}) - 1}{2(x/x_{\rm R}) - 1}\right) kG_k^{\rm RD}(\eta; \bar{\eta}) f(u, v, \bar{x}, x_{\rm R}). \qquad (\text{for } \eta > \eta_{\rm R}) \end{aligned} \tag{6.15}$$

As we can see from Eqs. (6.12) and (6.15), the induced GWs sensitively depend on the evolution of the gravitational potential Φ. In Refs. [107, 108], they assume that the gravitational potential remains unity until $\eta_{\rm R}$ and that the second line in Eq. (6.15), representing the contributions after $\eta_{\rm R}$, is subdominant and hence can be neglected. However, the gravitational potential gradually changes around the transition and therefore we need to take into account the evolution of the gravitational potential more carefully. The contributions after $\eta_{\rm R}$ also turn out to have non-negligible impacts on the induced GWs. These are the main issues we address in this section.

The Green functions in Eq. (6.15) are expressed as (see Eqs. (4.20) and (4.24))

$$kG_k^{\rm RD}(\eta; \bar{\eta}) = \sin(x - \bar{x}), \tag{6.16}$$

$$kG_k^{\rm eMD\to RD}(\eta; \bar{\eta}) = C(x, x_{\rm R}) \bar{x} j_1(\bar{x}) + D(x, x_{\rm R}) \bar{x} y_1(\bar{x}), \tag{6.17}$$

where the step function is omitted and $C(x, x_{\rm R})$ and $D(x, x_{\rm R})$ are defined as

$$C(x, x_{\rm R}) = \frac{\sin x - 2x_{\rm R}(\cos x + x_{\rm R} \sin x) + \sin(x - 2x_{\rm R})}{2x_{\rm R}^2}, \tag{4.25}$$

$$D(x, x_{\rm R}) = \frac{(2x_{\rm R}^2 - 1)\cos x - 2x_{\rm R} \sin x + \cos(x - 2x_{\rm R})}{2x_{\rm R}^2}. \tag{4.26}$$

Here, we consider the power spectrum given by

$$\mathcal{P}_\zeta = A_s \, \Theta(k - 30/\eta_{\rm eq}) \Theta(k_{\rm max} - k), \tag{6.18}$$

where A_s represents the amplitude. We focus on modes with $k > 30/\eta_{\rm eq}$ so that we can use the fitting formula for Φ, given in Eq. (6.9). In addition, we have introduced the

[3] Eq. (6.15) refines the relevant formula in Ref. [81]. In the limit of $x \to \infty$, the contribution of the first term to $\Omega_{\rm GW}$ decreases by 1/4 compared to the previous result.

cutoff scale $k_{\rm max}$. This cutoff scale corresponds to the horizon scale at the start of an eMD era, or the scale that is entering the non-linear regime at $\eta_{\rm R}$, i.e., the amplitude of matter density perturbations on such a scale becomes unity at $\eta_{\rm R}$.[4] Since the formulas shown above are invalid in the non-linear regime, we need to introduce this cutoff scale to limit our analysis to the linear regime when there exist scales that enter the non-linear regime before $\eta_{\rm R}$. From Eq. (6.5), the matter density perturbation during an eMD era on subhorizon scales is related to the gravitational potential as

$$\delta_{\rm m} \simeq -\frac{2}{3}k^2\mathcal{H}^{-2}\Phi_{\rm ini}. \tag{6.19}$$

Since the power spectrum of the gravitational potential is related to that of the curvature perturbations as $\mathcal{P}_\Phi = \frac{9}{25}\mathcal{P}_\zeta$, the initial value $\Phi_{\rm ini}$ can be estimated as $|\Phi_{\rm ini}| \sim \frac{3}{5}\mathcal{P}_\zeta^{1/2}$. Then, we can rewrite Eq. (6.19) as

$$|\delta_{\rm m}| \sim \frac{1}{10}(k\eta)^2\mathcal{P}_\zeta^{1/2}, \tag{6.20}$$

where we have used the relation $\mathcal{H} = 2/\eta$, satisfied during a MD era. From this equation, the non-linear scale, on which the matter density perturbation becomes unity at the reheating, can be approximated as

$$k_{\rm NL} \sim \sqrt{10}\,\eta_{\rm R}^{-1}\mathcal{P}_\zeta^{-1/4} \sim 470/\eta_{\rm R}, \tag{6.21}$$

where we have substituted $\mathcal{P}_\zeta = 2.1 \times 10^{-9}$ [17] to obtain the final expression. Therefore our calculations are valid only for $k_{\rm max} \lesssim 470/\eta_{\rm R}$. To make the differences from the previous works look clear, we take $k_{\rm max} = 450/\eta_{\rm R}$ in the following.

To calculate induced GWs, we substitute the fitting formulas of w and Φ for a gradual transition, given in Eqs. (6.7) and (6.9), into Eq. (6.12), thereby taking into account the graduality of the transition. Note that we neglect contributions from the oscillation phases of Φ because the oscillation amplitude is very small for $k > 30/\eta_{\rm eq}$, noting that the power spectrum of the induced GWs is basically proportional to the fourth power of Φ. For example, in Fig. 6.2, we can see that Φ with $k = 30/\eta_{\rm eq}$ starts to oscillate with the amplitude $\Phi \sim \mathcal{O}(10^{-6})$. Figure 6.4 shows the numerical results for the induced GWs. From this figure, we can see that the induced GWs (black solid line) are suppressed compared to those derived with the setups in the previous works (brown dotted line).

6.1.3 Discussion

Here, we discuss the result of the induced GWs in the gradual transition, given in Fig. 6.4.

From Fig. 6.4, we can see the suppression of the induced GWs with $k_{\rm R} < k < k_{\rm max}$, which corresponds to the modes entering the horizon before the transition. To see how the suppression of the induced GWs arises, we show the time dependence of $x|I|$ in Fig. 6.5. We use the concrete expression of I, given in Eqs. (6.13) and (6.15). Note that the time dependence of the energy density parameter is finally given as $\Omega_{\rm GW} \propto x^2\overline{I^2}$. From Fig. 6.5, we can see that xI grows when $\eta \ll \eta_{\rm R}$, but around the transition ($\eta \sim \eta_{\rm R}$), xI stops growing and starts to decrease due to the decay of Φ. After the transition

[4] Strictly speaking, since the transition is gradual, there is an uncertainty on the start of an eMD era. In this section, we regard $\eta_{\rm R}$ as the conformal at the start of the eMD era for simplicity because the scale factor can be fitted with the formula given in Eq. (6.6) well.

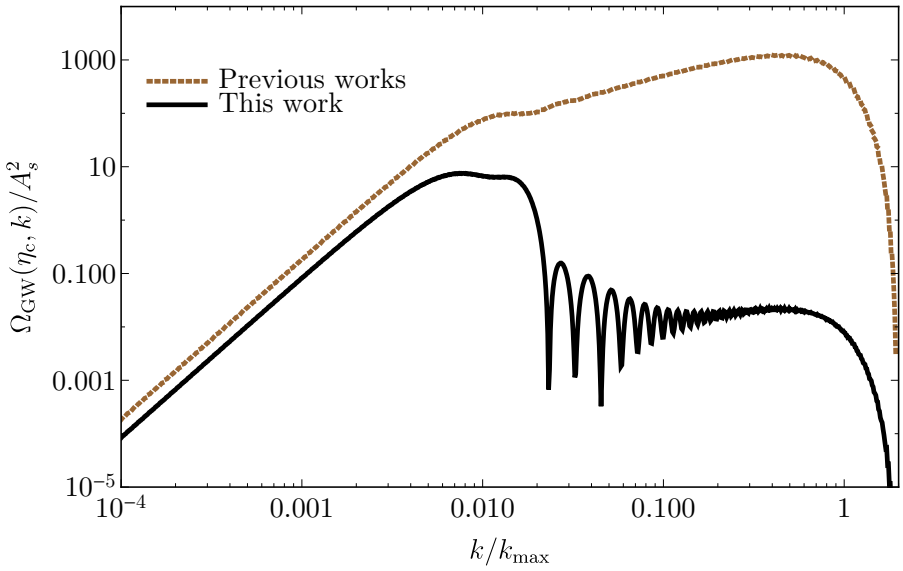

Figure 6.4: Spectrum of induced GWs at $\eta = \eta_{\rm c}$ associated with a gradual transition from an eMD era to the RD era (see Sec. 4.5 for the definition of $\eta_{\rm c}$). For all the plots, $k_{\rm max} = 450/\eta_{\rm R}$ is assumed and the primordial power spectrum is given in Eq. (6.18). Our result for $\Omega_{\rm GW}$ is shown by a black solid line. The brown dotted line shows the result using Ref. [81], additionally taking into account the factor 1/4 mentioned in footnote 3, with the same assumptions as in Refs. [107], under which $\Phi = 1$ until $\eta = \eta_{\rm R}$ and there is no GW source ($\Phi = 0$) for $\eta > \eta_{\rm R}$. In other words, we neglect the second line in Eq. (6.15) to derive the brown dotted line. Reduction from the brown dotted line to the black solid line shows the effects of the gradual transition.

($\eta > \mathcal{O}(1)\eta_{\rm R}$), xI oscillates with its amplitude being almost constant, which indicates that $\Omega_{\rm GW}$ becomes constant. Since the evolution of I corresponds to that of the tensor perturbations, the behavior of xI can be interpreted as follows. During an eMD era, since the source term in Eq. (4.15) is almost constant, the amplitude of the tensor perturbation is given as $h^\lambda_{\boldsymbol{k}} \simeq 4S^\lambda_{\boldsymbol{k}}/k^2$ in the subhorizon limit [42, 107]. Here, we consider a gradual transition from an eMD era to the RD era and therefore the amplitude of the tensor perturbations decays on subhorizon scales, following the gradual decay of the source during the transition, which corresponds to the decay of xI around $\eta \sim \eta_{\rm R}$. After a while, the tensor perturbations decouple from the source and behave as free-propagating GWs, which corresponds to the oscillation of xI for $\eta > \mathcal{O}(1)\eta_{\rm R}$. Note that, to obtain Fig. 6.5, we use the approximation formula $\Phi_{\rm fit}$ for Φ and neglect the oscillation behavior of Φ after its exponential decay. This also implies that the oscillation behavior of xI in Fig. 6.5 (already present before $\eta = 2\eta_{\rm eq} \simeq 2.4\eta_{\rm R}$)) has nothing to do with the oscillation behavior of Φ in Fig. 6.2 (appearing after $\eta = 2\eta_{\rm eq}$), and the contributions from the oscillations of Φ can be neglected because of its small amplitude if we consider $k > 30/\eta_{\rm eq}$, as we have already mentioned.

We stress that the main difference between the result in previous works [81, 107, 108] and our result comes from the decay of the tensor perturbations during the gradual transition, which we have taken into account for the first time.

For the large-scale tensor perturbations with $k < k_{\rm R}$ in Fig. 6.4, they feel that the transition occurs suddenly because the transition timescale ($\mathcal{O}(\eta_{\rm R})$) is much shorter than the oscillation timescale of the tensor perturbations ($1/k$). Thus, the large-scale tensor

perturbations do not experience the suppression during the transition, which occurs for the small-scale tensor perturbations. This is why the difference between this work and previous works is small on the large scales in Fig. 6.4. We can also see the oscillation behavior of the GW spectrum with $0.01 \lesssim k/k_{\rm max}$ in Fig. 6.4. Since the oscillation frequency in wavenumber, defined as $k_{\rm osc}$, satisfies $k_{\rm osc}\eta_{\rm eq} \sim \mathcal{O}(1)$, we can naively expect that the oscillation behavior comes from some resonances between the wavenumber of the tensor perturbations and the timescale of the gradual transition.

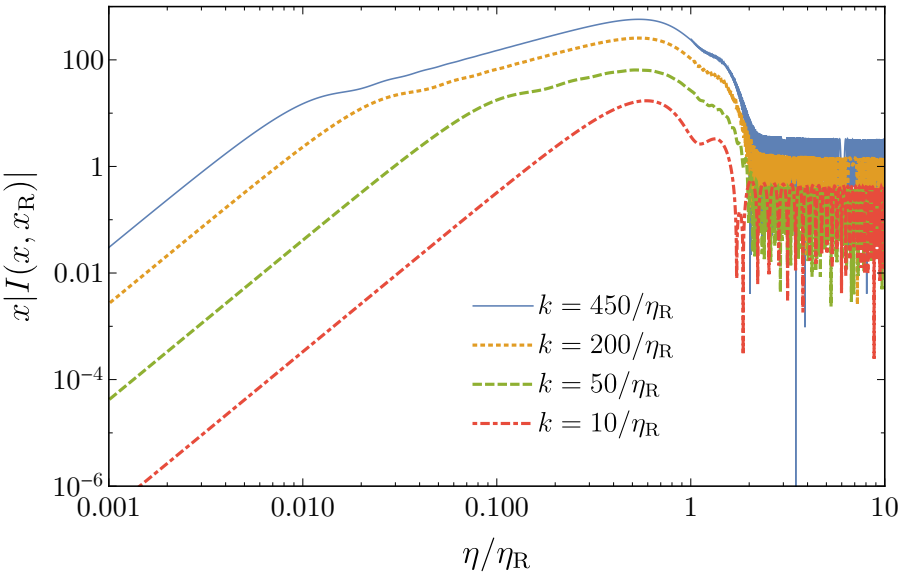

Figure 6.5: Time dependences of $x|I(x, x_{\rm R})|$, defined in Eq. (6.11). We omit the arguments u and v because we approximate Φ as $\Phi_{\rm fit}$, defined in Eq. (6.9), and hence I does not depend on u or v.

Before closing this section, we mention some uncertainties on our results. Throughout this section, to spotlight the effects of an eMD era on induced GWs, we have focused on the GWs induced by the perturbations entering the horizon during an eMD era. However, we have neglected the contributions from the perturbations entering the horizon during an eMD era but relatively near the transition ($1/\eta_{\rm R} < k < 30/\eta_{\rm eq}$) to avoid high computational costs. If we consider the scale-invariant spectrum of curvature perturbations, these perturbations could produce GWs in addition to the results in Fig. 6.4. We leave the analysis of these additional effects of an eMD era for future work. Besides, we have not considered the GWs induced by the perturbations entering the horizon much before the transition ($k > 470/\eta_{\rm R}$). If we consider the scale-invariant spectrum and a long-lasting eMD era, the perturbations on $k > 470/\eta_{\rm R}$ could also induce additional GWs. Such perturbations may have become non-linear during the eMD era and our formula, based on the linear perturbation theory, cannot be applied. Although there are works discussing GWs induced by non-linear scalar perturbations in this context [191, 192], there are still some uncertainties about the predictions [191, 192]. Therefore, the amount of the induced GWs predicted in this section can be regarded as lower bounds on the total induced GWs.

6.2 Sudden transition

In the previous section, we have found that if we carefully take into account the evolution of the gravitational potential around the transition from an eMD era to the RD era, the predictions for the induced GWs can change. In particular, we have shown that the induced GWs can be significantly suppressed for a gradual transition, whose timescale is comparable to the Hubble timescale at that time. In some cosmological scenarios (see Appendix A), however, the transition from an eMD era to the RD era occurs suddenly, i.e. the timescale of the transition (or reheating) is much shorter than the Hubble timescale at that time. The purpose of this section is to study the induced GWs in such sudden transition cases. The situation is different from the case of the gradual transition. The effects of a sudden transition on the induced GWs mainly come from the contributions of the GWs induced after the sudden transition, which are ignored in the previous works [81, 107, 108]. In this section, we point out that, in sudden-reheating scenarios, GWs induced during the RD era can be larger than the induced GWs predicted in the previous works by several orders of magnitude. We also discuss the possibility of the determination of the reheating temperature with the use of the enhanced induced GWs.

6.2.1 Formulas for induced GWs

Here, we briefly review the equations for induced GWs that we use in this section. We assume that an eMD era ended suddenly with the Universe entering into the RD era at a conformal time $\eta = \eta_{\rm R}$. Similarly to Sec. 6.1, the scale factor and the conformal Hubble parameter are given by (see also Sec. 2.3.2)

$$\frac{a(\eta)}{a(\eta_{\rm R})} = \begin{cases} \left(\dfrac{\eta}{\eta_{\rm R}}\right)^2 & (\eta < \eta_{\rm R}) \\ 2\dfrac{\eta}{\eta_{\rm R}} - 1 & (\eta \geq \eta_{\rm R}) \end{cases}, \tag{2.48}$$

$$\mathcal{H} = \begin{cases} \dfrac{2}{\eta} & (\eta < \eta_{\rm R}) \\ \dfrac{1}{\eta - \eta_{\rm R}/2} & (\eta \geq \eta_{\rm R}) \end{cases}. \tag{2.49}$$

The energy density parameter of GWs per logarithmic interval in k is given by

$$\Omega_{\rm GW}(\eta, k) = \frac{27}{1250}\left(\frac{k}{\mathcal{H}}\right)^2 \int_0^\infty {\rm d}v \int_{|1-v|}^{|1+v|} {\rm d}u \left[\frac{4v^2 - (1+v^2-u^2)^2}{4uv}\right]^2 \times \overline{I^2(u, v, x, x_{\rm R})}\mathcal{P}_\zeta(uk)\mathcal{P}_\zeta(vk). \tag{6.10}$$

$I(u, v, x, x_{\rm R})$ in $\eta > \eta_{\rm R}$ is given as

$$\begin{aligned} I(u, v, x, x_{\rm R}) =& \int_0^{x_{\rm R}} {\rm d}\bar{x} \left(\frac{1}{2(x/x_{\rm R}) - 1}\right)\left(\frac{\bar{x}}{x_{\rm R}}\right)^2 kG_k^{\rm eMD\to RD}(\eta; \bar{\eta}) f(u, v, \bar{x}, x_{\rm R}) \\ &+ \int_{x_{\rm R}}^{x} {\rm d}\bar{x} \left(\frac{2(\bar{x}/x_{\rm R}) - 1}{2(x/x_{\rm R}) - 1}\right) kG_k^{\rm RD}(\eta; \bar{\eta}) f(u, v, \bar{x}, x_{\rm R}) \qquad (6.15) \\ \equiv& I_{\rm eMD}(u, v, x, x_{\rm R}) + I_{\rm RD}(u, v, x, x_{\rm R}), \qquad (6.22) \end{aligned}$$

where we have defined the first and second lines of Eq. (6.15) as $I_{\rm eMD}(u,v,x,x_{\rm R})$ and $I_{\rm RD}(u,v,x,x_{\rm R})$, respectively. The concrete expressions of f and G_k are given in previous section (see Eqs. (6.12), (6.16), and (6.17)). Note again $f(u,v,\bar{x},x_{\rm R})$ in Eq. (6.15) is given with the transfer function of the gravitational potential as

$$f(u,v,\bar{x},x_{\rm R}) = \frac{1}{3(1+w)}\left(2(5+3w)\Phi(u\bar{x})\Phi(v\bar{x}) + 4\mathcal{H}^{-1}(\Phi'(u\bar{x})\Phi(v\bar{x}) + \Phi(u\bar{x})\Phi'(v\bar{x})) \right.$$
$$\left. +4\mathcal{H}^{-2}\Phi'(u\bar{x})\Phi'(v\bar{x})\right). \tag{6.12}$$

We approximate $\overline{I^2(u,v,x,x_{\rm R})}$ in Eq. (6.10) as

$$\overline{I^2(u,v,x,x_{\rm R})} \simeq \overline{I^2_{\rm eMD}(u,v,x,x_{\rm R})} + \overline{I^2_{\rm RD}(u,v,x,x_{\rm R})}. \tag{6.23}$$

As we will see in the next subsection, in the case of the sudden reheating, $\overline{I^2_{\rm RD}} \gg \overline{I^2_{\rm eMD}}$ is satisfied. However, since the contribution from $\overline{I^2_{\rm eMD}}$ corresponds to the induced GWs predicted in the previous works [81, 107, 108], we leave $\overline{I^2_{\rm eMD}}$ in Eq. (6.23) just for later use, though we neglect the contribution from $\overline{I_{\rm eMD}I_{\rm RD}}(\ll \overline{I^2_{\rm RD}})$. Correspondingly, we approximately split $\Omega_{\rm GW}$ into two parts as $\Omega_{\rm GW} \simeq \Omega_{\rm GW,eMD} + \Omega_{\rm GW,RD}$, where $\Omega_{\rm GW,eMD}$ and $\Omega_{\rm GW,RD}$ are calculated from $\overline{I^2_{\rm eMD}}$ and $\overline{I^2_{\rm RD}}$, respectively. Note that $\Omega_{\rm GW,eMD}$ is the same as the energy density parameter calculated in the previous works [81, 107, 108] up to factor of 1/4 (see footnote 4 in Sec. 6.1).

The main difference between this section and the previous section comes from the evolution of the gravitational potential around the transition. From Eq. (3.55), the evolution equation for the transfer function of the gravitational potential is given as

$$\Phi'' + \frac{6}{\eta}\Phi' = 0, \quad (\eta < \eta_{\rm R}) \tag{6.24}$$

$$\Phi'' + 4\mathcal{H}\Phi' + \frac{k^2}{3}\Phi = 0, \quad (\eta > \eta_{\rm R}) \tag{6.25}$$

where we have used the relation $\mathcal{H}' = -\mathcal{H}^2$ in $\eta > \eta_{\rm R}$ (see Eq. (2.49)). By solving this equation, we find

$$\Phi(x,x_{\rm R}) = \begin{cases} 1 & (\text{for } x \le x_{\rm R}), \\ A(x_{\rm R})\mathcal{J}(x) + B(x_{\rm R})\mathcal{Y}(x) & (\text{for } x \ge x_{\rm R}), \end{cases} \tag{6.26}$$

where we have dropped the decaying mode for $\eta < \eta_{\rm R}$. The functions $\mathcal{J}(x)$ and $\mathcal{Y}(x)$ are the independent solutions of Eq. (6.25), defined with the first and second spherical Bessel functions, $j_1(x)$ and $y_1(x)$, as

$$\mathcal{J}(x) = \frac{3\sqrt{3}\, j_1\left(\frac{x-x_{\rm R}/2}{\sqrt{3}}\right)}{x - x_{\rm R}/2}, \tag{6.27}$$

$$\mathcal{Y}(x) = \frac{3\sqrt{3}\, y_1\left(\frac{x-x_{\rm R}/2}{\sqrt{3}}\right)}{x - x_{\rm R}/2}, \tag{6.28}$$

and the coefficients $A(x_{\rm R})$ and $B(x_{\rm R})$ are determined so that $\Phi(x)$ and $\Phi'(x)$ are continuous at $x = x_{\rm R}$:

$$A(x_{\rm R}) = \frac{1}{\mathcal{J}(x_{\rm R}) - \frac{\mathcal{Y}(x_{\rm R})}{\mathcal{Y}'(x_{\rm R})}\mathcal{J}'(x_{\rm R})}, \tag{6.29}$$

$$B(x_{\rm R}) = -\frac{\mathcal{J}'(x_{\rm R})}{\mathcal{Y}'(x_{\rm R})}A(x_{\rm R}). \tag{6.30}$$

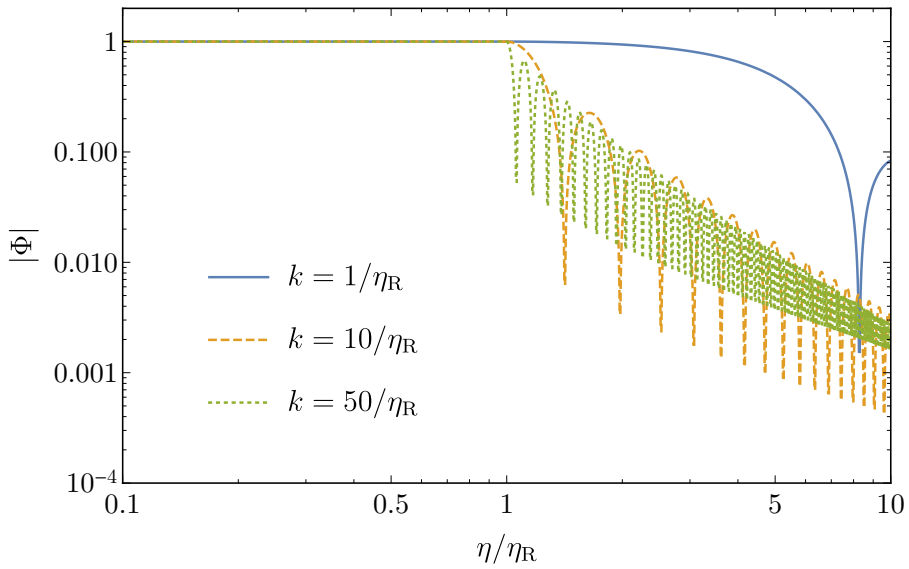

Figure 6.6: Evolution of the transfer function of the gravitational potential in a sudden-transition scenario, which is given by Eq. (6.26).

In Appendix A, we introduce a model realizing a sudden-reheating transition and check that the above analytic expression for Φ with these connection conditions coincides well with the numerical solution for Φ calculated in that model. Figure 6.6 shows the evolution of the transfer function of the gravitational potential, given by Eq. (6.26). We can see that, after the transition, the gravitational potential with $k \gg 1/\eta_{\rm R}$ starts to oscillate rapidly compared to the Hubble timescale at that time.

In Ref. [81], the authors derive the analytic formulas for $I_{\rm eMD}$ and $I_{\rm RD}$ with the expression of Φ given as Eq. (6.26). In the reference, they adopt an implicit assumption that GWs induced during the RD era by the perturbations having entered the horizon during an eMD era, which we focus on in this section, are subdominant compared to the GWs 1) which are induced during the eMD era ($\Omega_{\rm GW,eMD}$) and 2) which are induced by the perturbations entering the horizon after the reheating. However, this assumption is not true in realistic situations. In Sec. 6.1, we consider a gradual reheating transition and show that the contributions from $I_{\rm RD}$ play an important roll for the suppression of induced GWs (though we do not explicitly define $I_{\rm RD}$ there). In addition, in a sudden-reheating scenario, the dominant contribution comes from $I_{\rm RD}$ as we will show in the next subsection.

When we discuss the current value of the energy density parameter of the induced GWs, we take into account the late-time evolution as

$$\Omega_{\rm GW}(\eta_0, k)h^2 = 0.39 \left(\frac{g_{*,\rm c}}{106.75}\right)^{-1/3} \Omega_{\rm r,0}h^2 \Omega_{\rm GW}(\eta_{\rm c}, k), \tag{4.64}$$

where note again $\eta_{\rm c}$ is the conformal time when $\Omega_{\rm GW}$ becomes constant after their production, but much before the late matter-radiation equality time (see Sec. 4.5 for details).

6.2.2 Enhancement of induced GWs

Using the above equations and the analytic formulas in Ref. [81], we calculate induced GWs. To be specific, we assume the following power spectrum of the curvature pertur-

bation:

$$\mathcal{P}_\zeta(k) = \Theta(k_{\rm max} - k) A_s \left(\frac{k}{k_*}\right)^{n_s - 1}, \tag{6.31}$$

where A_s is the amplitude at the pivot scale k_* and n_s is the tilt of the power spectrum. We introduce $k_{\rm max}$ as the cutoff scale of the power spectrum. Similarly to the case in Sec. 6.1.2, the cutoff scale corresponds to the horizon scale at the start of the eMD era or the scale where the matter perturbations become unity at the sudden reheating. To ensure the validity of our analysis, we limit our analysis to cases with $k_{\rm max} \leq 450/\eta_{\rm R}$. That is, we do not take into account GWs that are generated from non-linear perturbations, and this means our analysis would lead to conservative estimations of the GW spectrum.

Figure 6.7 shows the scale dependence of the spectrum of induced GWs. In this figure, we take $n_s = 1$ for simplicity. We can see that $\Omega_{\rm GW,RD}$ is much larger than $\Omega_{\rm GW,eMD}$. This is because the GWs induced during the RD era by the subhorizon perturbations that entered the horizon during an eMD era, neglected in the previous works but taken into account in this work, are significant. For comparison, we also plot the GW spectra induced by the power spectra of $\mathcal{P}(k) = \Theta(k_{\rm max} - k)\Theta(k - 0.7k_{\rm max})A_s$ and $\mathcal{P}(k) = \Theta(0.7k_{\rm max} - k)\Theta(k - 0.4k_{\rm max})A_s$ with blue and red lines. As shown in the figure, the contributions from the smallest scales (blue dashed line) are the dominant contributions to the total spectrum (solid black line) except for the large-scale-side tail of the sharp peak ($0.3 \lesssim k/k_{\rm max} \lesssim 1$). This sharp peak is due to the resonance effect, which is a characteristic feature of GWs induced during the RD era [41], when the gravitational potential oscillates (see also Fig. 4.1). The tail of the sharp peak is formed by the envelope of the resonance effects on these scales (see the red dot-dashed line). In this way, the spectrum of the induced GWs is produced dominantly by the smallest scales, and the resonant amplification plays a key role. This understanding becomes clearer in Appendix B, where we derive approximate analytic formulas for induced GWs for sudden-reheating scenarios. On much larger scales, the contributions from the perturbations entering the horizon after the reheating dominate induced GWs, whose spectrum becomes scale invariant $\Omega_{\rm GW}(\eta_{\rm c}, k) \simeq 0.8222 A_s^2$ [81]. This can be observed in the GW spectrum for $k < 10^9 {\rm Mpc}^{-1}$ in Fig. 6.8, though in that figure a slightly scale-dependent primordial spectrum is assumed, leading to a slight scale dependence of $\Omega_{\rm GW}$.

The main reason why induced GWs are enhanced is that the gravitational potential Φ with large k ($\gg 1/\eta_{\rm R}$) is constant until $\eta = \eta_{\rm R}$ and, after the reheating, it oscillates with the timescale $\sim 1/k$, much shorter than its decay timescale $\sim \eta_{\rm R}$ (see Fig. 6.6). Due to the fast oscillations of perturbations with unsuppressed amplitudes, which remained constant until the moment of the reheating, induced GWs are significantly enhanced.[5] Note that the dominant contributions come from the last term in Eq. (6.12), which involves two time derivatives of the gravitational potential. This is because, at the beginning of the RD era, the last term can be approximated as $\mathcal{H}^{-2}\Phi'\Phi' \sim (k\eta_{\rm R})^2\Phi^2 \gg \Phi^2$ for the perturbations that entered the horizon well before the sudden reheating. In other words, the factor $(k\eta_{\rm R})^2$ in the source term and the amplitude of Φ that remained constant until the reheating are the main causes for the enhancement.

In addition to numerical solutions, we also obtain approximate analytic formulas of $\Omega_{\rm GW,RD}$ in Appendix B, with $\Omega_{\rm GW,RD}$ given by the sum of Eqs. (B.71) and (B.73). Using

[5] Although the perturbations entering the horizon during the RD era also oscillate with the timescale much shorter than their decay timescale well after (not soon after) the horizon entry, the amplitudes of the perturbations start to decay soon after the horizon entry, unlike during an eMD era, and therefore the enhancement is not caused by the perturbations entering the horizon during the RD era.

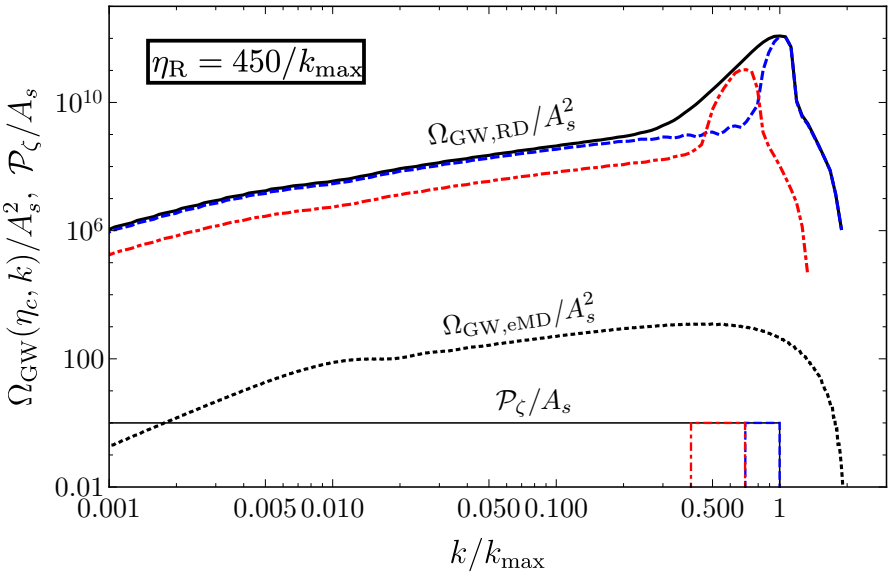

Figure 6.7: Energy density parameters of GWs, for each logarithmic interval of wavenumber, induced during the RD era ($\Omega_{\rm GW,RD}(\eta_{\rm c}, k)$) and during an eMD era ($\Omega_{\rm GW,eMD}(\eta_{\rm c}, k)$), as well as the power spectrum $\mathcal{P}_\zeta(k)$ of curvature perturbations. They are normalized by A_s^2 or A_s, respectively, and we take $\eta_{\rm R} = 450/k_{\rm max}$. The black lines are derived from $\mathcal{P}_\zeta(k) = \Theta(k_{\rm max} - k)A_s$. For comparison, the blue and red lines are also shown, which are derived from $\mathcal{P}_\zeta(k) = \Theta(k_{\rm max} - k)\Theta(k - 0.7k_{\rm max})A_s$ and $\mathcal{P}_\zeta(k) = \Theta(0.7k_{\rm max} - k)\Theta(k - 0.4k_{\rm max})A_s$, respectively. Note that the black dashed line ($\Omega_{\rm GW,eMD}(\eta_{\rm c}, k)$) is the same as the brown dashed line in Fig. 6.4.

these expressions, the GW spectrum is roughly expressed as

$$\frac{\Omega_{\rm GW}(\eta_{\rm c}, k)}{A_{\rm s}^2} \simeq \begin{cases} 0.8 & (x_{\rm R} \lesssim 150 x_{\rm max,R}^{-5/3}) \\ 3 \times 10^{-7} x_{\rm R}^3 x_{\rm max,R}^5 & (150 x_{\rm max,R}^{-5/3} \lesssim x_{\rm R} \ll 1) \\ 1 \times 10^{-6} x_{\rm R} x_{\rm max,R}^5 & (1 \ll x_{\rm R} \lesssim x_{\rm max,R}^{5/6}) \\ 3 \times 10^{-7} x_{\rm R}^7 & (x_{\rm max,R}^{5/6} \lesssim x_{\rm R} \lesssim x_{\rm max,R}) \\ (\text{sharp drop}) & (x_{\rm max,R} \lesssim x_{\rm R} \leq 2 x_{\rm max,R}) \end{cases}, \tag{6.32}$$

neglecting a logarithmic factor for the second line.

6.2.3 Determination of reheating temperature

In the previous subsection, we have shown that the induced GWs can be much larger than those previously reported [81, 107, 108]. In the following, we consider the GWs induced by the almost scale-invariant power spectrum, given in Eq. (6.31), with $A_s = 2.1 \times 10^{-9}$, $k_* = 0.05\,{\rm Mpc}^{-1}$, and $n_s = 0.96$ [17]. Figure 6.8 shows the sensitivity curves of current and future GW experiments and plots for $\Omega_{\rm GW}$ of the GWs induced by the power spectrum with $k_{\rm max} = 10^{14}{\rm Mpc}^{-1}$. This figure shows that the induced GWs associated with a sudden transition from an eMD era to the RD era could in principle be observable by future projects. Since the height and scale of the peak are determined by the scale of the reheating and the cutoff $k_{\rm max}$, we discuss what range of the reheating temperature could be probed by future observations searching for GWs.

Following the procedure and using the effective sensitivity curves in Chap. 5, we derive the cutoff scale and reheating temperature to make the signal-to-noise ratio unity

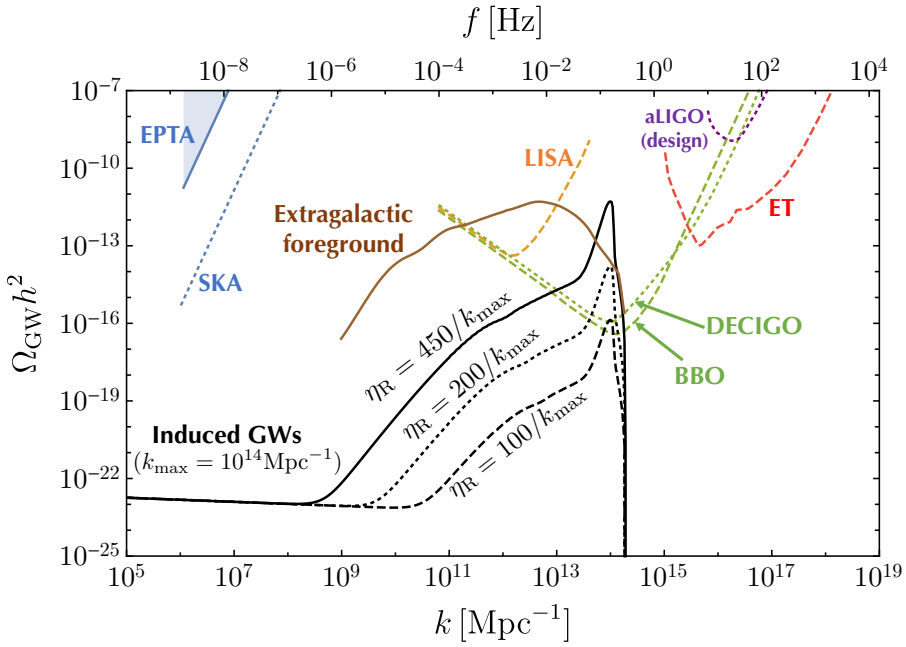

Figure 6.8: Effective sensitivities to stochastic GWs of current and future experiments. Note that we plot $\Omega_{\rm GW,eff}h^2/\sqrt{T_{\rm obs}f/10}$ as a sensitivity curve for each experiment and the foreground. We consider the same experiments and foreground and take the same parameters as in Fig. 5.1. See the section for details about the sensitivity curve of each experiment and the foreground. Black lines show the energy density parameters of the GWs induced by the power spectrum of $\mathcal{P}_\zeta(k) = 2.1 \times 10^{-9}(k/0.05\,{\rm Mpc}^{-1})^{-0.04}\Theta(k_{\rm max} - k)$. We take $k_{\rm max} = 10^{14}{\rm Mpc}^{-1}$ for all these three lines and $\eta_{\rm R} = 450/k_{\rm max}$, $\eta_{\rm R} = 200/k_{\rm max}$ and $\eta_{\rm R} = 100/k_{\rm max}$ for each line, respectively.

($SNR = 1$) for each project. The numerical results are shown in Fig. 6.9. When we derive the curves, we use the approximation formulas given in Eqs. (B.71), (B.73), and (B.75) to save the computational time. In this figure, we take $T_{\rm obs} = 20$ years for SKA and $T_{\rm obs} = 1$ year for the other projects and assume no foreground for simplicity. When we obtain these plots, we have used the following relation between the conformal time and the temperature (see Sec. 4.5)

$$\frac{1}{k_{\rm eq}\eta} = \frac{1}{\sqrt{2}} \left(\frac{g_{s*,\rm eq}}{g_{s*}}\right)^{1/3} \left(\frac{g_*}{g_{\rm eq}}\right)^{1/2} \frac{T}{T_{\rm eq}} \tag{4.66}$$

$$\Rightarrow \frac{\eta_{\rm R}}{10^{-14}{\rm Mpc}} = \left(\frac{g_s}{106.75}\right)^{1/3} \left(\frac{g}{106.75}\right)^{-1/2} \left(\frac{T_{\rm R}}{1.2\times 10^7 {\rm GeV}}\right)^{-1}. \tag{6.33}$$

We also plot the parameter region that could be contaminated by the extragalactic foreground, imposing that the energy density parameter of the foreground should be smaller than that of the induced GWs at the peak scale. Note again that the peak scale of the induced GWs corresponds to $k \sim k_{\rm max}$, not $k \sim 1/\eta_{\rm R}$. Figure 6.9 shows that, in the case of $k_{\rm max}\eta_{\rm R} = 450$, the ranges of reheating temperature that future observations could investigate are $T_{\rm R} \lesssim 7\times 10^{-2}\,{\rm GeV}$ for SKA, $20\,{\rm GeV} \lesssim T_{\rm R} \lesssim 4\times 10^3\,{\rm GeV}$ for LISA, $20\,{\rm GeV} \lesssim T_{\rm R} \lesssim 1\times 10^7\,{\rm GeV}$ for DECIGO, $20\,{\rm GeV} \lesssim T_{\rm R} \lesssim 2\times 10^7\,{\rm GeV}$ for BBO, and $4\times 10^5\,{\rm GeV} \lesssim T_{\rm R} \lesssim 2\times 10^7\,{\rm GeV}$ for ET. Note that we have implicitly assumed the standard thermal history (no entropy production after the sudden reheating) in this section, as we do in Chap. 5. If entropy production occurs after the GWs are induced, the parameter region in $T_{\rm R}$ and $k_{\rm max}\eta_{\rm R}$ that can be investigated would become smaller.

6.2.4 Discussion

In this subsection, we discuss the results.

Since the enhancement of the induced GWs we find is so significant, one may wonder whether the backreaction, which we have not taken into account, is important or not. We have seen that the energy density of the induced GWs is $\Omega_{\rm GW}(\eta_{\rm c}) \sim 10^{12} A_s^2 \sim \mathcal{O}(10^{-6})$ even for $k_{\rm max}\eta_{\rm R} = 450$ and $\mathcal{P}_\zeta = 2.1\times 10^{-9}$. Since the tensor perturbations are expected to be produced dominantly soon after the sudden transition, the power spectrum of the tensor perturbations soon after the transition is roughly estimated as $\mathcal{P}_h \sim \mathcal{O}(10\,\Omega_{\rm GW}(\eta_{\rm c}))$ (see Eq. (4.32)). The induced tensor perturbations can affect the evolution of the scalar perturbations only with the non-linear interactions. In our case, since the amplitude of the scalar perturbation $\Phi_{\boldsymbol{k}} (\sim \mathcal{O}(10^{-5}))$ is the same order of magnitude as the second-order (first $\times$ first) tensor perturbations ($\sim \mathcal{P}_h \sim \mathcal{O}(10^{-5})$), the backreaction could affect the evolution of the scalar perturbations for $k_{\rm max}\eta_{\rm R} \gtrsim 450$, the analysis of which is beyond the scope of this thesis. However, since we restrict ourselves to the case of $k_{\rm max}\eta_{\rm R} \leq 450$ to avoid the non-linear effects, we can expect the backreaction does not affect our result so much.

Next, we mention how the induced GWs depend on the amplitude of the curvature perturbations. Throughout this section, we assume that the curvature perturbations have almost scale-invariant spectrum. However, the curvature perturbations could be enhanced on the small scales, which are often discussed in the context of PBHs. In addition to the fact that the induced GWs depend on the amplitude of the scalar perturbations, the cutoff scale also depends on the amplitude. That is, the larger amplitude of the curvature perturbation leads to the larger cutoff scale (smaller $k_{\rm NL}$), which limits us to the case

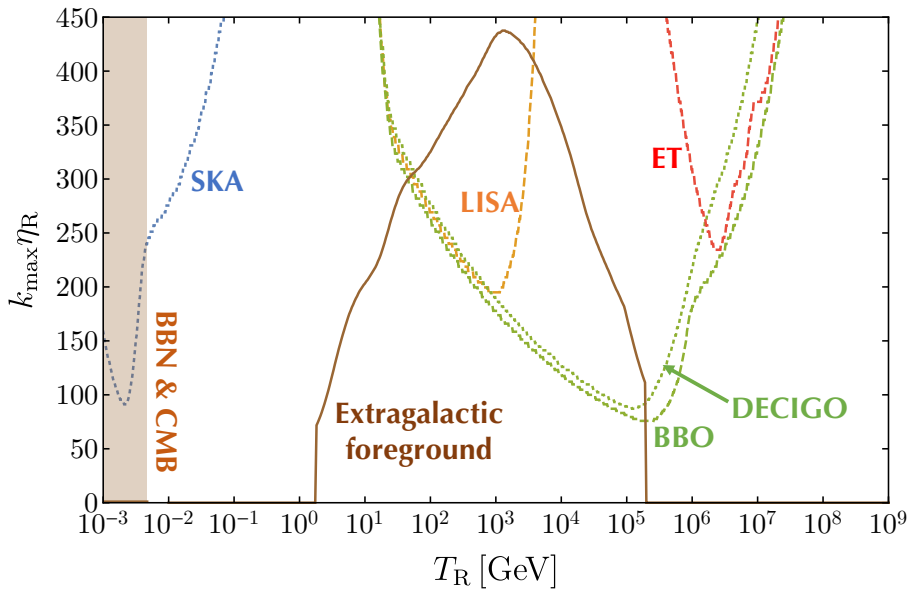

Figure 6.9: Relation between the cutoff scale multiplied by $\eta_{\rm R}$ and the reheating temperature that can be probed by the future observations. We take $T_{\rm obs} = 20$ years for SKA and $T_{\rm obs} = 1$ year for the others. The curves correspond to the values of $k_{\max}\eta_{\rm R}$ required to reach the signal-to-noise ratio of unity ($SNR = 1$) for the experiments at each reheating temperature. The regions above the dotted and dashed lines are accessible by the future observations. The brown shaded region is already excluded by the BBN and the Planck data [193]. The brown solid line shows the foreground and the region below the solid line could be contaminated by the foreground.

of shorter length of an eMD era. Here, we roughly estimate the maximum height of the GW spectrum that we can predict with the linear theory taking into account the dependence of non-linear cutoff scale on the amplitude of the curvature perturbations. From Eq. (6.21), we can see that the non-linear scale is related to the power spectrum as $k_{\rm NL}\eta_{\rm R} \propto \mathcal{P}_\zeta^{-1/4}$. Then, from Eq. (6.32), we find that the maximum height of the GW spectrum is related to the power spectrum as

$$\begin{aligned}\Omega_{\rm GW}(k_{\rm NL}, \eta_{\rm c}) &\sim \mathcal{O}(10^{12}) \left(\frac{k_{\rm NL}\eta_{\rm R}}{450}\right)^7 \mathcal{P}_\zeta^2 \\ &\sim \mathcal{O}(10^{-6}) \left(\frac{\mathcal{P}_\zeta}{2.1 \times 10^{-9}}\right)^{1/4} . \end{aligned} \tag{6.34}$$

Note again that, as we mentioned in Sec. 6.1.3, if the eMD era lasts long, the non-linear structures could also induce the GWs, which cannot be calculated with the linear theory. In this sense, our predictions for the induced GWs in this section are conservative.

Finally, we comment on the relation between the reheating temperature, the inflation energy scale, and the length of an eMD era. Here, we assume that an eMD era starts right after the inflation era due to the oscillation of the inflaton. Since the energy density decays proportionally to $a^{-3} \propto \eta^{-6}$ during an eMD era, the energy density at the reheating ($\rho_{\rm R}$) is related to that during the inflation ($\rho_{\rm inf}$) as

$$\frac{\rho_{\rm R}}{\rho_{\rm inf}} \sim \left(\frac{\eta_{\rm eMD,start}}{\eta_{\rm R}}\right)^6 , \tag{6.35}$$

where $\eta_{\rm eMD,start}$ is the conformal time at the beginning of the eMD era. In the case where the duration of the eMD era is given as $\eta_{\rm R} \sim \mathcal{O}(100)\eta_{\rm eMD,start}$, which we mainly consider throughout this section, the energy density at the reheating can be expressed as $\rho_{\rm R} \sim \mathcal{O}(10^{-12}\rho_{\rm inf})$.

Chapter 7

Conclusion

In this thesis, we have discussed the GWs induced by scalar perturbations in the early Universe. In Part I (Chaps. 2-4), we have derived the basic formulas for the induced GWs from the Einstein equation. Using the derived formulas, we have studied the induced GWs from two aspects in Part II. One is the aspect of the amplitude of small-scale perturbations (Chap. 5) and the other is the aspect of the effects of an eMD era on the induced GWs (Chap. 6).

In Chap. 5, we have discussed the constraints on the small-scale perturbations with the use of the induced GWs. Although the small-scale perturbations could produce PBHs and therefore have drawn attention from many authors, the amplitude of the small-scale perturbations are difficult to measure from CMB or LSS observations. On the other hand, if the small-scale scalar perturbations are large, the induced GWs also could become so large that the future GW detectors can measure the GWs. From this fact, we have derived the amplitude of the scalar perturbations that the future detectors can investigate (Fig. 5.4). Since Assadullahi & Wands studied this topic in Ref. [146], we briefly emphasize what is new in our work again. First, we have updated the formulas for the induced GWs because the formulas have been corrected since the previous work appeared. Second, we have improved the analyses taking into account the profile of the power spectrum of the curvature perturbations and the signal-to-noise ratio for each future observation, which have not been considered in the previous work.

In Chap. 6, we have studied the effects of an eMD era on the induced GWs. Although the effects of an eMD era are discussed in the previous works [81, 107, 108], we have shown that the results in the previous works are not correct, taking into account the evolution of the perturbations before, during, and after the transition from an eMD era to the RD era carefully. As concrete examples, we have considered two cases. One is the gradual transition, whose timescale is comparable to the Hubble timescale at that time, and the other is the sudden transition, whose timescale is much shorter than the Hubble timescale.

In Sec. 6.1, we have discussed the effects in the case of the gradual transition. To be concrete, we have considered the case where the massive particles dominating the Universe during the eMD era decay to radiation with a constant decay rate. Then, we have found that the gravitational potential decays gradually during the transition (Fig. 6.2) and it leads to the decay of tensor perturbations during the transition (Fig. 6.5). We have taken into account the decay of tensor perturbations during the transition for the first time and shown the induced GWs are suppressed compared to the previous results (Fig. 6.4).

In Sec. 6.2, we have considered the case of the sudden transition. In this case, the

GWs are mainly induced by the scalar perturbations that entered the horizon during an eMD era, whose contributions have been implicitly ignored in the previous works. After the sudden transition, the scalar perturbations start to oscillate with the timescale much shorter than the Hubble timescale at that time. This fast oscillation of the scalar perturbation enhances the induced GWs much (Fig. 6.7). The enhanced GWs could be detected by future observations (Fig. 6.8) and enable us to determine the reheating temperature (Fig. 6.9).

Before closing this thesis, we stress that the results in this thesis can be a platform to discuss the early Universe in terms of the induced GWs. From our results, we can say that a detection or null detection of the induced GWs with the future detectors could shed light on the evolution of the early Universe from the viewpoints of the amplitude of small-scale perturbations or the reheating following an eMD era.

Acknowledgments

First of all, I would like to express my utmost gratitude to my advisor, Masahiro Kawasaki, for his advice during my Ph.D. course. Thanks to him, I learned the fun of working on cosmology. I am also grateful to my collaborators, Kazunori Kohri, Tomohiro Nakama, and Takahiro Terada for their enthusiastic discussions. Without their collaborations, I could not complete this thesis. I would also like to thank the examiners, Jun'ichi Yokoyama (chair), Yasushi Suto, Koichi Hamaguchi, Masahiro Takada, and Shinji Miyoki, for constructive comments on this thesis. I am also thankful to the members of ICRR theory group for exciting discussions. Thanks to them, I got broad interests in cosmology. I would also like to express my thanks to Aya Minami, Shun Minami and Nozomi Morimura for fruitful conversations at Kashiwa Open Campus. Thanks to the conversations, I got more motivation.

Finally, I would like to express my deepest gratitude to my parents, Masaru and Miyuki Inomata, for their continuous support. Thanks to them, I had a really good time in my Ph.D. course.

Appendix A

A model that realizes a sudden-reheating transition

In this appendix, we build a concrete model in which the reheating happens in a timescale much shorter than the Hubble timescale at that time. This ensures that Φ does not decay during the reheating transition, leading to the enhancement of induced GWs, shown in Sec. 6.2.

Our idea for a sudden reheating is to initially block the decay of the field ϕ, dominating the energy density in the eMD era, into relativistic daughter particles, collectively denoted by χ, for some reason related to kinematics or symmetry, and then to remove the cause of the blocking in a dynamical manner. For this purpose, we introduce a field τ, which dynamically triggers the decay of ϕ into χ. We dub such a field τ 'triggeron'. In the models we discuss below, the mass of χ is dependent on the field value of τ and a quick change of that field value causes a sudden decay of ϕ to χ, which we identify as a sudden reheating.

A.1 A scenario for a sudden reheating triggered by a fast-rolling field

The main ideas of this model are as follows. At first, the initial triggeron value is sufficiently large so that the decay of ϕ into two χ particles is kinematically forbidden. When the Hubble parameter becomes comparable to the triggeron mass m, the triggeron starts to roll down its potential quickly, and it passes through some critical value at which the decay channel of ϕ opens. If the decay rate is much larger than the Hubble scale, the reheating transition completes quickly.

We consider a simple model that involves three canonically normalized real scalar fields ϕ, τ, and χ to demonstrate the ideas. One can easily generalize this model by considering e.g. complex scalar fields, fermions, or gauge bosons. The Lagrangian density we assume is

$$\mathcal{L} = -\frac{1}{2}\partial^\mu\phi\partial_\mu\phi - \frac{1}{2}\partial^\mu\chi\partial_\mu\chi - \frac{1}{2}\partial^\mu\tau\partial_\mu\tau - V, \tag{A.1}$$

$$V = \frac{1}{2}M^2\phi^2 + \frac{1}{2}m^2\tau^2 + \frac{\lambda}{4}\tau^2\chi^2 + \frac{c}{2}M\phi\chi^2, \tag{A.2}$$

where M and m denote the masses of ϕ and τ, respectively, satisfying $M^2 \gg m^2$, and λ and c are dimensionless coupling constants. The third term in the potential can be

interpreted as the τ-dependent mass term for χ, and the last term provides the decay channel of ϕ into 2 χ particles, once the decay becomes kinematically allowed. The decay rate of ϕ into 2 χ particles is [126]

$$\Gamma = \frac{c^2 M}{32\pi}\sqrt{1 - \frac{m_{\chi,\mathrm{eff}}^2}{(M/2)^2}}\Theta\left(M^2 - 4m_{\chi,\mathrm{eff}}^2\right), \tag{A.3}$$

where $m_{\chi,\mathrm{eff}}^2 = \langle\lambda\tau^2/2\rangle$ is the effective mass squared of χ and it is determined by the time-dependent expectation value of τ, as mentioned above. Note that the decay rate is non-zero only when the decay is kinematically possible, i.e., $m_{\chi,\mathrm{eff}} < M/2$, otherwise, it vanishes. The critical value of triggeron field at which the decay channel opens is $\tau_\mathrm{c} = M/\sqrt{2\lambda}$.[1]

There are some conditions for this scenario to work. Obviously, the initial field value of triggeron τ_0 should be large enough to satisfy $\tau_0 > \tau_\mathrm{c}$. (We may assume $\tau_0 \geq 0$ without loss of generality.) To make the reheating transition quick, the speed of τ needs to be sufficiently large when it passes through the critical point τ_c, hence we assume $\tau_0 \gg \tau_\mathrm{c}$. On the other hand, the triggeron field should not dominate the energy density, and so τ_0 should be much less than the reduced Planck mass M_P. Thus, the required condition for τ_0 is

$$\tau_\mathrm{c} \ll \tau_0 \ll M_\mathrm{P}. \tag{A.4}$$

Second, once the decay becomes kinematically possible, the typical decay rate should be much larger than the Hubble scale, $\Gamma \gg H$. This requires $c^2 M \gg m$. We also assume that τ eventually decays into radiation before it would dominate the energy density.

Let us present the time evolution of the gravitational potential Φ to show how this model works. Figure A.1 shows the evolution of Φ. We have used the equations for perturbations given in Sec. 3.4 to take into account the decay of ϕ to χ. This figure shows that the analytical expression of Φ, given in Eq. (6.26), is satisfactorily accurate in sudden-reheating scenarios.

Since ϕ and τ are independent degrees of freedom, fluctuations in τ will introduce additional curvature perturbations and non-Gaussianity due to the modulated reheating mechanism [195–199]. To estimate those quantities, let us first note that the time evolution of the triggeron is given by $\tau = \tau_0 \sin(mt)/(mt)$. The time when it reaches the minimum ($\tau = 0$) is $mt = \pi$, but it reaches the critical value slightly before. The decay time is thus estimated to be

$$mt = \pi\left(1 - \frac{\tau_c}{\tau_0}\right). \tag{A.5}$$

[1] To follow the evolution of the mass of the daughter particles χ after the decay of ϕ, we need to take into account the backreaction of the particle production effect to the dynamics of τ, whose dedicated analysis is beyond the scope of this thesis. Once most of the energy density in ϕ has been converted to a large number of χ particles when they are almost massless, energy conservation implies that τ cannot move significantly. A similar backreaction effect is discussed in the context of preheating [194]. We expect that τ is trapped around the origin and assume that the daughter particles χ remain relativistic in the following analyses. Even if the daughter particles do not behave as relativistic particles due to its varying mass, the sudden reheating is realized in the case where the daughter particles decay or annihilate to other light particles, including the Standard Model particles, within a timescale much shorter than the Hubble timescale at that time.

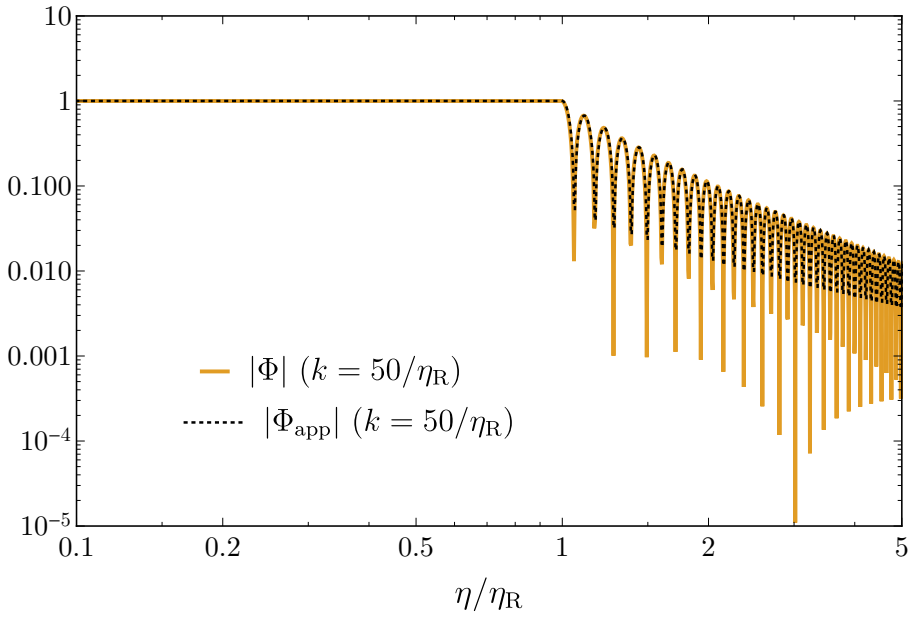

Figure A.1: Numerical results for the evolution of the gravitational potential Φ. We also plot the analytical formula of Φ, given by Eq. (6.26), with the black dotted line. We take $\lambda = 0.1$, $c = 0.1$, and $\tau_0 = 1000M$.

As discussed e.g. in Ref. [200], the e-folding number is related to the decay time as

$$e^N \propto t^{1/6}. \tag{A.6}$$

Thus, we can calculate $N' = (1/6)t'/t$ and $N'' = (1/6)(t''/t - (t'/t)^2)$ where the prime denotes differentiation with respect to τ_0, and t is evaluated at the decay time. Explicitly,

$$N' \simeq \frac{\tau_{\rm c}}{6\tau_0^2}, \qquad N'' \simeq -\frac{\tau_{\rm c}}{3\tau_0^3}, \tag{A.7}$$

noting $\tau_c \ll \tau_0$. Using these values, we obtain

$$\mathcal{P}_{\zeta^{(\tau)}} = (N'\delta\tau_0)^2 \simeq \frac{1}{36}\left(\frac{\tau_c}{\tau_0}\right)^2\left(\frac{H_{\rm inf}}{2\pi\tau_0}\right)^2, \tag{A.8}$$

where $\zeta^{(\tau)}$ is the contribution to the total curvature perturbation (ζ) from τ. We can see that if $\tau_0 \gg \tau_{\rm c}$ is satisfied, we can naively expect $\mathcal{P}_{\zeta^{(\tau)}} \ll \mathcal{P}_\zeta$. We also mention the non-Gaussianity parameter $f_{\rm NL}$, which is related to the three-point correlation function as [200]

$$\langle\zeta_{\boldsymbol{k}_1}\zeta_{\boldsymbol{k}_2}\zeta_{\boldsymbol{k}_3}\rangle = (2\pi)^3\delta(\boldsymbol{k}_1+\boldsymbol{k}_2+\boldsymbol{k}_3)\frac{6}{5}f_{\rm NL}\left[\frac{2\pi^2}{k_1^3}\mathcal{P}_\zeta(k_1)\frac{2\pi^2}{k_2^3}\mathcal{P}_\zeta(k_2) + \text{cyclic permutations}\right]. \tag{A.9}$$

Using Eq. (A.7), we obtain

$$f_{\rm NL} = \frac{5}{6}\left(\frac{\mathcal{P}_{\zeta^{(\tau)}}}{\mathcal{P}_\zeta}\right)^2\frac{N''}{(N')^2} \simeq -10\left(\frac{\mathcal{P}_{\zeta^{(\tau)}}}{\mathcal{P}_\zeta}\right)^2\frac{\tau_0}{\tau_c}. \tag{A.10}$$

Note that $f_{\rm NL}$ appears to contain a large factor τ_0/τ_c, but the above expression implicitly contains the inverse of this factor with a higher power in $(\mathcal{P}_{\zeta^{(\tau)}}/\mathcal{P}_\zeta)^2$. Hence, $f_{\rm NL}$ can be sufficiently small. We conclude that non-Gaussianity can be small enough to be consistent with observations provided that $\tau_0 \gg \tau_{\rm c}$ is satisfied.

Let us interpret the above model. It is quite natural that the decay of a field is prohibited by some symmetry. For example, the lightest particle charged under some unbroken symmetry is absolutely stable. This is usually applied to dark matter model building to explain its stability [201]. Thus, we assume that the dominant field ϕ is charged under some symmetry. If the scalar field is real, as in the above toy model, the possible charge assignment is limited, and so the scalar fields will be complex in a more realistic situation. In this context, the trigger field τ must be assumed to be a singlet (non-charged) with respect to the symmetry that protects ϕ's stability because otherwise its initial nonzero expectation value spontaneously breaks the symmetry. The daughter particle χ can be interpreted as some charged particle, initially heavier than ϕ due to its τ-dependent mass. However, it subsequently becomes lighter than ϕ, which triggers the ϕ decay. For example, we can assign ϕ charge $+2$ and χ charge -1. Or, we can assign ϕ and χ the same charge and introduce a chargeless field χ' with an interaction such as $\phi\chi^\dagger\chi'$. In this way, various generalizations of our simple model would be possible. The produced relativistic χ particles and antiparticles are assumed to produce a thermal bath containing Standard Model particles through scattering and annihilation, which reheats the Universe.

Alternatively, we may interpret τ as some symmetry breaking field. When a symmetry is broken, it is often the case that charged fields (corresponding to χ) become massive. For example, the Higgs mechanism makes gauge bosons massive. In the Standard Model, it also makes fermions massive through Yukawa interactions. One of the flat directions in the minimal supersymmetric standard model [202] would be a good candidate for this purpose since most of the fields in the theory (corresponding to χ) can be massive when it obtains a finite expectation value. In this case, all the possible decay channels of ϕ must be kinematically blocked or sufficiently suppressed.

A.2 Another sudden-reheating scenario realized by a field that experiences a first-order phase transition

Suppose that ϕ is protected by a symmetry from decaying, without any decay channels of ϕ to lighter particles. Let us further assume that τ is charged under the symmetry and is too heavy for ϕ to decay into. There may be an interaction term of the form

$$\mathcal{L} = c\tau\phi\chi\chi + \dots, \tag{A.11}$$

where c is a coupling constant. Suppose that initially the field value of τ is zero, to be contrasted with the previous model. Then the decay of ϕ becomes possible once τ acquires a finite vacuum expectation value, thereby spontaneously breaking the symmetry.

Such a symmetry-breaking phase transition can occur suddenly if the phase transition is first order. The transition occurs through the tunneling effect, and the tunneling rate is exponentially sensitive to the cosmic temperature (to be more precise, the temperature of the thermal bath to which τ is coupled), and hence such a transition is sudden [203].

After the transition, ϕ becomes able to decay into χ particles. Provided that this decay rate is much larger than the Hubble parameter, the decay completes within a timescale much shorter than the Hubble timescale at that time. Associated with the decay of ϕ, the temperature increases, which may restore the symmetry temporarily. Thus, the importance of the backreaction to the decay of ϕ requires a further study. Eventually, the temperature decreases and τ settles to the symmetry-breaking vacuum.

One way to suppress the backreaction may be to assume that the initial thermal bath is made up of a hidden sector with τ being a portal to the visible sector. Then, the increase in the temperature felt by τ would not be significantly affected by the decay of ϕ.

Appendix B

Approximate analytic formulas for induced gravitational waves

In this Appendix, we derive approximate analytic formulas for the spectrum of induced GWs in sudden-reheating scenarios.

B.1 General integral formulas for GWs induced during RD era

First, we briefly summarize the general integral formulas to calculate GWs induced during a RD era, derived in Ref. [81].

For convenience, we consider the following quantity

$$\mathcal{I}_{\rm RD}(u,v,x_1,x_2)=\int_{x_1}^{x_2}{\rm d}\bar{x}\,\bar{x}(C\sin\bar{x}+D\cos\bar{x})\tilde{f}_{\rm RD}(u,v,\bar{x})|_{\Phi(\bar{x})=3\sqrt{3}(Aj_1(\bar{x}/\sqrt{3})+By_1(\bar{x}/\sqrt{3}))/\bar{x}}, \tag{B.1}$$

where A and B are coefficients that might depend on k and η_1 and C and D are coefficients that might depend on k and η_2. The function $\tilde{f}_{\rm RD}$ is defined as[1]

$$\tilde{f}_{\rm RD}(u,v,\bar{x})=3\Phi(u\bar{x})\Phi(v\bar{x})+\bar{\eta}(\Phi'(u\bar{x})\Phi(v\bar{x})+\Phi(u\bar{x})\Phi'(v\bar{x}))+\bar{\eta}^2\Phi'(u\bar{x})\Phi'(v\bar{x}). \tag{B.2}$$

Since we introduce the coefficients A and B, $\tilde{f}_{\rm RD}$ can be different from $f_{\rm RD}$, defined in Eq. (4.49). After substituting $\Phi(\bar{x})=3\sqrt{3}(Aj_1(\bar{x}/\sqrt{3})+By_1(\bar{x}/\sqrt{3}))/\bar{x}$, we derive

$$\begin{aligned}\tilde{f}_{\rm RD}(u,v,\bar{x})=&\frac{9}{4u^3v^3\bar{x}^6}\left(E^{\cos,v-u}\cos\frac{(v-u)\bar{x}}{\sqrt{3}}+E^{\sin,v-u}\sin\frac{(v-u)\bar{x}}{\sqrt{3}}\right.\\&\left.+E^{\cos,v+u}\cos\frac{(v+u)\bar{x}}{\sqrt{3}}+E^{\sin,v+u}\sin\frac{(v+u)\bar{x}}{\sqrt{3}}\right),\end{aligned} \tag{B.3}$$

[1]Note that the coefficients in $\tilde{f}_{\rm RD}$ are different from those in $f_{\rm RD}$ in Ref. [81] because the normalization of f in this thesis is different from that adopted in Ref. [81].

where the functions E are given as

$$\begin{aligned}
E^{\cos,v-u} =&6\Big(2\sqrt{3}(A(u)B(v)-A(v)B(u))(u-v)\bar{x}(9+uv\bar{x}^2)\\
&+(A(u)A(v)+B(u)B(v))(54-6(u^2+v^2-3uv)\bar{x}^2+u^2v^2\bar{x}^4)\Big), \qquad \text{(B.4)}\\
E^{\cos,v+u} =&-6\Big(2\sqrt{3}(A(u)B(v)+A(v)B(u))(u+v)\bar{x}(-9+uv\bar{x}^2)\\
&+(A(u)A(v)-B(u)B(v))(54-6(u^2+v^2+3uv)\bar{x}^2+u^2v^2\bar{x}^4)\Big), \qquad \text{(B.5)}\\
E^{\sin,v-u} =&-6\Big(2\sqrt{3}(A(u)A(v)+B(u)B(v))(u-v)\bar{x}(9+uv\bar{x}^2)\\
&+(A(v)B(u)-A(u)B(v))(54-6(u^2+v^2-3uv)\bar{x}^2+u^2v^2\bar{x}^4)\Big), \qquad \text{(B.6)}\\
E^{\sin,v+u} =&6\Big(2\sqrt{3}(A(u)A(v)-B(u)B(v))(u+v)\bar{x}(-9+uv\bar{x}^2)\\
&+(A(u)B(v)+A(v)B(u))(-54+6(u^2+v^2+3uv)\bar{x}^2-u^2v^2\bar{x}^4)\Big), \qquad \text{(B.7)}
\end{aligned}$$

where we explicitly write the arguments u and v for A and B because they might depend on k. To perform the integral in $\mathcal{I}_{\rm RD}$ with Mathematica, we rearrange the integrand as

$$\begin{aligned}
\mathcal{I}_{\rm RD}(u,v,x_1,x_2)=\frac{9}{4}\int_{x_1}^{x_2}\mathrm{d}\bar{x}\sum_{m=1}^{5}\Bigg(&\frac{M_m^{\cos,--}}{\bar{x}^m}\cos y^{--}+\frac{M_m^{\cos,+-}}{\bar{x}^m}\cos y^{+-}+\frac{M_m^{\cos,-+}}{\bar{x}^m}\cos y^{-+}\\
&+\frac{M_m^{\cos,++}}{\bar{x}^m}\cos y^{++}+\frac{M_m^{\sin,--}}{\bar{x}^m}\sin y^{--}+\frac{M_m^{\sin,+-}}{\bar{x}^m}\sin y^{+-}\\
&+\frac{M_m^{\sin,-+}}{\bar{x}^m}\sin y^{-+}+\frac{M_m^{\sin,++}}{\bar{x}^m}\sin y^{++}\Bigg), \qquad \text{(B.8)}
\end{aligned}$$

where the coefficient M_m is independent of $\bar{x}$ and the function y is given as $y^{\pm\pm}=\left(1\pm\frac{v\pm u}{\sqrt{3}}\right)\bar{x}$, e.g. $y^{-+}=\left(1-\frac{v+u}{\sqrt{3}}\right)\bar{x}$. The concrete expressions of M_m are given by

$$\begin{aligned}
M_1^{\cos,--}&=\frac{3}{uv}H^{--}, \qquad \text{(B.9)}\\
M_2^{\cos,--}&=-\frac{6\sqrt{3}(u-v)}{u^2v^2}I^{--}, \qquad \text{(B.10)}\\
M_3^{\cos,--}&=-\frac{18(u^2-3uv+v^2)}{u^3v^3}H^{--}, \qquad \text{(B.11)}\\
M_4^{\cos,--}&=-\frac{54\sqrt{3}(u-v)}{u^3v^3}I^{--}, \qquad \text{(B.12)}\\
M_5^{\cos,--}&=\frac{162}{u^3v^3}H^{--}, \qquad \text{(B.13)}\\
M_1^{\cos,+-}&=\frac{3}{uv}H^{+-}, \qquad \text{(B.14)}\\
M_2^{\cos,+-}&=\frac{6\sqrt{3}(u-v)}{u^2v^2}I^{+-}, \qquad \text{(B.15)}\\
M_3^{\cos,+-}&=-\frac{18(u^2-3uv+v^2)}{u^3v^3}H^{+-}, \qquad \text{(B.16)}\\
M_4^{\cos,+-}&=\frac{54\sqrt{3}(u-v)}{u^3v^3}I^{+-}, \qquad \text{(B.17)}\\
M_5^{\cos,+-}&=\frac{162}{u^3v^3}H^{+-}, \qquad \text{(B.18)}
\end{aligned}$$

$$M_1^{\cos,-+} = \frac{3}{uv} H^{-+}, \tag{B.19}$$

$$M_2^{\cos,-+} = -\frac{6\sqrt{3}(u+v)}{u^2v^2} I^{-+}, \tag{B.20}$$

$$M_3^{\cos,-+} = -\frac{18(u^2+3uv+v^2)}{u^3v^3} H^{-+}, \tag{B.21}$$

$$M_4^{\cos,-+} = \frac{54\sqrt{3}(u+v)}{u^3v^3} I^{-+}, \tag{B.22}$$

$$M_5^{\cos,-+} = \frac{162}{u^3v^3} H^{-+}, \tag{B.23}$$

$$M_1^{\cos,++} = \frac{3}{uv} H^{++}, \tag{B.24}$$

$$M_2^{\cos,++} = \frac{6\sqrt{3}(u+v)}{u^2v^2} I^{++}, \tag{B.25}$$

$$M_3^{\cos,++} = -\frac{18(u^2+3uv+v^2)}{u^3v^3} H^{++}, \tag{B.26}$$

$$M_4^{\cos,++} = -\frac{54\sqrt{3}(u+v)}{u^3v^3} I^{++}, \tag{B.27}$$

$$M_5^{\cos,++} = \frac{162}{u^3v^3} H^{++}, \tag{B.28}$$

$$M_1^{\sin,--} = \frac{3}{uv} I^{--}, \tag{B.29}$$

$$M_2^{\sin,--} = \frac{6\sqrt{3}(u-v)}{u^2v^2} H^{--}, \tag{B.30}$$

$$M_3^{\sin,--} = -\frac{18(u^2-3uv+v^2)}{u^3v^3} I^{--}, \tag{B.31}$$

$$M_4^{\sin,--} = \frac{54\sqrt{3}(u-v)}{u^3v^3} H^{--}, \tag{B.32}$$

$$M_5^{\sin,--} = \frac{162}{u^3v^3} I^{--}, \tag{B.33}$$

$$M_1^{\sin,+-} = \frac{3}{uv} I^{+-}, \tag{B.34}$$

$$M_2^{\sin,+-} = -\frac{6\sqrt{3}(u-v)}{u^2v^2} H^{+-}, \tag{B.35}$$

$$M_3^{\sin,+-} = -\frac{18(u^2-3uv+v^2)}{u^3v^3} I^{+-}, \tag{B.36}$$

$$M_4^{\sin,+-} = -\frac{54\sqrt{3}(u-v)}{u^3v^3} H^{+-}, \tag{B.37}$$

$$M_5^{\sin,+-} = \frac{162}{u^3v^3} I^{+-}, \tag{B.38}$$

$$M_1^{\sin,-+} = \frac{3}{uv} I^{-+}, \tag{B.39}$$

$$M_2^{\sin,-+} = \frac{6\sqrt{3}(u+v)}{u^2v^2} H^{-+}, \tag{B.40}$$

$$M_3^{\sin,-+} = -\frac{18(u^2+3uv+v^2)}{u^3v^3} I^{-+}, \tag{B.41}$$

$$M_4^{\sin,-+} = -\frac{54\sqrt{3}(u+v)}{u^3v^3}H^{-+}, \tag{B.42}$$

$$M_5^{\sin,-+} = \frac{162}{u^3v^3}I^{-+}, \tag{B.43}$$

$$M_1^{\sin,++} = \frac{3}{uv}I^{++}, \tag{B.44}$$

$$M_2^{\sin,++} = -\frac{6\sqrt{3}(u+v)}{u^2v^2}H^{++}, \tag{B.45}$$

$$M_3^{\sin,++} = -\frac{18(u^2+3uv+v^2)}{u^3v^3}I^{++}, \tag{B.46}$$

$$M_4^{\sin,++} = \frac{54\sqrt{3}(u+v)}{u^3v^3}H^{++}, \tag{B.47}$$

$$M_5^{\sin,++} = \frac{162}{u^3v^3}I^{++}, \tag{B.48}$$

where I and H are defined as

$$\begin{aligned}
H^{--} =&(A(u)A(v)+B(u)B(v))D+(A(u)B(v)-A(v)B(u))C, && \text{(B.49)}\\
H^{+-} =&(A(u)A(v)+B(u)B(v))D+(A(v)B(u)-A(u)B(v))C, && \text{(B.50)}\\
H^{-+} =&-((A(u)A(v)-B(u)B(v))D+(A(u)B(v)+A(v)B(u))C), && \text{(B.51)}\\
H^{++} =&-((A(u)A(v)-B(u)B(v))D-(A(u)B(v)+A(v)B(u))C), && \text{(B.52)}\\
I^{--} =&(A(u)A(v)+B(u)B(v))C+(A(v)B(u)-A(u)B(v))D, && \text{(B.53)}\\
I^{+-} =&(A(u)A(v)+B(u)B(v))C+(A(u)B(v)-A(v)B(u))D, && \text{(B.54)}\\
I^{-+} =&-((A(u)A(v)-B(u)B(v))C-(A(u)B(v)+A(v)B(u))D), && \text{(B.55)}\\
I^{++} =&-((A(u)A(v)-B(u)B(v))C+(A(u)B(v)+A(v)B(u))D). && \text{(B.56)}
\end{aligned}$$

To simplify the expression for $m \geq 2$, we use the integration by parts given as

$$\begin{aligned}
\int_{x_1}^{x_2} \mathrm{d}\bar{x}\frac{\sin(\alpha\bar{x}+\phi)}{x^m} =& \left[\sum_{k=0}^{m-2}\frac{(m-k-2)!}{(m-1)!}\alpha^k \sin\left(\alpha x+\phi+\frac{(k+2)}{2}\pi\right)x^{1+k-m}\right]_{x_1}^{x_2}\\
&-\frac{\alpha^{m-1}}{(m-1)!}\int_{x_1}^{x_2}\mathrm{d}\bar{x}\frac{1}{\bar{x}}\sin\left(\alpha x+\phi+\frac{(m+1)}{2}\pi\right). \qquad \text{(B.57)}
\end{aligned}$$

Finally, we derive

$$\begin{aligned}
\mathcal{I}_{\mathrm{RD}}(u,v,x_1,x_2) =& \frac{27}{16u^3v^3}\left[\frac{1}{\bar{x}^4}\left(F^{--}\cos y^{--}+F^{+-}\cos y^{+-}+F^{-+}\cos y^{-+}+F^{++}\cos y^{++}\right.\right.\\
&\qquad +G^{--}\sin y^{--}+G^{+-}\sin y^{+-}\\
&\qquad \left.\left.+G^{-+}\sin y^{-+}+G^{++}\sin y^{++}\right)\right]_{x_1}^{x_2}\\
&+\frac{27(u^2+v^2-3)^2}{16u^3v^3}\left[H^{--}\mathrm{Ci}(y^{--})+H^{+-}\mathrm{Ci}(y^{+-})\right.\\
&\qquad +H^{-+}\mathrm{Ci}(|y^{-+}|)+H^{++}\mathrm{Ci}(y^{++})\\
&\qquad +I^{--}\mathrm{Si}(y^{--})+I^{+-}\mathrm{Si}(y^{+-})\\
&\qquad \left.+I^{-+}\mathrm{Si}(y^{-+})+I^{++}\mathrm{Si}(y^{++})\right]_{x_1}^{x_2}, \qquad \text{(B.58)}
\end{aligned}$$

where the functions F and G are given as

$$\begin{aligned}
F^{--} =& I^{--}\left(18(-1+\sqrt{3}(u-v))\bar{x}+(-3+\sqrt{3}(u-v))((u+v)^2-3)\bar{x}^3\right)\\
&-H^{--}\left(54-3(3+u^2+v^2-6uv+2\sqrt{3}(v-u))\bar{x}^2\right), \qquad \text{(B.59)}\\
F^{+-} =& -I^{+-}\left(18(1+\sqrt{3}(u-v))\bar{x}+(3+\sqrt{3}(u-v))((u+v)^2-3)\bar{x}^3\right)\\
&-H^{+-}\left(54-3(3+u^2+v^2-6uv+2\sqrt{3}(u-v))\bar{x}^2\right), \qquad \text{(B.60)}\\
F^{-+} =& -I^{-+}\left(18(1+\sqrt{3}(u+v))\bar{x}+(3+\sqrt{3}(u+v))((u-v)^2-3)\bar{x}^3\right)\\
&-H^{-+}\left(54-3(3+u^2+v^2+6uv+2\sqrt{3}(u+v))\bar{x}^2\right), \qquad \text{(B.61)}\\
F^{++} =& I^{++}\left(18(-1+\sqrt{3}(u+v))\bar{x}+(-3+\sqrt{3}(u+v))((u-v)^2-3)\bar{x}^3\right)\\
&-H^{++}\left(54-3(3+u^2+v^2+6uv-2\sqrt{3}(u+v))\bar{x}^2\right), \qquad \text{(B.62)}\\
G^{--} =& -H^{--}\left(18(-1+\sqrt{3}(u-v))\bar{x}+(-3+\sqrt{3}(u-v))((u+v)^2-3)\bar{x}^3\right)\\
&-I^{--}\left(54-3(3+u^2+v^2-6uv+2\sqrt{3}(v-u))\bar{x}^2\right), \qquad \text{(B.63)}\\
G^{+-} =& H^{+-}\left(18(1+\sqrt{3}(u-v))\bar{x}+(3+\sqrt{3}(u-v))((u+v)^2-3)\bar{x}^3\right)\\
&-I^{+-}\left(54-3(3+u^2+v^2-6uv+2\sqrt{3}(u-v))\bar{x}^2\right), \qquad \text{(B.64)}\\
G^{-+} =& H^{-+}\left(18(1+\sqrt{3}(u+v))\bar{x}+(3+\sqrt{3}(u+v))((u-v)^2-3)\bar{x}^3\right)\\
&-I^{-+}\left(54-3(3+u^2+v^2+6uv+2\sqrt{3}(u+v))\bar{x}^2\right), \qquad \text{(B.65)}\\
G^{++} =& -H^{++}\left(18(-1+\sqrt{3}(u+v))\bar{x}+(-3+\sqrt{3}(u+v))((u-v)^2-3)\bar{x}^3\right)\\
&-I^{++}\left(54-3(3+u^2+v^2+6uv-2\sqrt{3}(u+v))\bar{x}^2\right). \qquad \text{(B.66)}
\end{aligned}$$

Note that if we substitute $A=1$, $B=0$, $C=-\cos x$, $D=\sin x$, $x_1\to 0$, and $x_2=x$ into Eq. (B.58), we can see that $\lim_{x\to\infty}x^{-1}\mathcal{I}_{\rm RD}$ reproduces Eq. (4.52).

B.2 Analytical formulas for sudden reheating

Now, we discuss the case of the sudden reheating. As we can see in Fig. A.1, Φ can be well approximated by Eq. (6.26) in sudden-reheating scenarios. The explicit forms of the coefficients A and B in Eqs. (6.29) and (6.30) are

$$A(x_{\rm R})=\left(-\frac{x_{\rm R}^2}{36}+1\right)\cos\frac{x_{\rm R}}{2\sqrt{3}}+\frac{\sqrt{3}}{6}x_{\rm R}\sin\frac{x_{\rm R}}{2\sqrt{3}}, \qquad \text{(B.67)}$$

$$B(x_{\rm R})=\left(-\frac{x_{\rm R}^2}{36}+1\right)\sin\frac{x_{\rm R}}{2\sqrt{3}}-\frac{\sqrt{3}}{6}x_{\rm R}\cos\frac{x_{\rm R}}{2\sqrt{3}}. \qquad \text{(B.68)}$$

We substitute the above A and B as well as $C=-\cos(x-x_{\rm R}/2)$ and $D=\sin(x-x_{\rm R}/2)$ into Eq. (B.58) with x_1 and x_2 replaced by $x_{\rm R}/2$ and $x-x_{\rm R}/2$, respectively. The function I is split into two terms as in Eq. (6.22). The contribution generated during an eMD

era, $I_{\rm eMD}$, has been derived in Ref. [107] and revised in Ref. [81], and so we here mainly discuss the contribution generated during the RD era, $I_{\rm RD}$. As explained in Sec. 6.2, this behaves very differently from the counterpart for a pure RD era, which is obtained in the limit $x_{\rm R} \to 0$, because of fast oscillations of the modes that are already inside the horizon at the reheating transition. Extracting the redshift factor from the function, $I_{\rm RD} = \frac{1}{x - x_{\rm R}/2}\mathcal{I}_{\rm RD}$, we first calculate $\mathcal{I}_{\rm RD}$, which can be expressed as Eq. (B.58).

Below, we use two different approximations to obtain two main contributions. The first approximation is valid for the large-scale modes with $k \ll k_{\rm max}$, and the second approximation extracts the resonant contributions at $k \lesssim 2k_{\rm max}/\sqrt{3}$. The sum of these two contributions turns out to explain the results of numerical integrations well.

B.2.1 Large-scale approximation

As long as the scale k^{-1} under consideration is much larger than the smallest scale $k_{\rm max}^{-1}$, the integrations over u and v, wavenumbers in units of k, are dominated by the large $t(\equiv u+v-1)$ region ($t \sim x_{\rm max,R}/x_{\rm R}$), hence $tx_{\rm R} \sim x_{\rm max,R} \gg 1$. After taking the late-time ($x \gg 1$) oscillation average and changing variables from u and v to t and $s(\equiv u - v)$, we find

$$\begin{aligned}
\overline{\mathcal{I}_{\rm RD}^2} \simeq \frac{t^4 x_{\rm R}^8}{2359296}\Bigg(&\pi^2 + \pi^2\cos\frac{sx_{\rm R}}{\sqrt{3}} + 2{\rm Ci}\left(\frac{x_{\rm R}}{2} - \frac{sx_{\rm R}}{2\sqrt{3}}\right)^2 + 2{\rm Ci}\left(\frac{x_{\rm R}}{2} + \frac{sx_{\rm R}}{2\sqrt{3}}\right)^2 \\
&+ 4\cos\frac{sx_{\rm R}}{\sqrt{3}}{\rm Ci}\left(\frac{x_{\rm R}}{2} + \frac{sx_{\rm R}}{2\sqrt{3}}\right){\rm Ci}\left(\frac{x_{\rm R}}{2} - \frac{sx_{\rm R}}{2\sqrt{3}}\right) \\
&+ 2\pi\sin\frac{sx_{\rm R}}{\sqrt{3}}\left({\rm Ci}\left(\frac{x_{\rm R}}{2} + \frac{sx_{\rm R}}{2\sqrt{3}}\right) - {\rm Ci}\left(\frac{x_{\rm R}}{2} - \frac{sx_{\rm R}}{2\sqrt{3}}\right)\right) \\
&- 2\pi\left(1 + \cos\frac{sx_{\rm R}}{\sqrt{3}}\right)\left({\rm Si}\left(\frac{x_{\rm R}}{2} - \frac{sx_{\rm R}}{2\sqrt{3}}\right) + {\rm Si}\left(\frac{x_{\rm R}}{2} + \frac{sx_{\rm R}}{2\sqrt{3}}\right)\right) \\
&+ 4\sin\frac{sx_{\rm R}}{\sqrt{3}}\left({\rm Ci}\left(\frac{x_{\rm R}}{2} - \frac{sx_{\rm R}}{2\sqrt{3}}\right){\rm Si}\left(\frac{x_{\rm R}}{2} + \frac{sx_{\rm R}}{2\sqrt{3}}\right)\right. \\
&\qquad \left. - {\rm Ci}\left(\frac{x_{\rm R}}{2} + \frac{sx_{\rm R}}{2\sqrt{3}}\right){\rm Si}\left(\frac{x_{\rm R}}{2} - \frac{sx_{\rm R}}{2\sqrt{3}}\right)\right) \\
&+ 2{\rm Si}\left(\frac{x_{\rm R}}{2} - \frac{sx_{\rm R}}{2\sqrt{3}}\right)^2 + 2{\rm Si}\left(\frac{x_{\rm R}}{2} + \frac{sx_{\rm R}}{2\sqrt{3}}\right)^2 \\
&+ 4\cos\frac{sx_{\rm R}}{\sqrt{3}}{\rm Si}\left(\frac{x_{\rm R}}{2} + \frac{sx_{\rm R}}{2\sqrt{3}}\right){\rm Si}\left(\frac{x_{\rm R}}{2} - \frac{sx_{\rm R}}{2\sqrt{3}}\right)\Bigg),
\end{aligned} \tag{B.69}$$

where we have kept only terms with highest powers of t. When we vary s, the above quantity varies approximately by a factor of two at most. However, the angular factor (the factor in front of I^2 in Eq. (4.46)) in the large t limit is $(s^2-1)^2$, which suppresses the nonzero s part, and so it turns out that setting $s = 0$ is a good approximation for calculating $\Omega_{\rm GW}$ with 10% errors at most. If we set $s = 0$, it is simplified as

$$\overline{\mathcal{I}_{\rm RD}^2}|_{s=0} \simeq \frac{t^4 x_{\rm R}^8\left(4{\rm Ci}\left(\frac{x_{\rm R}}{2}\right)^2 + \left(\pi - 2{\rm Si}\left(\frac{x_{\rm R}}{2}\right)\right)^2\right)}{1179648}. \tag{B.70}$$

This expression is so simple that we can analytically integrate it over t and s. The integration region is $0 \le s \le 1$ and $0 \le t \le -s + 2\frac{x_{\rm max,R}}{x_{\rm R}} - 1$ for $x_{\rm R} \le x_{\rm max,R}$, and

$0 \le s \le 2\frac{x_{\rm max,\,R}}{x_{\rm R}} - 1$ and $0 \le t \le -s + 2\frac{x_{\rm max,R}}{x_{\rm R}} - 1$ for $x_{\rm R} > x_{\rm max,R}$. For each case, there is also an integration region obtained by the replacement $s \to -s$, but the symmetry under this inversion ensures that the total result is obtained by doubling the result obtained from the integration region with $s > 0$. Then the GW spectrum under the large-scale (LS) approximation is given as

$$\begin{aligned}\Omega^{\rm (LS)}_{\rm GW,RD}(\eta_{\rm c}, k) \simeq & \frac{4{\rm Ci}\left(\frac{x_{\rm R}}{2}\right)^2 + \left(\pi - 2{\rm Si}\left(\frac{x_{\rm R}}{2}\right)\right)^2}{86016000000} A_{\rm s}^2 x_{\rm R}^3 x_{\rm max,R}^5 \times \\ & \Big(\Theta(x_{\rm max,R} - x_{\rm R})\left(5376 - 17640\widetilde{k} + 23760\widetilde{k}^2 - 16425\widetilde{k}^3 + 5825\widetilde{k}^4 - 847\widetilde{k}^5\right) \\ & + \Theta(x_{\rm R} - x_{\rm max,R})\widetilde{k}^{-5}\left(2 - \widetilde{k}\right)^6\left(4 - 8\widetilde{k} - 9\widetilde{k}^2 + 13\widetilde{k}^3 + 49\widetilde{k}^4\right)\Big)\,,\end{aligned} \tag{B.71}$$

where $\widetilde{k} = x_{\rm R}/x_{\rm max,R} = k/k_{\rm max}$.

B.2.2 The resonant peak contributions

Here, we focus on a specific contribution in sudden-reheating scenarios which corresponds to the resonance-like peak (logarithmic divergence) at $t = \sqrt{3} - 1$ in the case of the monochromatic source in a pure RD era (see Sec. 4.4.2). The origin of the peak is the limit $x_{\rm R} \to 0$ of the Ci function. In the present case, we do not take the limit $x_{\rm R} \to 0$, but instead, we focus on contributions from the region where the integration variable t hits the zero of the Ci function, possibly causing an enhancement. For this purpose, we do not take the large t limit. Instead, we can take the large $x_{\rm R}$ limit since it turns out that this effect is most efficient for the smallest-scale modes (see Sec. 6.2.2).

We focus on the terms containing the Ci function whose argument can vanish, neglecting the other terms. Furthermore, we take the late-time limit $x \to \infty$ as well as the oscillation average. With these approximations, we find

$$\overline{\mathcal{I}^2_{\rm RD}} \approx \frac{(-5 + s^2 + 2t + t^2)^4 x_{\rm R}^8}{1179648(1 - s + t)^2(1 + s + t)^2}{\rm Ci}\left(|y|\right)^2\,, \tag{B.72}$$

where $y \equiv (t - \sqrt{3} + 1)x_{\rm R}/(2\sqrt{3})$. We focus on spiky contributions around $y = 0$ or equivalently $t = \sqrt{3} - 1$. Except for the argument of the Ci function, we may set $t = \sqrt{3} - 1$, which enables us to do the integration over s. Then, the resonant contribution to the GW spectrum is

$$\begin{aligned}\Omega^{\rm (res)}_{\rm GW,RD}(\eta_{\rm c}, k) \simeq & \int_{-s_0(x_{\rm R})}^{s_0(x_{\rm R})} {\rm d}s \frac{3(1 - s^2)^2}{81920000} A_{\rm s}^2 x_{\rm R}^8 \times 2\int_0^1 {\rm d}y {\rm Ci}(y)^2 \frac{2\sqrt{3}}{x_{\rm R}} \\ = & \frac{2.30285}{102400000}\sqrt{3} A_{\rm s}^2 x_{\rm R}^7 s_0(x_{\rm R}) \times \left(15 - 10 s_0^2(x_{\rm R}) + 3 s_0^4(x_{\rm R})\right)\,,\end{aligned} \tag{B.73}$$

where

$$s_0(x_{\rm R}) = \begin{cases} 1 & x_{\rm R} \le \frac{2x_{\rm max,R}}{1+\sqrt{3}} \\ 2\frac{x_{\rm max,R}}{x_{\rm R}} - \sqrt{3} & \frac{2x_{\rm max,R}}{1+\sqrt{3}} \le x_{\rm R} \le \frac{2x_{\rm max,R}}{\sqrt{3}} \\ 0 & \frac{2x_{\rm max,R}}{\sqrt{3}} \le x_{\rm R} \end{cases}\,. \tag{B.74}$$

In the first equality in Eq. (B.73), we have changed the integration variable from t to y with the Jacobian factor $2\sqrt{3}/x_{\rm R}$. This integration is for the spiky part, and so we limit the integration region to $|y| < 1$. The choice of the integration boundary here is somewhat arbitrary, and this causes uncertainties of order unity.

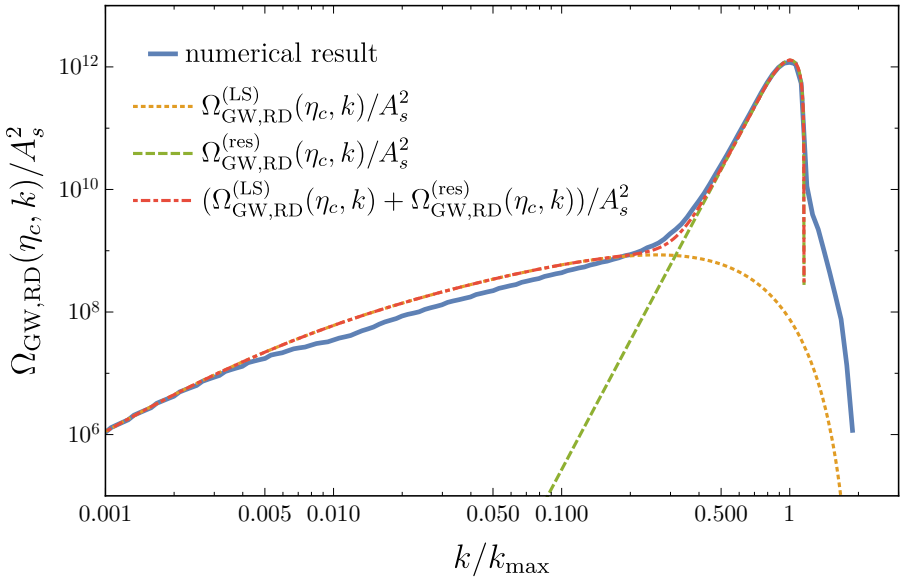

Figure B.1: Comparison of the analytic and numerical results for the induced GWs. The blue solid line shows the numerical result. The orange dotted, greed dashed, and red dot-dashed lines show the large-scale approximation [Eq. (B.71)], the resonant contribution [Eq. (B.73)], and their sum, respectively. We take the power spectrum given in Eq. (6.31) with $k_{\rm max} = 450/\eta_{\rm R}$ and $n_s = 1$.

The total spectrum is approximated by the contribution produced after the reheating transition, $\Omega_{\rm GW} \simeq \Omega_{\rm GW,RD}$, which is given by the sum of Eqs. (B.71) and (B.73):

$$\Omega_{\rm GW,RD} \simeq \Omega^{(\rm LS)}_{\rm GW,RD} + \Omega^{(\rm res)}_{\rm GW,RD}. \tag{B.75}$$

This is compared with the numerical result in Fig. B.1. From this figure, we can see that those approximate analytic formulas fit the numerical result very well.

The k dependence of $\Omega_{\rm GW}$ is summarized as follows. It is proportional to k^3, neglecting a logarithmic factor, for $k \lesssim 1/\eta_{\rm R}$, then it scales as k for $k \gtrsim 1/\eta_{\rm R}$. The slope of the resonant contribution is k^7, which peaks at $k \simeq k_{\rm max}$. Finally, it decreases sharply and vanishes at $k = 2k_{\rm max}$. This behavior is summarized in Eq. (6.32).

Bibliography

[1] **Virgo, LIGO Scientific** Collaboration, B. P. Abbott et. al., *Observation of Gravitational Waves from a Binary Black Hole Merger*, Phys. Rev. Lett. **116** (2016), no. 6 061102 [arXiv:1602.03837].

[2] A. Einstein, *Approximative Integration of the Field Equations of Gravitation*, Sitzungsber. Preuss. Akad. Wiss. Berlin (Math. Phys.) **1916** (1916) 688–696.

[3] R. A. Hulse and J. H. Taylor, *Discovery of a pulsar in a binary system*, Astrophys. J. **195** (1975) L51–L53.

[4] J. H. Taylor and J. M. Weisberg, *A new test of general relativity: Gravitational radiation and the binary pulsar PS R 1913+16*, Astrophys. J. **253** (1982) 908–920.

[5] G. Lemaitre, *A homogeneous universe of constant mass and increasing radius accounting for the radial velocity of extra-galactic nebulae*, Mon. Not. Roy. Astron. Soc. **91** (1931) 483–490.

[6] H. Bondi and T. Gold, *The Steady-State Theory of the Expanding Universe*, Mon. Not. Roy. Astron. Soc. **108** (1948) 252.

[7] F. Hoyle, *A New Model for the Expanding Universe*, Mon. Not. Roy. Astron. Soc. **108** (1948) 372–382.

[8] A. A. Penzias and R. W. Wilson, *A Measurement of excess antenna temperature at 4080-Mc/s*, Astrophys. J. **142** (1965) 419–421.

[9] R. H. Dicke, P. J. E. Peebles, P. G. Roll and D. T. Wilkinson, *Cosmic Black-Body Radiation*, Astrophys. J. **142** (1965) 414–419.

[10] R. A. Alpher, H. Bethe and G. Gamow, *The origin of chemical elements*, Phys. Rev. **73** (1948) 803–804.

[11] G. Gamow, *The Origin of Elements and the Seyaration of Galaxies*, Phys. Rev. **74** (1948) 505–506.

[12] C. Hayashi, *Proton-Neutron Concentration Ratio in the Expanding Universe at the Stages preceding the Formation of the Elements*, Prog. Theor. Phys. **5** (1950), no. 2 224–235.

[13] G. J. Mathews, M. Kusakabe and T. Kajino, *Introduction to Big Bang Nucleosynthesis and Modern Cosmology*, Int. J. Mod. Phys. **E26** (2017), no. 08 1741001 [arXiv:1706.03138].

[14] W. H. McCrea, *Cosmology after half a century*, Science **160** (1968), no. 3834 1295–1299.

[15] C. W. Misner, *Mixmaster universe*, Phys. Rev. Lett. **22** (1969) 1071–1074.

[16] R. Dicke, *Gravitation and the universe, volume 78 of memoirs of the american philosophical society, jayne lecture for 1969*, American Philosophical Society, Philadelphia, USA **82** (1970).

[17] **Planck** Collaboration, N. Aghanim et. al., *Planck 2018 results. VI. Cosmological parameters*, arXiv:1807.06209.

[18] A. A. Starobinsky, *A New Type of Isotropic Cosmological Models Without Singularity*, Phys. Lett. **91B** (1980) 99–102. [,771(1980)].

[19] K. Sato, *First Order Phase Transition of a Vacuum and Expansion of the Universe*, Mon. Not. Roy. Astron. Soc. **195** (1981) 467–479.

[20] K. Sato, *Cosmological Baryon Number Domain Structure and the First Order Phase Transition of a Vacuum*, Phys. Lett. **99B** (1981) 66–70. [Adv. Ser. Astrophys. Cosmol.3,134(1987)].

[21] D. Kazanas, *Dynamics of the Universe and Spontaneous Symmetry Breaking*, Astrophys. J. **241** (1980) L59–L63.

[22] A. H. Guth, *The Inflationary Universe: A Possible Solution to the Horizon and Flatness Problems*, Phys. Rev. **D23** (1981) 347–356. [Adv. Ser. Astrophys. Cosmol.3,139(1987)].

[23] D. H. Lyth, *What would we learn by detecting a gravitational wave signal in the cosmic microwave background anisotropy?*, Phys. Rev. Lett. **78** (1997) 1861–1863 [arXiv:hep-ph/9606387].

[24] U. Seljak, *Measuring polarization in cosmic microwave background*, Astrophys. J. **482** (1997) 6 [arXiv:astro-ph/9608131].

[25] U. Seljak and M. Zaldarriaga, *Signature of gravity waves in polarization of the microwave background*, Phys. Rev. Lett. **78** (1997) 2054–2057 [arXiv:astro-ph/9609169].

[26] M. Kamionkowski, A. Kosowsky and A. Stebbins, *A Probe of primordial gravity waves and vorticity*, Phys. Rev. Lett. **78** (1997) 2058–2061 [arXiv:astro-ph/9609132].

[27] T. Vachaspati and A. Vilenkin, *Gravitational Radiation from Cosmic Strings*, Phys. Rev. **D31** (1985) 3052.

[28] M. Sakellariadou, *Gravitational waves emitted from infinite strings*, Phys. Rev. **D42** (1990) 354–360. [Erratum: Phys. Rev.D43,4150(1991)].

[29] T. Damour and A. Vilenkin, *Gravitational wave bursts from cosmic strings*, Phys. Rev. Lett. **85** (2000) 3761–3764 [arXiv:gr-qc/0004075].

[30] A. Kosowsky, M. S. Turner and R. Watkins, *Gravitational radiation from colliding vacuum bubbles*, Phys. Rev. **D45** (1992) 4514–4535.

[31] A. Kosowsky, M. S. Turner and R. Watkins, *Gravitational waves from first order cosmological phase transitions*, Phys. Rev. Lett. **69** (1992) 2026–2029.

[32] A. Kosowsky and M. S. Turner, *Gravitational radiation from colliding vacuum bubbles: envelope approximation to many bubble collisions*, Phys. Rev. **D47** (1993) 4372–4391 [arXiv:astro-ph/9211004].

[33] M. Kamionkowski, A. Kosowsky and M. S. Turner, *Gravitational radiation from first order phase transitions*, Phys. Rev. **D49** (1994) 2837–2851 [arXiv:astro-ph/9310044].

[34] R. Easther and E. A. Lim, *Stochastic gravitational wave production after inflation*, JCAP **0604** (2006) 010 [arXiv:astro-ph/0601617].

[35] J. Garcia-Bellido and D. G. Figueroa, *A stochastic background of gravitational waves from hybrid preheating*, Phys. Rev. Lett. **98** (2007) 061302 [arXiv:astro-ph/0701014].

[36] J. Garcia-Bellido, D. G. Figueroa and A. Sastre, *A Gravitational Wave Background from Reheating after Hybrid Inflation*, Phys. Rev. **D77** (2008) 043517 [arXiv:0707.0839].

[37] J. F. Dufaux, A. Bergman, G. N. Felder, L. Kofman and J.-P. Uzan, *Theory and Numerics of Gravitational Waves from Preheating after Inflation*, Phys. Rev. **D76** (2007) 123517 [arXiv:0707.0875].

[38] K. Tomita, *Non-linear theory of gravitational instability in the expanding universe*, Progress of Theoretical Physics **37** (1967), no. 5 831–846.

[39] S. Matarrese, O. Pantano and D. Saez, *General relativistic dynamics of irrotational dust: Cosmological implications*, Phys. Rev. Lett. **72** (1994) 320–323 [arXiv:astro-ph/9310036].

[40] S. Matarrese, S. Mollerach and M. Bruni, *Second order perturbations of the Einstein-de Sitter universe*, Phys. Rev. **D58** (1998) 043504 [arXiv:astro-ph/9707278].

[41] K. N. Ananda, C. Clarkson and D. Wands, *The Cosmological gravitational wave background from primordial density perturbations*, Phys. Rev. **D75** (2007) 123518 [arXiv:gr-qc/0612013].

[42] D. Baumann, P. J. Steinhardt, K. Takahashi and K. Ichiki, *Gravitational Wave Spectrum Induced by Primordial Scalar Perturbations*, Phys. Rev. **D76** (2007) 084019 [arXiv:hep-th/0703290].

[43] R. Saito and J. Yokoyama, *Gravitational wave background as a probe of the primordial black hole abundance*, Phys. Rev. Lett. **102** (2009) 161101 [arXiv:0812.4339]. [Erratum: Phys. Rev. Lett.107,069901(2011)].

[44] R. Saito and J. Yokoyama, *Gravitational-Wave Constraints on the Abundance of Primordial Black Holes*, Prog. Theor. Phys. **123** (2010) 867–886 [arXiv:0912.5317]. [Erratum: Prog. Theor. Phys.126,351(2011)].

[45] L. Lentati et. al., *European Pulsar Timing Array Limits On An Isotropic Stochastic Gravitational-Wave Background*, Mon. Not. Roy. Astron. Soc. **453** (2015), no. 3 2576–2598 [arXiv:1504.03692].

[46] R. M. Shannon et. al., *Gravitational waves from binary supermassive black holes missing in pulsar observations*, Science **349** (2015), no. 6255 1522–1525 [arXiv:1509.07320].

[47] **NANOGrav** Collaboration, Z. Arzoumanian et. al., *The NANOGrav Nine-year Data Set: Limits on the Isotropic Stochastic Gravitational Wave Background*, Astrophys. J. **821** (2016), no. 1 13 [arXiv:1508.03024].

[48] C. J. Moore, R. H. Cole and C. P. L. Berry, *Gravitational-wave sensitivity curves*, Class. Quant. Grav. **32** (2015), no. 1 015014 [arXiv:1408.0740].

[49] G. Janssen et. al., *Gravitational wave astronomy with the SKA*, PoS **AASKA14** (2015) 037 [arXiv:1501.00127].

[50] **Virgo, LIGO Scientific** Collaboration, B. P. Abbott et. al., *GW170817: Implications for the Stochastic Gravitational-Wave Background from Compact Binary Coalescences*, Phys. Rev. Lett. **120** (2018), no. 9 091101 [arXiv:1710.05837].

[51] Virgo. http://www.virgo-gw.eu/.

[52] KAGRA. https://gwcenter.icrr.u-tokyo.ac.jp/en/.

[53] B. S. Sathyaprakash and B. F. Schutz, *Physics, Astrophysics and Cosmology with Gravitational Waves*, Living Rev. Rel. **12** (2009) 2 [arXiv:0903.0338].

[54] Einstein Telescope. http://www.et-gw.eu/.

[55] **LIGO Scientific** Collaboration, B. P. Abbott et. al., *Exploring the Sensitivity of Next Generation Gravitational Wave Detectors*, Class. Quant. Grav. **34** (2017), no. 4 044001 [arXiv:1607.08697].

[56] **LISA** Collaboration, H. Audley et. al., *Laser Interferometer Space Antenna*, arXiv:1702.00786.

[57] N. Seto, S. Kawamura and T. Nakamura, *Possibility of direct measurement of the acceleration of the universe using 0.1-Hz band laser interferometer gravitational wave antenna in space*, Phys. Rev. Lett. **87** (2001) 221103 [arXiv:astro-ph/0108011].

[58] K. Yagi and N. Seto, *Detector configuration of DECIGO/BBO and identification of cosmological neutron-star binaries*, Phys. Rev. **D83** (2011) 044011 [arXiv:1101.3940]. [Erratum: Phys. Rev.D95,no.10,109901(2017)].

[59] E. Phinney et. al., Big Bang Observer mission concept study. 2003.

[60] J. Silk, *Cosmic black body radiation and galaxy formation*, Astrophys. J. **151** (1968) 459–471.

[61] H. Satō, *Mass of a galaxy and dissipative process in the hot universe*, Progress of Theoretical Physics **45** (1971), no. 2 370–385.

[62] G. Nicholson and C. R. Contaldi, *Reconstruction of the primordial power spectrum using temperature and polarisation data from multiple experiments*, JCAP **0907** (2009) 011 [arXiv:0903.1106].

[63] G. Nicholson, C. R. Contaldi and P. Paykari, *Reconstruction of the primordial power spectrum by direct inversion*, JCAP **1001** (2010) 016 [arXiv:0909.5092].

[64] S. Bird, H. V. Peiris, M. Viel and L. Verde, *Minimally parametric power spectrum reconstruction from the lyman α forest*, Mon. Not. Roy. Astron. Soc. **413** (2011), no. 3 1717–1728 [arXiv:1010.1519].

[65] J. Yokoyama, *Chaotic new inflation and formation of primordial black holes*, Phys. Rev. **D58** (1998) 083510 [arXiv:astro-ph/9802357].

[66] M. Kawasaki and T. Yanagida, *Primordial black hole formation in supergravity*, Phys. Rev. **D59** (1999) 043512 [arXiv:hep-ph/9807544].

[67] S. Kasuya and M. Kawasaki, *Axion isocurvature fluctuations with extremely blue spectrum*, Phys. Rev. **D80** (2009) 023516 [arXiv:0904.3800].

[68] J. Garcia-Bellido and E. Ruiz Morales, *Primordial black holes from single field models of inflation*, Phys. Dark Univ. **18** (2017) 47–54 [arXiv:1702.03901].

[69] M. Sasaki, T. Suyama, T. Tanaka and S. Yokoyama, *Primordial black holes—perspectives in gravitational wave astronomy*, Class. Quant. Grav. **35** (2018), no. 6 063001 [arXiv:1801.05235].

[70] M. Ricotti and A. Gould, *A New Probe of Dark Matter and High-Energy Universe Using Microlensing*, Astrophys. J. **707** (2009) 979–987 [arXiv:0908.0735].

[71] P. Scott and S. Sivertsson, *Gamma-Rays from Ultracompact Primordial Dark Matter Minihalos*, Phys. Rev. Lett. **103** (2009) 211301 [arXiv:0908.4082]. [Erratum: Phys. Rev. Lett.105,119902(2010)].

[72] K. Kohri, T. Nakama and T. Suyama, *Testing scenarios of primordial black holes being the seeds of supermassive black holes by ultracompact minihalos and CMB μ-distortions*, Phys. Rev. **D90** (2014), no. 8 083514 [arXiv:1405.5999].

[73] T. Nakama, T. Suyama, K. Kohri and N. Hiroshima, *Constraints on small-scale primordial power by annihilation signals from extragalactic dark matter minihalos*, Phys. Rev. **D97** (2018), no. 2 023539 [arXiv:1712.08820].

[74] B. Carr, F. Kuhnel and M. Sandstad, *Primordial Black Holes as Dark Matter*, Phys. Rev. **D94** (2016), no. 8 083504 [arXiv:1607.06077].

[75] K. Inomata, M. Kawasaki, K. Mukaida, Y. Tada and T. T. Yanagida, *Inflationary Primordial Black Holes as All Dark Matter*, Phys. Rev. **D96** (2017), no. 4 043504 [arXiv:1701.02544].

[76] K. Inomata, M. Kawasaki, K. Mukaida and T. T. Yanagida, *Double inflation as a single origin of primordial black holes for all dark matter and LIGO observations*, Phys. Rev. **D97** (2018), no. 4 043514 [arXiv:1711.06129].

[77] S. Bird, I. Cholis, J. B. Muñoz, Y. Ali-Haïmoud, M. Kamionkowski, E. D. Kovetz, A. Raccanelli and A. G. Riess, *Did LIGO detect dark matter?*, Phys. Rev. Lett. **116** (2016), no. 20 201301 [arXiv:1603.00464].

[78] S. Clesse and J. García-Bellido, *The clustering of massive Primordial Black Holes as Dark Matter: measuring their mass distribution with Advanced LIGO*, Phys. Dark Univ. **15** (2017) 142–147 [arXiv:1603.05234].

[79] M. Sasaki, T. Suyama, T. Tanaka and S. Yokoyama, *Primordial Black Hole Scenario for the Gravitational-Wave Event GW150914*, Phys. Rev. Lett. **117** (2016), no. 6 061101 [arXiv:1603.08338].

[80] J. R. Espinosa, D. Racco and A. Riotto, *A Cosmological Signature of the SM Higgs Instability: Gravitational Waves*, JCAP **1809** (2018), no. 09 012 [arXiv:1804.07732].

[81] K. Kohri and T. Terada, *Semianalytic calculation of gravitational wave spectrum nonlinearly induced from primordial curvature perturbations*, Phys. Rev. **D97** (2018), no. 12 123532 [arXiv:1804.08577].

[82] R.-g. Cai, S. Pi and M. Sasaki, *Gravitational Waves Induced by non-Gaussian Scalar Perturbations*, arXiv:1810.11000.

[83] N. Bartolo, V. De Luca, G. Franciolini, M. Peloso and A. Riotto, *The Primordial Black Hole Dark Matter - LISA Serendipity*, arXiv:1810.12218.

[84] N. Bartolo, V. De Luca, G. Franciolini, M. Peloso, D. Racco and A. Riotto, *Testing Primordial Black Holes as Dark Matter through LISA*, arXiv:1810.12224.

[85] C. Unal, *Imprints of Primordial Non-Gaussianity on Gravitational Wave Spectrum*, arXiv:1811.09151.

[86] C. T. Byrnes, P. S. Cole and S. P. Patil, *Steepest growth of the power spectrum and primordial black holes*, arXiv:1811.11158.

[87] K. Inomata and T. Nakama, *Gravitational waves induced by scalar perturbations as probes of the small-scale primordial spectrum*, Phys. Rev. **D99** (2019), no. 4 043511 [arXiv:1812.00674].

[88] S. Clesse, J. García-Bellido and S. Orani, *Detecting the Stochastic Gravitational Wave Background from Primordial Black Hole Formation*, arXiv:1812.11011.

[89] R.-G. Cai, S. Pi, S.-J. Wang and X.-Y. Yang, *Resonant multiple peaks in the induced gravitational waves*, JCAP **1905** (2019), no. 05 013 [arXiv:1901.10152].

[90] Y.-F. Cai, C. Chen, X. Tong, D.-G. Wang and S.-F. Yan, *When Primordial Black Holes from Sound Speed Resonance Meet a Stochastic Background of Gravitational Waves*, Phys. Rev. **D100** (2019), no. 4 043518 [arXiv:1902.08187].

[91] S. Wang, T. Terada and K. Kohri, *Prospective constraints on the primordial black hole abundance from the stochastic gravitational-wave backgrounds produced by coalescing events and curvature perturbations*, Phys. Rev. **D99** (2019), no. 10 103531 [arXiv:1903.05924].

[92] I. Ben-Dayan, B. Keating, D. Leon and I. Wolfson, *Constraints on scalar and tensor spectra from N_{eff}*, JCAP **1906** (2019), no. 06 007 [arXiv:1903.11843].

[93] Y. Tada and S. Yokoyama, *Primordial black hole tower: Dark matter, earth-mass, and LIGO black holes*, Phys. Rev. **D100** (2019), no. 2 023537 [arXiv:1904.10298].

[94] K. Inomata, K. Kohri, T. Nakama and T. Terada, *Gravitational Waves Induced by Scalar Perturbations during a Gradual Transition from an Early Matter Era to the Radiation Era*, JCAP **1910** (2019), no. 10 071 [arXiv:1904.12878].

[95] K. Inomata, K. Kohri, T. Nakama and T. Terada, *Enhancement of Gravitational Waves Induced by Scalar Perturbations due to a Sudden Transition from an Early Matter Era to the Radiation Era*, Phys. Rev. **D100** (2019), no. 4 043532 [arXiv:1904.12879].

[96] C. Yuan, Z.-C. Chen and Q.-G. Huang, *Probing Primordial-Black-Hole Dark Matter with Scalar Induced Gravitational Waves*, arXiv:1906.11549.

[97] W.-T. Xu, J. Liu, T.-J. Gao and Z.-K. Guo, *Low-frequency Gravitational Waves from Double-inflection-point Inflation*, arXiv:1907.05213.

[98] R.-G. Cai, S. Pi, S.-J. Wang and X.-Y. Yang, *Pulsar Timing Array Constraints on the Induced Gravitational Waves*, arXiv:1907.06372.

[99] Y. Lu, Y. Gong, Z. Yi and F. Zhang, *Constraints on primordial curvature perturbations from primordial black hole dark matter and secondary gravitational waves*, arXiv:1907.11896.

[100] C. Yuan, Z.-C. Chen and Q.-G. Huang, *Log-dependent slope of scalar induced gravitational waves in the infrared regions*, arXiv:1910.09099.

[101] Z.-C. Chen, C. Yuan and Q.-G. Huang, *Pulsar Timing Array Constraints on Primordial Black Holes with NANOGrav 11-Year Data Set*, arXiv:1910.12239.

[102] F. Hajkarim and J. Schaffner-Bielich, *Thermal History of the Early Universe and Primordial Gravitational Waves from Induced Scalar Perturbations*, arXiv:1910.12357.

[103] M. S. Turner, *Coherent Scalar Field Oscillations in an Expanding Universe*, Phys. Rev. **D28** (1983) 1243.

[104] M. Khlopov, B. A. Malomed and I. B. Zeldovich, *Gravitational instability of scalar fields and formation of primordial black holes*, Mon. Not. Roy. Astron. Soc. **215** (1985) 575–589.

[105] T. Harada, C.-M. Yoo, K. Kohri, K.-i. Nakao and S. Jhingan, *Primordial black hole formation in the matter-dominated phase of the Universe*, Astrophys. J. **833** (2016), no. 1 61 [arXiv:1609.01588].

[106] T. Harada, C.-M. Yoo, K. Kohri and K.-I. Nakao, *Spins of primordial black holes formed in the matter-dominated phase of the Universe*, Phys. Rev. **D96** (2017), no. 8 083517 [arXiv:1707.03595].

[107] H. Assadullahi and D. Wands, *Gravitational waves from an early matter era*, Phys. Rev. **D79** (2009) 083511 [arXiv:0901.0989].

[108] L. Alabidi, K. Kohri, M. Sasaki and Y. Sendouda, *Observable induced gravitational waves from an early matter phase*, JCAP **1305** (2013) 033 [arXiv:1303.4519].

[109] C. Pitrou, X. Roy and O. Umeh, *xPand: An algorithm for perturbing homogeneous cosmologies*, Class. Quant. Grav. **30** (2013) 165002 [arXiv:1302.6174].

[110] D. J. Fixsen, *The Temperature of the Cosmic Microwave Background*, Astrophys. J. **707** (2009) 916–920 [arXiv:0911.1955].

[111] A. G. Riess, S. Casertano, W. Yuan, L. M. Macri and D. Scolnic, *Large Magellanic Cloud Cepheid Standards Provide a 1% Foundation for the Determination of the Hubble Constant and Stronger Evidence for Physics beyond ΛCDM*, Astrophys. J. **876** (2019), no. 1 85 [arXiv:1903.07603].

[112] **WMAP** Collaboration, G. Hinshaw et. al., *Nine-Year Wilkinson Microwave Anisotropy Probe (WMAP) Observations: Cosmological Parameter Results*, Astrophys. J. Suppl. **208** (2013) 19 [arXiv:1212.5226].

[113] **Planck** Collaboration, P. A. R. Ade et. al., *Planck 2015 results. XIII. Cosmological parameters*, Astron. Astrophys. **594** (2016) A13 [arXiv:1502.01589].

[114] L. F. Abbott, E. Farhi and M. B. Wise, *Particle Production in the New Inflationary Cosmology*, Phys. Lett. **117B** (1982) 29.

[115] K. Harigaya and K. Mukaida, *Thermalization after/during Reheating*, JHEP **05** (2014) 006 [arXiv:1312.3097].

[116] H. Kodama and T. Hamazaki, *Evolution of cosmological perturbations in a stage dominated by an oscillatory scalar field*, Prog. Theor. Phys. **96** (1996) 949–970 [arXiv:gr-qc/9608022].

[117] T. Hamazaki and H. Kodama, *Evolution of cosmological perturbations during reheating*, Prog. Theor. Phys. **96** (1996) 1123–1146 [arXiv:gr-qc/9609036].

[118] D. Jeong, J. Pradler, J. Chluba and M. Kamionkowski, *Silk damping at a redshift of a billion: a new limit on small-scale adiabatic perturbations*, Phys. Rev. Lett. **113** (2014) 061301 [arXiv:1403.3697].

[119] V. Mukhanov, Physical Foundations of Cosmology. Cambridge Univ. Press, Cambridge, 2005.

[120] T. Kobayashi, M. Yamaguchi and J. Yokoyama, *G-inflation: Inflation driven by the Galileon field*, Phys. Rev. Lett. **105** (2010) 231302 [arXiv:1008.0603].

[121] Y.-F. Cai, J.-O. Gong, S. Pi, E. N. Saridakis and S.-Y. Wu, *On the possibility of blue tensor spectrum within single field inflation*, Nucl. Phys. **B900** (2015) 517–532 [arXiv:1412.7241].

[122] M. Satoh and J. Soda, *Higher Curvature Corrections to Primordial Fluctuations in Slow-roll Inflation*, JCAP **0809** (2008) 019 [arXiv:0806.4594].

[123] M. Satoh, *Slow-roll Inflation with the Gauss-Bonnet and Chern-Simons Corrections*, JCAP **1011** (2010) 024 [arXiv:1008.2724].

[124] Z.-K. Guo and D. J. Schwarz, *Slow-roll inflation with a Gauss-Bonnet correction*, Phys. Rev. **D81** (2010) 123520 [arXiv:1001.1897].

[125] Y. Mishima and T. Kobayashi, *Revisiting slow-roll dynamics and the tensor tilt in general single-field inflation*, arXiv:1911.02143.

[126] M. Srednicki, Quantum Field Theory. Cambridge Univ. Press, Cambridge, 2007.

[127] V. Poulin, P. D. Serpico and J. Lesgourgues, *A fresh look at linear cosmological constraints on a decaying dark matter component*, JCAP **1608** (2016), no. 08 036 [arXiv:1606.02073].

[128] M. Maggiore, Gravitational waves. Oxford Univ. Press, Oxford, 2008.

[129] T. Nakama, J. Silk and M. Kamionkowski, *Stochastic gravitational waves associated with the formation of primordial black holes*, Phys. Rev. **D95** (2017), no. 4 043511 [arXiv:1612.06264].

[130] J. Garcia-Bellido, M. Peloso and C. Unal, *Gravitational Wave signatures of inflationary models from Primordial Black Hole Dark Matter*, JCAP **1709** (2017), no. 09 013 [arXiv:1707.02441].

[131] E. W. Kolb and M. S. Turner, The early universe. Frontiers in Physics. Westview Press, Boulder, CO, 1990.

[132] S. Dodelson, Modern cosmology. Academic Press, San Diego, CA, 2003.

[133] J. Chluba, R. Khatri and R. A. Sunyaev, *CMB at 2x2 order: The dissipation of primordial acoustic waves and the observable part of the associated energy release*, Mon. Not. Roy. Astron. Soc. **425** (2012) 1129–1169 [arXiv:1202.0057].

[134] J. Chluba, A. L. Erickcek and I. Ben-Dayan, *Probing the inflaton: Small-scale power spectrum constraints from measurements of the CMB energy spectrum*, Astrophys. J. **758** (2012) 76 [arXiv:1203.2681].

[135] T. Nakama, T. Suyama and J. Yokoyama, *Reheating the Universe Once More: The Dissipation of Acoustic Waves as a Novel Probe of Primordial Inhomogeneities on Even Smaller Scales*, Phys. Rev. Lett. **113** (2014) 061302 [arXiv:1403.5407].

[136] K. Inomata, M. Kawasaki and Y. Tada, *Revisiting constraints on small scale perturbations from big-bang nucleosynthesis*, Phys. Rev. **D94** (2016), no. 4 043527 [arXiv:1605.04646].

[137] T. Bringmann, P. Scott and Y. Akrami, *Improved constraints on the primordial power spectrum at small scales from ultracompact minihalos*, Phys. Rev. **D85** (2012) 125027 [arXiv:1110.2484].

[138] H. Niikura, M. Takada, S. Yokoyama, T. Sumi and S. Masaki, *Constraints on Earth-mass primordial black holes from OGLE 5-year microlensing events*, Phys. Rev. **D99** (2019), no. 8 083503 [arXiv:1901.07120].

[139] A. S. Josan, A. M. Green and K. A. Malik, *Generalised constraints on the curvature perturbation from primordial black holes*, Phys. Rev. **D79** (2009) 103520 [arXiv:0903.3184].

[140] G. Sato-Polito, E. D. Kovetz and M. Kamionkowski, *Constraints on the primordial curvature power spectrum from primordial black holes*, Phys. Rev. **D100** (2019), no. 6 063521 [arXiv:1904.10971].

[141] A. Kalaja, N. Bellomo, N. Bartolo, D. Bertacca, S. Matarrese, I. Musco, A. Raccanelli and L. Verde, *From Primordial Black Holes Abundance to Primordial Curvature Power Spectrum (and back)*, JCAP **1910** (2019), no. 10 031 [arXiv:1908.03596].

[142] T. Nakama, T. Harada, A. G. Polnarev and J. Yokoyama, *Identifying the most crucial parameters of the initial curvature profile for primordial black hole formation*, JCAP **1401** (2014) 037 [arXiv:1310.3007].

[143] K. Ando, K. Inomata and M. Kawasaki, *Primordial black holes and uncertainties in the choice of the window function*, Phys. Rev. **D97** (2018), no. 10 103528 [arXiv:1802.06393].

[144] C.-M. Yoo, T. Harada, J. Garriga and K. Kohri, *PBH abundance from random Gaussian curvature perturbations and a local density threshold*, arXiv:1805.03946.

[145] S. Young, *The primordial black hole formation criterion re-examined: parameterisation, timing, and the choice of window function*, arXiv:1905.01230.

[146] H. Assadullahi and D. Wands, *Constraints on primordial density perturbations from induced gravitational waves*, Phys. Rev. **D81** (2010) 023527 [arXiv:0907.4073].

[147] E. Thrane and J. D. Romano, *Sensitivity curves for searches for gravitational-wave backgrounds*, Phys. Rev. **D88** (2013), no. 12 124032 [arXiv:1310.5300].

[148] B. Allen and J. D. Romano, *Detecting a stochastic background of gravitational radiation: Signal processing strategies and sensitivities*, Phys. Rev. **D59** (1999) 102001 [arXiv:gr-qc/9710117].

[149] X. Siemens, J. Ellis, F. Jenet and J. D. Romano, *The stochastic background: scaling laws and time to detection for pulsar timing arrays*, Class. Quant. Grav. **30** (2013) 224015 [arXiv:1305.3196].

[150] **VIRGO, KAGRA, LIGO Scientific** Collaboration, B. P. Abbott et. al., *Prospects for Observing and Localizing Gravitational-Wave Transients with Advanced LIGO, Advanced Virgo and KAGRA*, Living Rev. Rel. **21** (2018) 3 [arXiv:1304.0670]. [Living Rev. Rel.19,1(2016)].

[151] S. Kuroyanagi, K. Nakayama and J. Yokoyama, *Prospects of determination of reheating temperature after inflation by DECIGO*, PTEP **2015** (2015), no. 1 013E02 [arXiv:1410.6618].

[152] T. L. Smith, E. Pierpaoli and M. Kamionkowski, *A new cosmic microwave background constraint to primordial gravitational waves*, Phys. Rev. Lett. **97** (2006) 021301 [arXiv:astro-ph/0603144].

[153] A. J. Farmer and E. S. Phinney, *The gravitational wave background from cosmological compact binaries*, Mon. Not. Roy. Astron. Soc. **346** (2003) 1197 [arXiv:astro-ph/0304393].

[154] H. Kudoh, A. Taruya, T. Hiramatsu and Y. Himemoto, *Detecting a gravitational-wave background with next-generation space interferometers*, Phys. Rev. **D73** (2006) 064006 [arXiv:gr-qc/0511145].

[155] C. Cutler, *Angular resolution of the LISA gravitational wave detector*, Phys. Rev. **D57** (1998) 7089–7102 [arXiv:gr-qc/9703068].

[156] M. Tinto, J. W. Armstrong and F. B. Estabrook, *Discriminating a gravitational wave background from instrumental noise in the LISA detector*, Phys. Rev. **D63** (2001) 021101.

[157] C. J. Hogan and P. L. Bender, *Estimating stochastic gravitational wave backgrounds with Sagnac calibration*, Phys. Rev. **D64** (2001) 062002 [arXiv:astro-ph/0104266].

[158] M. R. Adams and N. J. Cornish, *Discriminating between a Stochastic Gravitational Wave Background and Instrument Noise*, Phys. Rev. **D82** (2010) 022002 [arXiv:1002.1291].

[159] M. R. Adams and N. J. Cornish, *Detecting a Stochastic Gravitational Wave Background in the presence of a Galactic Foreground and Instrument Noise*, Phys. Rev. **D89** (2014), no. 2 022001 [arXiv:1307.4116].

[160] M. Anholm, S. Ballmer, J. D. E. Creighton, L. R. Price and X. Siemens, *Optimal strategies for gravitational wave stochastic background searches in pulsar timing data*, Phys. Rev. **D79** (2009) 084030 [arXiv:0809.0701].

[161] S. J. Chamberlin, J. D. E. Creighton, X. Siemens, P. Demorest, J. Ellis, L. R. Price and J. D. Romano, *Time-domain Implementation of the Optimal Cross-Correlation Statistic for Stochastic Gravitational-Wave Background Searches in Pulsar Timing Data*, Phys. Rev. **D91** (2015), no. 4 044048 [arXiv:1410.8256].

[162] R. w. Hellings and G. s. Downs, *UPPER LIMITS ON THE ISOTROPIC GRAVITATIONAL RADIATION BACKGROUND FROM PULSAR TIMING ANALYSIS*, Astrophys. J. **265** (1983) L39–L42.

[163] R. Schneider, V. Ferrari, S. Matarrese and S. F. Portegies Zwart, *Gravitational waves from cosmological compact binaries*, Mon. Not. Roy. Astron. Soc. **324** (2001) 797 [arXiv:astro-ph/0002055].

[164] R. Schneider, S. Marassi and V. Ferrari, *Stochastic backgrounds of gravitational waves from extragalactic sources*, Class. Quant. Grav. **27** (2010) 194007 [arXiv:1005.0977].

[165] K. Inomata, M. Kawasaki, K. Mukaida, Y. Tada and T. T. Yanagida, *Inflationary primordial black holes for the LIGO gravitational wave events and pulsar timing array experiments*, Phys. Rev. **D95** (2017), no. 12 123510 [arXiv:1611.06130].

[166] J. M. Ezquiaga, J. Garcia-Bellido and E. Ruiz Morales, *Primordial Black Hole production in Critical Higgs Inflation*, Phys. Lett. **B776** (2018) 345–349 [arXiv:1705.04861].

[167] R.-G. Cai, S. Pi and M. Sasaki, *Universal infrared scaling of gravitational wave background spectra*, arXiv:1909.13728.

[168] T. Suyama, T. Tanaka, B. Bassett and H. Kudoh, *Are black holes over-produced during preheating?*, Phys. Rev. **D71** (2005) 063507 [arXiv:hep-ph/0410247].

[169] C. Caprini and D. G. Figueroa, *Cosmological Backgrounds of Gravitational Waves*, Class. Quant. Grav. **35** (2018), no. 16 163001 [arXiv:1801.04268].

[170] A. Sesana, A. Vecchio and C. N. Colacino, *The stochastic gravitational-wave background from massive black hole binary systems: implications for observations with Pulsar Timing Arrays*, Mon. Not. Roy. Astron. Soc. **390** (2008) 192 [arXiv:0804.4476].

[171] A. Sesana, *Systematic investigation of the expected gravitational wave signal from supermassive black hole binaries in the pulsar timing band*, Mon. Not. Roy. Astron. Soc. **433** (2013) 1 [arXiv:1211.5375].

[172] C. M. F. Mingarelli, T. J. W. Lazio, A. Sesana, J. E. Greene, J. A. Ellis, C.-P. Ma, S. Croft, S. Burke-Spolaor and S. R. Taylor, *The Local Nanohertz Gravitational-Wave Landscape From Supermassive Black Hole Binaries*, Nat. Astron. **1** (2017), no. 12 886–892 [arXiv:1708.03491].

[173] L. Barack et. al., *Black holes, gravitational waves and fundamental physics: a roadmap*, arXiv:1806.05195.

[174] S. R. Taylor and J. R. Gair, *Searching For Anisotropic Gravitational-wave Backgrounds Using Pulsar Timing Arrays*, Phys. Rev. **D88** (2013) 084001 [arXiv:1306.5395].

[175] S. R. Taylor et. al., *Limits on anisotropy in the nanohertz stochastic gravitational-wave background*, Phys. Rev. Lett. **115** (2015), no. 4 041101 [arXiv:1506.08817].

[176] C. Cutler and D. E. Holz, *Ultra-high precision cosmology from gravitational waves*, Phys. Rev. **D80** (2009) 104009 [arXiv:0906.3752].

[177] T. Regimbau, M. Evans, N. Christensen, E. Katsavounidis, B. Sathyaprakash and S. Vitale, *Digging deeper: Observing primordial gravitational waves below the binary black hole produced stochastic background*, Phys. Rev. Lett. **118** (2017), no. 15 151105 [arXiv:1611.08943].

[178] D. J. Fixsen, E. S. Cheng, J. M. Gales, J. C. Mather, R. A. Shafer and E. L. Wright, *The Cosmic Microwave Background spectrum from the full COBE FIRAS data set*, Astrophys. J. **473** (1996) 576 [arXiv:astro-ph/9605054].

[179] P. Hunt and S. Sarkar, *Search for features in the spectrum of primordial perturbations using Planck and other datasets*, JCAP **1512** (2015), no. 12 052 [arXiv:1510.03338].

[180] K. Inomata and T. Terada, *Gauge Independence of Induced Gravitational Waves*, arXiv:1912.00785.

[181] F. Arroja, H. Assadullahi, K. Koyama and D. Wands, *Cosmological matching conditions for gravitational waves at second order*, Phys. Rev. **D80** (2009) 123526 [arXiv:0907.3618].

[182] G. Domènech and M. Sasaki, *Hamiltonian approach to second order gauge invariant cosmological perturbations*, Phys. Rev. **D97** (2018), no. 2 023521 [arXiv:1709.09804].

[183] J.-O. Gong, *Analytic integral solutions for induced gravitational waves*, arXiv:1909.12708.

[184] K. Tomikawa and T. Kobayashi, *On the gauge dependence of gravitational waves generated at second order from scalar perturbations*, arXiv:1910.01880.

[185] V. De Luca, G. Franciolini, A. Kehagias and A. Riotto, *On the Gauge Invariance of Cosmological Gravitational Waves*, arXiv:1911.09689.

[186] C. Yuan, Z.-C. Chen and Q.-G. Huang, *Scalar Induced Gravitational Waves in Different Gauges*, arXiv:1912.00885.

[187] S. Kuroyanagi, "Gravitational waves from 2nd order scalar perturbations." a talk in the 2nd LeCosPA Symposium, December, 2015.

[188] J.-c. Hwang, *Roles of a coherent scalar field on the evolution of cosmic structures*, Phys. Lett. **B401** (1997) 241–246 [arXiv:astro-ph/9610042].

[189] J. A. R. Cembranos, A. L. Maroto and S. J. Núñez Jareño, *Cosmological perturbations in coherent oscillating scalar field models*, JHEP **03** (2016) 013 [arXiv:1509.08819].

[190] H. Kodama and M. Sasaki, *Cosmological Perturbation Theory*, Prog. Theor. Phys. Suppl. **78** (1984) 1–166.

[191] K. Jedamzik, M. Lemoine and J. Martin, *Collapse of Small-Scale Density Perturbations during Preheating in Single Field Inflation*, JCAP **1009** (2010) 034 [arXiv:1002.3039].

[192] K. Jedamzik, M. Lemoine and J. Martin, *Generation of gravitational waves during early structure formation between cosmic inflation and reheating*, JCAP **1004** (2010) 021 [arXiv:1002.3278].

[193] P. F. de Salas, M. Lattanzi, G. Mangano, G. Miele, S. Pastor and O. Pisanti, *Bounds on very low reheating scenarios after Planck*, Phys. Rev. **D92** (2015), no. 12 123534 [arXiv:1511.00672].

[194] L. Kofman, A. D. Linde, X. Liu, A. Maloney, L. McAllister and E. Silverstein, *Beauty is attractive: Moduli trapping at enhanced symmetry points*, JHEP **05** (2004) 030 [arXiv:hep-th/0403001].

[195] L. Kofman, *Probing string theory with modulated cosmological fluctuations*, arXiv:astro-ph/0303614.

[196] G. Dvali, A. Gruzinov and M. Zaldarriaga, *Cosmological perturbations from inhomogeneous reheating, freezeout, and mass domination*, Phys. Rev. **D69** (2004) 083505 [arXiv:astro-ph/0305548].

[197] M. Zaldarriaga, *Non-Gaussianities in models with a varying inflaton decay rate*, Phys. Rev. **D69** (2004) 043508 [arXiv:astro-ph/0306006].

[198] L. Ackerman, C. W. Bauer, M. L. Graesser and M. B. Wise, *Light scalars and the generation of density perturbations during preheating or inflaton decay*, Phys. Lett. **B611** (2005) 53–59 [arXiv:astro-ph/0412007].

[199] D. I. Podolsky, G. N. Felder, L. Kofman and M. Peloso, *Equation of state and beginning of thermalization after preheating*, Phys. Rev. **D73** (2006) 023501 [arXiv:hep-ph/0507096].

[200] K. Kohri, D. H. Lyth and C. A. Valenzuela-Toledo, *Preheating and the non-gaussianity of the curvature perturbation*, JCAP **1002** (2010) 023 [arXiv:0904.0793]. [Erratum: JCAP1009,E01(2011)].

[201] G. Bertone, D. Hooper and J. Silk, *Particle dark matter: Evidence, candidates and constraints*, Phys. Rept. **405** (2005) 279–390 [arXiv:hep-ph/0404175].

[202] K. Enqvist and A. Mazumdar, *Cosmological consequences of MSSM flat directions*, Phys. Rept. **380** (2003) 99–234 [arXiv:hep-ph/0209244].

[203] P. Binetruy, A. Bohe, C. Caprini and J.-F. Dufaux, *Cosmological Backgrounds of Gravitational Waves and eLISA/NGO: Phase Transitions, Cosmic Strings and Other Sources*, JCAP **1206** (2012) 027 [arXiv:1201.0983].